NATIONAL ADVISORY COMMITTEE
)R AERONAUTICS

TECHNICAL NOTE

No. 1351

COMPARISON BETWEEN THE MEASURED AND THEORETICAL SPAN LOADINGS ON A MODERATELY SWEPT-FORWARD AND A MODERATELY SWEPT-BACK SEMISPAN WING

By Robert A. Mendelsohn and Jack D. Brewer

Langley Memorial Aeronautical Laboratory
Langley Field, Va.

Washington

July 1947

E R R A T A

NACA TN 1351

COMPARISON BETWEEN THE MEASURED AND THEORETICAL SPAN LOADINGS ON A MODERATELY SWEPT-FORWARD AND A MODERATELY SWEPT-BACK SEMISPAN WING

By Robert A. Mendelsohn and Jack D. Brewer

July 1947

The curves of figure 10(a) are in error because of the use of the incorrect root chord in conversion of the results to the form given in the figure. All curves of figure 10(a) should be corrected by multiplying the ordinates of the curves by the factor 0.865.

The term "uniform geometric twist," as used in this paper, is defined as that twist which is given by connection of constant-percent-chord stations of the root and tip airfoil sections by straight lines. The quarter-chord line of the swept-back wing has no dihedral.

NACA-Langley - 3-8-50 - 950

NATIONAL ADVISORY COMMITTEE FOR AERONAUTICS

TECHNICAL NOTE NO. 1351

COMPARISON BETWEEN THE MEASURED AND THEORETICAL SPAN LOADINGS ON A MODERATELY SWEPT-FORWARD AND A MODERATELY SWEPT-BACK SEMISPAN WING

By Robert A. Mendelsohn and Jack D. Brewer

SUMMARY

An investigation has been conducted in the Langley stability tunnel on two semispan swept-wing models — one swept forward 12° and the other swept back 23° at the quarter-chord line — in order to determine experimentally the span-load distributions and to compare the experimental with theoretical results. In addition, lift, drag, pitching moment, and stalling characteristics were determined. In order to check the validity of the semispan tests, the full-span swept-back wing from which the semispan model was made was first tested in the Langley propellor-research tunnel. A comparison between span loadings obtained from the data of the two wind tunnels and those calculated by lifting-line and lifting-surface theory indicated that differences between the results from the two wind tunnels, though small, were as great as the differences between the results from the lifting-line and lifting-surface calculations. The theoretical curves approximated the experimental curves within the accuracy necessary for engineering calculations.

The experimental results indicated that a small loss in load, presumably caused by the tunnel-wall boundary layer, occurred near the root for both semispan wings. Because of this loss in load and because of distortions in the chordwise loading near the root, semispan tests of highly swept wings may give errors in pitching moment. The aerodynamic centers of both semispan wings were found to move forward at high lift coefficients. A tailless swept-wing airplane, similar to the wing used for these tests, may therefore become longitudinally unstable at high lift coefficients. Profile-drag measurements indicated an appreciable outflow of the boundary layer on the swept-back wing.

INTRODUCTION

A great amount of work has been done to determine span-loading characteristics of swept wings from purely theoretical considerations, and many computation methods are now available, some based on lifting-line theory and some based on lifting-surface theory. These methods give the span loading to various degrees of accuracy, depending on the assumptions made, which in turn govern the amount of labor expended to obtain a solution. The purpose of this investigation was, therefore, to compare theoretical span-loading results with measured values to determine the practicability of using the simpler computation methods on wings having moderate amounts of sweep.

Tests were conducted in the 6- by 6-foot section of the Langley stability tunnel on two models - a semispan wing swept forward 12° and a semispan wing swept back 23° - in order to determine span loading, lift, drag, pitching moment, and stalling characteristics. The semispan swept-back wing was the left panel of a full-span swept-back wing that had previously been tested in the Langley propeller-research tunnel. (See appendix.) The tests described in the appendix were conducted on the swept-back wing alone and on the same wing with a center plate and spoiler which simulated the boundary layer on the tunnel wall for the semispan tests. The purpose of the full-span tests was to determine the effect of the tunnel-wall boundary layer on the span loading of the semispan model. The spanwise variation of profile drag was also determined in the full-span tests. Data from the tests described in the appendix are included herein for comparison.

The test models had no elevons but, by integration of pressures, generalized curves of the variation of hinge-moment coefficient with angle of attack were calculated for several assumed elevon plan forms.

SYMBOLS

The coefficients and symbols used are defined as follows:

C_L wing lift coefficient (L/qS)

c_l lift coefficient at a section (l/qc)

c_{l_a} additional lift coefficient at a section

c_{l_b} basic lift coefficient at a section $\left(C_L = 0\right)$

C_D wing drag coefficient (D/qS)

c_{d_o} profile-drag coefficient at a section (d/qc)

C_m wing pitching-moment coefficient (M/qSc')

c_m pitching-moment coefficient at a section (m/qc^2)

c_h elevon hinge-moment coefficient at a section

$$\left(\frac{1}{c_a{}^2}\int_{x_1}^{c} P\,(x - x_1)\,dx\right)$$

C_h elevon hinge-moment coefficient $\left(\frac{1}{\bar{c}_a{}^2 b_a}\int_{y_i}^{y_o} c_a{}^2 c_h\,dy\right)$

C_{h_α} rate of change of elevon hinge-moment coefficient with angle of attack $(\partial C_h/\partial\alpha)$

P pressure coefficient $\left(\frac{p - p_o}{q}\right)$

P_α rate of change of pressure coefficient with angle of attack $(\partial P/\partial\alpha)$

$\Delta P/\Delta\alpha$ pressure-coefficient increment resulting from an angle-of-attack change from 0° divided by the angle-of-attack change

L wing lift

l lift at a section

D wing drag

d profile drag at a section

M wing pitching moment about $\bar{c}/4$

m pitching moment about $c/4$ at a section

S wing area

y spanwise distance normal to plane of symmetry

y_i spanwise distance from plane of symmetry to inboard end of elevon

y_o	spanwise distance from plane of symmetry to outboard end of elevon
b	wing span normal to plane of symmetry
b_a	elevon span normal to plane of symmetry
x	distance from leading edge along chord line
x_1	distance from leading edge of wing to chord line of assumed elevon hinge axis
c	local wing chord parallel to plane of symmetry
$\bar{c}$	mean aerodynamic wing chord
c_s	wing root chord
c_a	local chord of assumed elevon parallel to plane of symmetry
$\bar{c}_a$	root-mean-square chord of assumed elevon
q	free-stream dynamic pressure $\left(\frac{1}{2}\rho V^2\right)$
p	local static pressure
p_o	free-stream static pressure
V	free-stream velocity
ρ	density of air
α	angle of attack, measured at root section

APPARATUS AND METHODS

Models

Two semispan tapered wing models were used for the tests, one having 12° sweepforward of the quarter-chord line with no geometric twist and the other having 23° sweepback of the quarter-chord line with −4° uniform geometric twist. Both models were constructed of laminated mahogany and had 25 pressure orifices spaced at constant percentages of the local chord for each of nine spanwise stations.

(See fig. 1.) The swept-back wing is the left panel of the model used for the tests described in the appendix, except that an additional row of orifices was installed 1 inch from the root section, and the model was completely refinished.

Some geometric constants for the models are:

	Swept-forward wing	Swept-back wing
Area of full-span wing, sq ft	16.72	13.55
Wing span, ft (full span)	10.10	10.10
Mean aerodynamic chord, ft	1.81	1.51
Aspect ratio	6.10	7.51
Taper ratio	0.327	0.243
Sweep of quarter-chord line, deg	-12	23
Uniform geometric twist (washout), deg	0	4
Root airfoil section	NACA 4415	NACA 4418
Tip airfoil section	NACA 4412	NACA 4418

Installation and Tests

Each model was mounted horizontally (with zero dihedral) on the side support of the tunnel balance frame, completely free from the tunnel wall except for a flexible seal used to prevent flow through the gap between the tunnel wall and the wing support block. (See fig. 2.)

In order to allow movement of the part of the wing that extended beyond the tunnel disk, the swept-forward wing had a gap of approximately $\frac{1}{8}$ inch left unsealed between the tunnel wall and the root section behind the 67-percent-chord point. For the swept-back wing, a similar gap was left unsealed forward of the 17-percent-chord point. Check tests were made on the swept-back wing to determine whether the fabric seal and open gap affected the loading near the root section. For these tests, plasteline was used to seal all gaps and to continue the wing contour to the tunnel wall.

Because the wings were expected to deflect under load, a determination of the wing twist was made. For the swept-forward wing, the twist was calculated by a method using the measured span loading and the known wing rigidity as determined from static tests. For the swept-back wing, the spanwise variation of twist of the wing under load was determined by measuring the displacement of beams of light reflected from mirrors mounted on the wing.

Span-loading, force, and tuft tests were made for this investigation at a dynamic pressure of 98.3 pounds per square foot for angles of attack up to and including 9°, and at a dynamic pressure of 39.7

pounds per square foot for angles of attack from 9° through the stall. These dynamic pressures correspond to airspeeds of 196 miles per hour and 124.6 miles per hour, respectively, under standard sea-level atmospheric conditions. For the same speeds, Reynolds numbers for the swept-forward wing, based on the mean aerodynamic chord of the model, were 3.31×10^6 and 2.10×10^6 and Reynolds numbers for the swept-back wing, based on the mean aerodynamic chord of the model, were 2.77×10^6 and 1.76×10^6. No turbulence factor was used in the calculation of Reynolds numbers because the turbulence level in the stability tunnel is very low.

CORRECTIONS

The force and moment coefficients and the angle of attack were corrected for the effects of the tunnel jet boundaries by the general method given in reference 1. In addition, corrections were applied to the angle of attack for model deflections. Because the angle-of-attack correction for jet boundaries and model twist varied along the span, the coefficients at each section were corrected for conditions at each section. For the force tests of the wing, the angle of attack was corrected by an average value, weighted according to the chord. The angles of attack shown on the pressure-distribution plots are the average wing angles of attack, because the pressure distributions are presented as measured and are for the nonrigid models. No corrections were applied for the effects of the tunnel-wall boundary layer or for the clearance gaps between the root section and the tunnel wall.

The equations used in correcting the force data for jet boundary and model deflections were:

Swept-forward wing:

$$\alpha = \alpha_U + 1.717C_{L_U} - 0.02; \quad q = 39.7 \text{ lb/sq ft}$$

$$\alpha = \alpha_U + 1.863C_{L_U} - 0.05; \quad q = 98.3 \text{ lb/sq ft}$$

$$C_L = C_{L_U}$$

$$C_D = C_{D_U} + 0.0176C_{L_U}^2$$

$$C_m = C_{m_U} + 0.0013C_{L_U}$$

Swept-back wing:

$$\alpha = \alpha_U + 1.132C_{L_U} - 0.02; \quad q = 39.7 \text{ lb/sq ft}$$

$$\alpha = \alpha_U + 0.923C_{L_U} - 0.04; \quad q = 98.3 \text{ lb/sq ft}$$

$$C_L = C_{L_U}$$

$$C_D = C_{D_U} + 0.0173C_{L_U}^2$$

$$C_m = C_{m_U}$$

where the subscript U denotes uncorrected values.

The maximum twist correction near the tip at a dynamic pressure of 98.3 pounds per square foot and at an angle of attack of 9° was 0.54° for the swept-forward wing and 0.77° for the swept-back wing.

PRESENTATION OF RESULTS

Pressure distributions.- The measured section pressure distributions are presented in figures 3 and 4. In order to obtain a better estimate of the pressure distributions corresponding to a rigid wing in free air, cross plots of pressure coefficients at several chordwise locations for each spanwise station were made against corrected angle of attack. From these plots, the parameters P_α and $\Delta P/\Delta\alpha$ were determined. (See figs. 5 and 6.) These pressure distributions deviate slightly from free-air conditions since, although the chordwise load was corrected for the effect of jet boundaries, there was no correction for the distortion in the load caused by induced camber. Except for this approximation, free-air pressure distributions can be estimated from figures 5 and 6 for angles of attack up to 12° by the following relations:

$$P = \alpha(P_\alpha) + P_{(\alpha=0)}$$

or

$$P = \alpha\left(\frac{\Delta P}{\Delta\alpha}\right) + P_{(\alpha=0)}$$

Span loading.- The pressure distributions at each section were integrated to obtain normal-force coefficients, chord-force coefficients, and pitching-moment coefficients. The lift coefficients at each section were calculated and, together with the pitching-moment coefficients at each section, are plotted against corrected angle of attack in figures 7 and 8.

Loading diagrams corresponding to a rigid wing in free air were obtained by cross-plotting the lift curves at each section at constant angles of attack. (See fig. 9.)

The parameter representing the rate of change of additional loading with lift coefficient $\left(cc_{l_a}/C_L c_s\right)$ was obtained from a plot of cc_{l_a}/c_s against C_L. Figure 10 shows this additional loading and the basic (or zero lift) loading. For the linear range of lift coefficient up to $C_L = 0.8$, the total loading on either wing may be obtained by the equation

$$\frac{cc_l}{c_s} = \frac{cc_{l_b}}{c_s} + C_L \frac{cc_{l_a}}{C_L c_s}$$

The basic and additional loads for the swept-back wing, as determined from the Langley stability and propeller-research tunnels, are compared in figure 10(b). Included in this figure are theoretical basic and additional loadings computed by the lifting-line theories described in references 2 and 3, respectively, neither of which accounts for sweep, and also an additional loading computed by the lifting-surface theory described in reference 4, which takes sweep into account.

Elevon characteristics.- The elevon hinge-moment coefficient at each section c_h was computed by integration of the measured pressures. The values of c_h were then plotted against spanwise location and integrated to determine C_h for two typical elevons. The constant-chord elevon ($c_a = 0.168c$) extends from the 36.4-percent section to the 71-percent section. On the swept-back model, this elevon closely resembles that currently used on a tailless airplane. The constant-percentage-chord elevon ($c_a = 0.200c$) extends from the 40-percent-span section to the tip. (See fig. 11.) The elevon hinge-moment parameter C_{h_α} was determined for various elevon spans and locations (see fig. 12) by appropriately integrating the P_α-curves (figs. 5 and 6).

Force tests.- Force and moment-coefficient data from the wind-tunnel balance readings are given in figure 13 for the swept-back and swept-forward wings. The data are plotted against corrected angle of attack.

Profile-drag characteristics.- The spanwise variation of section profile-drag coefficient for the swept-back wing, measured in the Langley propeller-research-tunnel tests (see appendix), is shown in figure 14.

Stall patterns.- The flow conditions over the wing at various angles of attack are shown by figure 15. The stall patterns were determined from photographs of tufts attached to the upper surface of the wings.

DISCUSSION

Pressure distribution.- The pressure distributions of figure 4 show irregular results for the original tests of sections H and I for the swept-back wing. After the tests had been completed, photographs taken to record stall patterns revealed that the fabric seal, which was used to prevent leakage between the model and the tunnel wall, had bulged inward; hence the local velocities near the root region were presumably changed. Check tests on the swept-back wing having plasteline to fair the wing contour to the tunnel wall indicated that, although the chordwise pressure distribution was distorted by the seal, the total load remained the same. The check tests also indicated that very little loss in loading was caused by the $\frac{1}{8}$-inch clearance gap between a part of the wing root and the tunnel wall and that a distortion of the inboard load occurred with a fabric seal regardless of whether it bulged into the air stream.

Span loading.- For the swept-forward wing, a comparison of the measured additional loading with the lifting-line loading, as calculated from reference 3, shows very good agreement except near the root section where a loss in load is indicated by the test data. (See fig. 10(a).) Inasmuch as the wing had constant camber and no geometric twist, theory would indicate a zero basic loading; however, a small basic loading was indicated by the measurements. This apparent basic loading may be caused by construction irregularities, boundary-layer effects, and errors in correcting for twist due to load.

The results for the swept-back wing show a loss in additional load near the root similar to that found for the swept-forward wing. This loss was not shown by the full-span data of the tests described in the appendix, even when the tunnel wall was simulated by a center plate but, since no measurements were made for $\frac{y}{b/2}$ stations less than 0.10 in that investigation, it is possible that the loss in load occurred but was not measured. For highly swept wings, semispan tests may give errors in pitching moment about the aerodynamic center because of distortions in chordwise loading near the wing root and because of changes in span loading caused by tunnel-wall boundary-layer effects. Unpublished data of the span loading over a two-dimensional wing completely spanning a tunnel test section indicate that a loss in load of approximately 5 percent may have been caused at section I by tunnel-wall boundary-

layer effects. The present swept-back-wing tests indicate a higher outboard loading than is shown by the tests described in the appendix or by lifting-line or lifting-surface theory. This apparent discrepancy is partly caused by the necessary vertical shift in the load curve to obtain a uniform total area even though a loss in load occurs near the root. The differences between the two test results are as great as the differences between the theoretical curves. The theoretical curves approximate the experimental ones within the accuracy necessary for engineering calculations. The induced drag corresponding to the various loadings are all very similar as shown in the following table:

Source of span loading	Induced-drag coefficient caused by additional loading
Present swept-back-wing data	$0.0427C_L^2$
Appendix test data	$0.0432C_L^2$
Lifting-line theory	$0.0436C_L^2$
Lifting-surface theory	$0.0429C_L^2$

The difference in the results of the two sets of tests may be attributed to differences in tunnel-correction methods, possible tunnel-wall boundary-layer effect, changes caused by refinishing the model after the tests described in the appendix, the accuracy with which a span loading can be determined from pressure measurements, and differences in air-stream angularity.

The basic loading computed by lifting-line theory indicates a greater load due to geometric twist than is shown by measurements.

Elevon characteristics.- The variation of elevon hinge moment with angle of attack (fig. 11) shows that, for both wing models, there is a large increase in the tendency of the elevon to float with the wind at angles of attack above 4°. Stick-force reversal may therefore occur on a tailless swept-wing airplane with elevons having the assumed dimensions.

The thicker boundary layer near the tip, the large trailing-edge angle, and the sweep cause a reversal of the P_α-curves near the trailing edge. (See figs. 5 and 6.) Plain elevon characteristics estimated from pressure integrations thus indicate that small-chord elevons on this swept-forward or swept-back wing have a positive C_{h_α}. (See fig. 12.) With an increase in elevon chord, C_{h_α} becomes more negative, but with an increase in elevon span, C_{h_α} changes little.

Balance data.- From the force and moment data (fig. 13), it was found that the aerodynamic center of the swept-forward wing remained at 22.1 percent of the mean aerodynamic chord for lift coefficients up to 0.80 and moved forward for higher lift coefficients. For the swept-back wing, the aerodynamic center remained at 28.2 percent of the mean aerodynamic chord for lift coefficients up to 0.28 and moved forward for higher lift coefficients. Thus, a swept-back tailless airplane of this plan form may become longitudinally unstable at high lift coefficients. This characteristic is also shown by the stalling patterns of figure 15. Because of the sweepback, stalling begins near the tip region and progresses inward. Inasmuch as the tip region is behind the moment center, decreases in loading produce more positive pitching moments.

Included in figure 13(b) is a comparison between the lift curve taken from the data of the tests described in the appendix and the present swept-back semispan wing tests. Good agreement is shown. Pressure integration for wing forces and moments gave results which compared very well with balance readings.

Profile-drag characteristics.- As shown in figure 14, the measured section profile-drag coefficients for the swept-back wing are lowest near the center of the wing and increase as the distance from the center increases. If the variation in local angle of attack caused by wing twist and the spanwise variation in Reynolds number were taken into account, an increase in profile drag toward the tip would be expected, but the magnitude of the increase shown by the tests indicates an appreciable outflow of the boundary layer.

Stall patterns.- Figure 15 shows that there is an inflow of air over the swept-forward wing, causing inboard stall, and an outboard flow over the swept-back wing, causing outboard stall. The progression of stall shown by these diagrams are probably influenced to some extent by jet-boundary effects, constriction effects, and model twist.

CONCLUSIONS

An investigation has been conducted in the Langley stability tunnel on two semispan swept-wing models, one swept forward 12° and the other swept back 23° at the quarter-chord line, in order to determine the span-load distributions and to compare the experimental and theoretical results. The full-span swept-back-wing model from which the semispan model was made was first tested in the Langley propeller-research tunnel in order to check the validity of the semispan tests.

The results of these tests indicate the following conclusions:

1. Although the differences between span loadings determined from tests in two wind tunnels were small, they were as great as the differences between span loadings determined from a lifting-line and lifting-surface theory. The theoretical curves approximated the experimental ones within the accuracy required for engineering calculations.

2. A small loss in load, presumably caused by the tunnel-wall boundary layer, occurred near the root for both semispan wings. Because of this loss in load and because of distortions in the chordwise loading near the root, semispan tests of highly swept wings may give errors in pitching moment.

3. The aerodynamic center of both semispan wings moved forward at high lift coefficients. A tailless swept-wing airplane, similar to the wing used for these tests, may therefore become longitudinally unstable at high lift coefficients.

4. Profile-drag measurements indicated an appreciable outflow of the boundary layer on the swept-back wing.

Langley Memorial Aeronautical Laboratory
National Advisory Committee for Aeronautics
Langley Field, Va., August 8, 1946

APPENDIX

WIND-TUNNEL INVESTIGATION OF THE LOAD DISTRIBUTION ON A FULL-SPAN SWEPT-BACK-WING MODEL

By Carl A. Sandahl

Because several semispan wings that were large with respect to the tunnel throat were to be tested, and because of the possibility that a tunnel-wall boundary layer would affect the span loading, one of the models was tested in a larger tunnel to obtain data which could be compared with the semispan data to show possible changes caused by testing methods. This preliminary investigation was conducted in the 20-foot Langley propeller-research tunnel with a 10.1-foot full-span swept-back-wing model. Tests were made with and without a center-plate spoiler arrangement attached to the wing in the plane of symmetry. A spoiler deflection which simulated the boundary-layer displacement thickness for the semispan tests was used. A photograph of the test arrangement is shown in figure 16.

The left panel of the wing model was completely refinished and equipped with an additional row of orifices 1 inch from the model center line for the swept-back wing semispan tests.

The tests in the Langley propeller-research tunnel were run at approximately 100 miles per hour, which corresponds to a Reynolds number based on the mean aerodynamic chord of 1.30×10^6. The wing angle of attack and the drag coefficients were corrected for jet-boundary interference; the variation in jet-boundary induced angle across the span was small enough to be neglected. A determination of the section profile drag was made from wake profiles at a number of spanwise stations 20 percent of the local wing chord behind the trailing edge.

The span loadings for the wing alone and for the wing equipped with center plate and spoiler were determined for various angles of attack. It was found that the spoiler extension which most closely simulated the boundary layer for the semispan tests had very little effect on the basic or additional-load distribution. It is noted that no pressure measurements were made on the inboard 10 percent of the span and that the load curve was extrapolated to zero slope at the center of the wing.

REFERENCES

1. Swanson, Robert S., and Toll, Thomas A.: Jet-Boundary Corrections for Reflection-Plane Models in Rectangular Wind Tunnels. NACA ARR No. 3E22, 1943.

2. Pearson, Henry A., and Jones, Robert T.: Theoretical Stability and Control Characteristics of Wings with Various Amounts of Taper and Twist. NACA Rep. No. 635, 1938.

3. Anderson, Raymond F.: Determination of the Characteristics of Tapered Wings. NACA Rep. No. 572, 1936.

4. Cohen, Doris: A Method for Determining the Camber and Twist of a Surface to Support a Given Distribution of Lift. NACA TN No. 855, 1942.

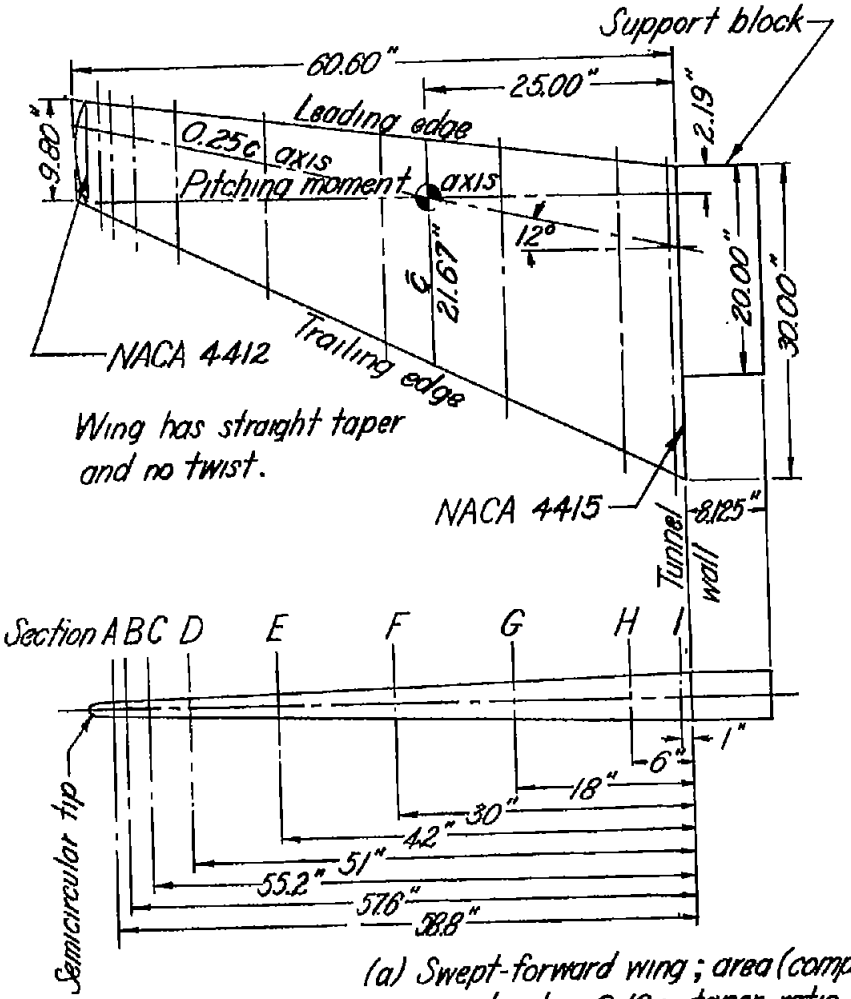

Orifice	Station percent c
1	0
2-14	1.0
3-15	2.5
4-16	5.0
5-17	10.0
6-18	18.125
7-19	28.30
8-20	39.50
9-21	50.50
10-22	61.50
11-23	72.50
12-24	83.50
13-25	94.50

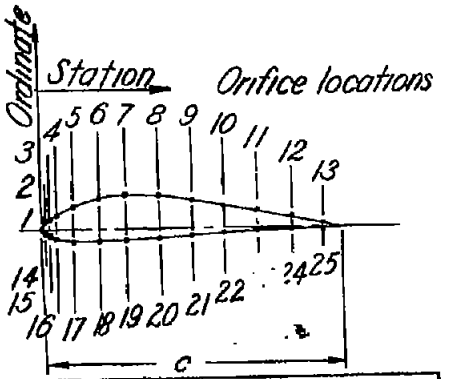

Tip Section		
NACA 4412 Airfoil		
Station percent c	Ordinates percent c	
	Upper	Lower
0	-	0
1.25	2.44	-1.43
2.5	3.39	-1.95
5.0	4.73	-2.49
7.5	5.76	-2.74
10.0	6.59	-2.86
15	7.89	-2.88
20	8.80	-2.74
25	9.41	-2.50
30	9.76	-2.26
40	9.80	-1.80
50	9.19	-1.40
60	8.14	-1.00
70	6.69	-0.65
80	4.89	-0.39
90	2.71	-0.22
95	1.47	-0.16
100	(.33)	(-0.13)
L.E. Rad. = 1.58		

Root Section		
NACA 4415 Airfoil		
Station percent c	Ordinates percent c	
	Upper	Lower
0	-	0
1.25	3.07	-1.79
2.50	4.17	-2.48
5.0	5.74	-3.27
7.5	6.91	-3.71
10.0	7.84	-3.98
15	9.27	-4.18
20	10.25	-4.15
25	10.92	-3.98
30	11.25	-3.73
40	11.25	-3.23
50	10.53	-2.72
60	9.30	-2.14
70	7.69	-1.58
80	5.85	-1.08
90	3.68	-0.57
95	1.67	-0.36
100	(0.16)	(-0.14)
L.E. Rad. = 2.48		

(a) Swept-forward wing; area (complete wing), 16.72 square feet; aspect ratio, 6.10; taper ratio, 0.327.

NATIONAL ADVISORY COMMITTEE FOR AERONAUTICS

Figure 1.- Details of the swept-wing models.

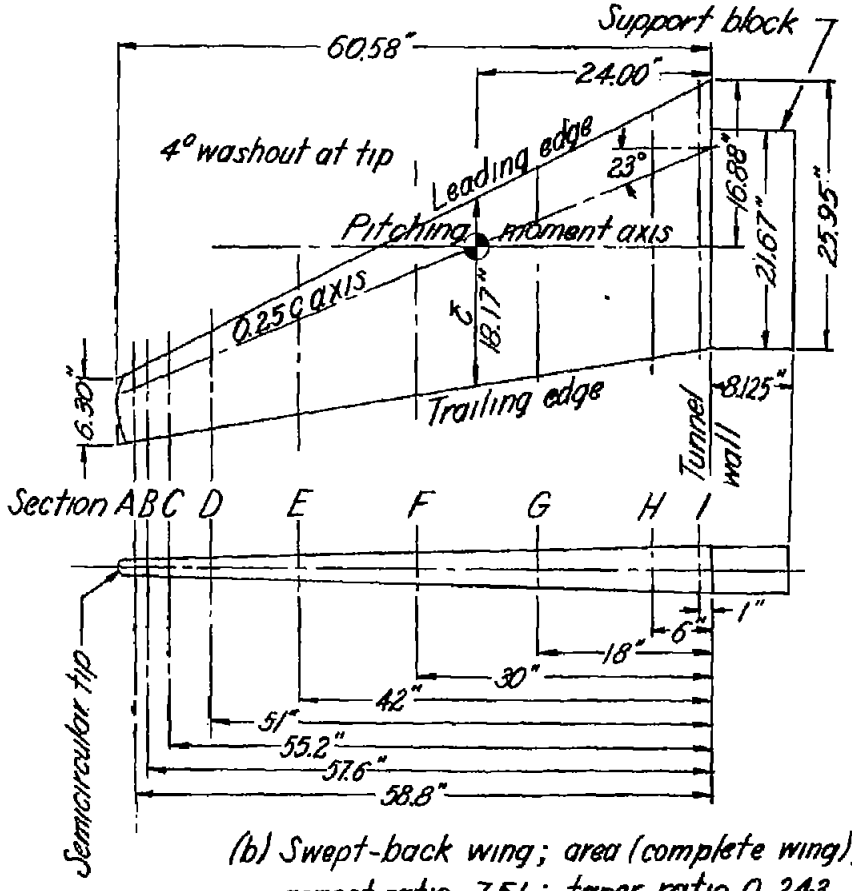

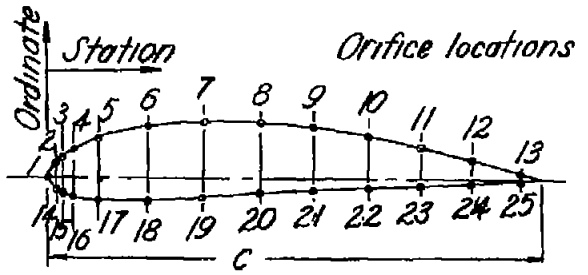

NACA 4418 Airfoil		
Station percent c	Ordinates percent c	
	Upper	Lower
0	-	0
1.25	3.36	-2.11
2.50	3.80	-2.99
5.00	6.73	-4.06
7.50	8.26	-4.67
10.00	9.11	-5.06
15.00	10.66	-5.49
20.00	11.72	-5.36
25.00	12.40	-5.49
30.00	12.76	-5.26
40.00	12.70	-4.70
50.00	11.85	-4.02
60.00	10.44	-3.24
70.00	8.55	-2.45
80.00	6.22	-1.67
90.00	3.46	-0.98
95.00	1.89	-0.55
100.00	(0.19)	(-0.19)
L.E. Rad. = 3.56		

Orifice	Station percent c
1	0
2-14	1.0
3-15	2.5
4-16	5.0
5-17	10.0
6-18	15.125
7-19	28.50
8-20	39.50
9-21	50.50
10-22	61.50
11-23	72.50
12-24	83.50
13-25	94.50

(b) Swept-back wing; area (complete wing), 13.55 square feet; aspect ratio, 7.51; taper ratio 0.243.

NATIONAL ADVISORY COMMITTEE FOR AERONAUTICS

Figure 1.- Concluded.

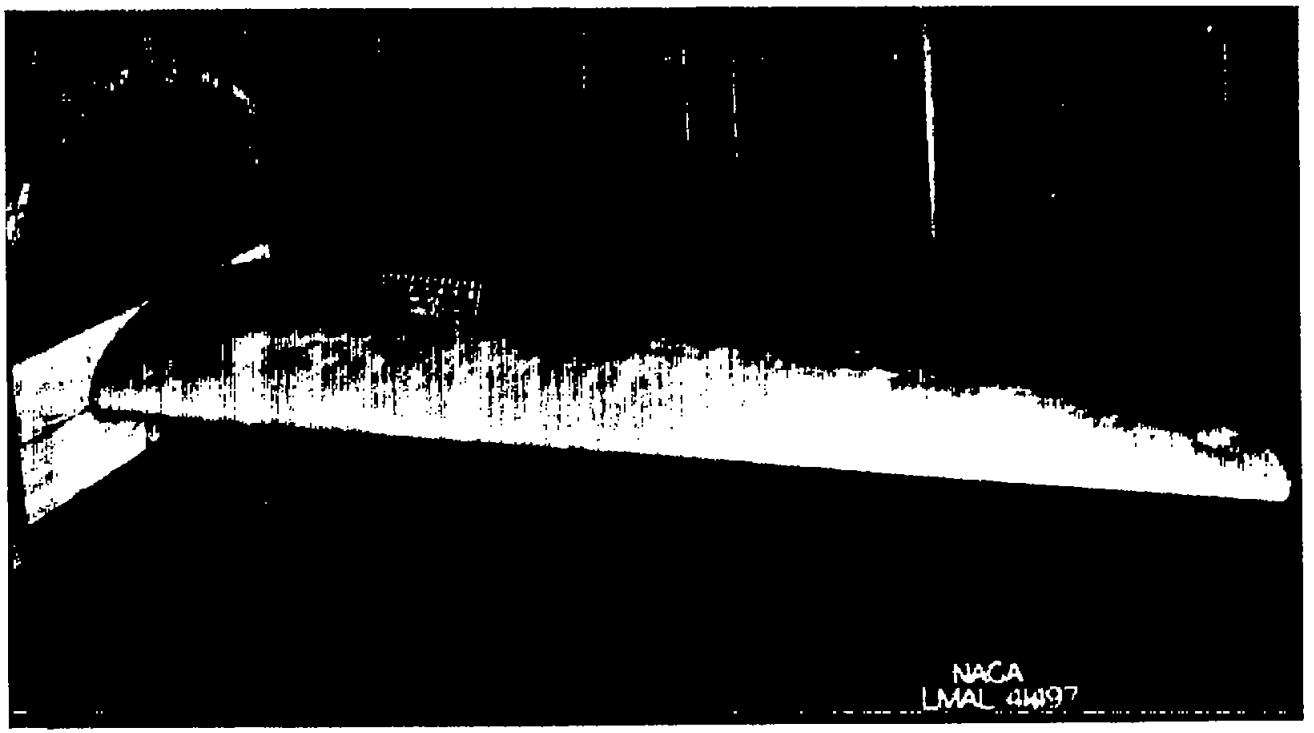

(a) Swept-forward wing. Front view.

Figure 2.- View of sweptwing models in the 6- by 6-foot section of the Langley stability tunnel.

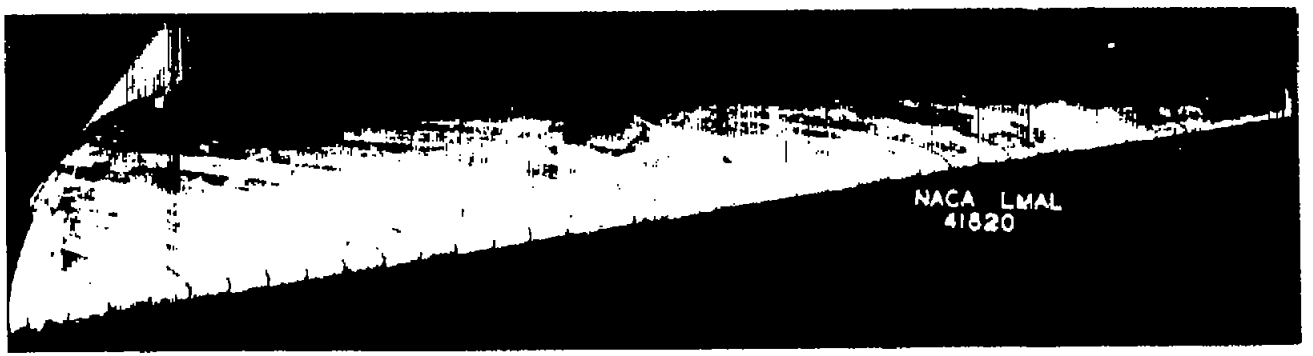

(c) Swept-back wing. Front view.

Figure 2.- Continued.

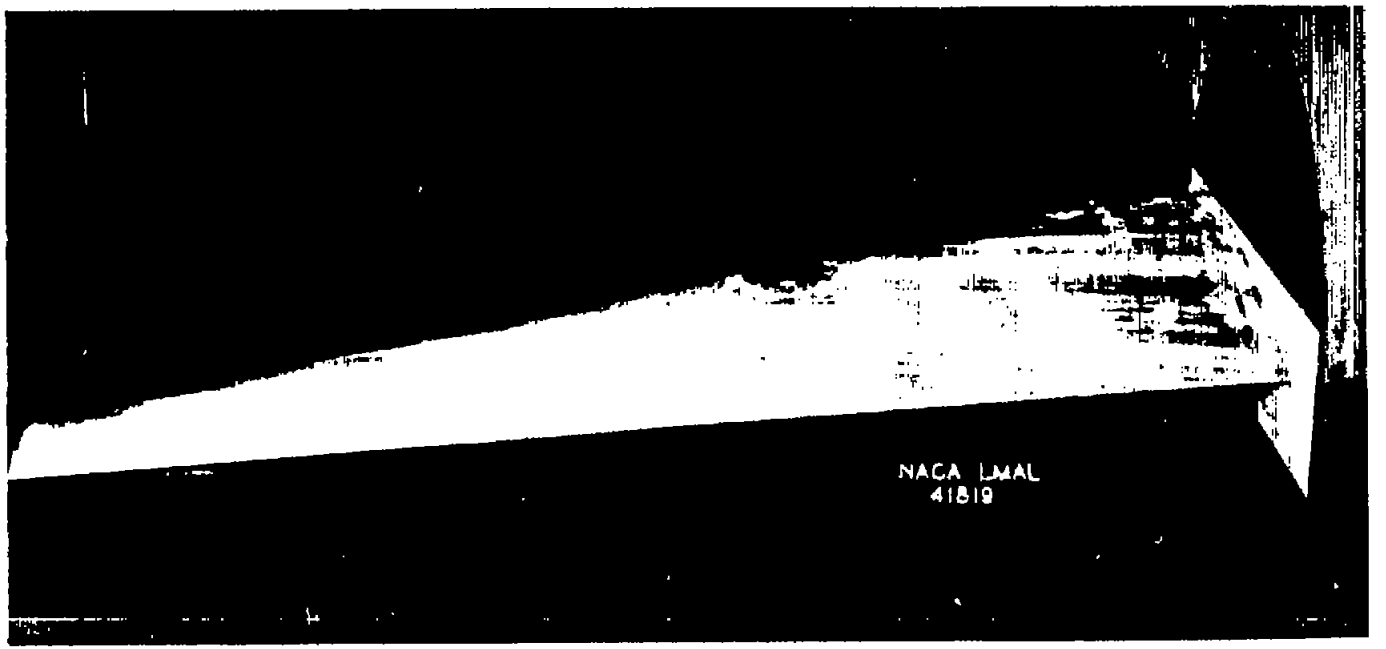

(d) Swept-back wing. Rear view.

Figure 2.- Concluded.

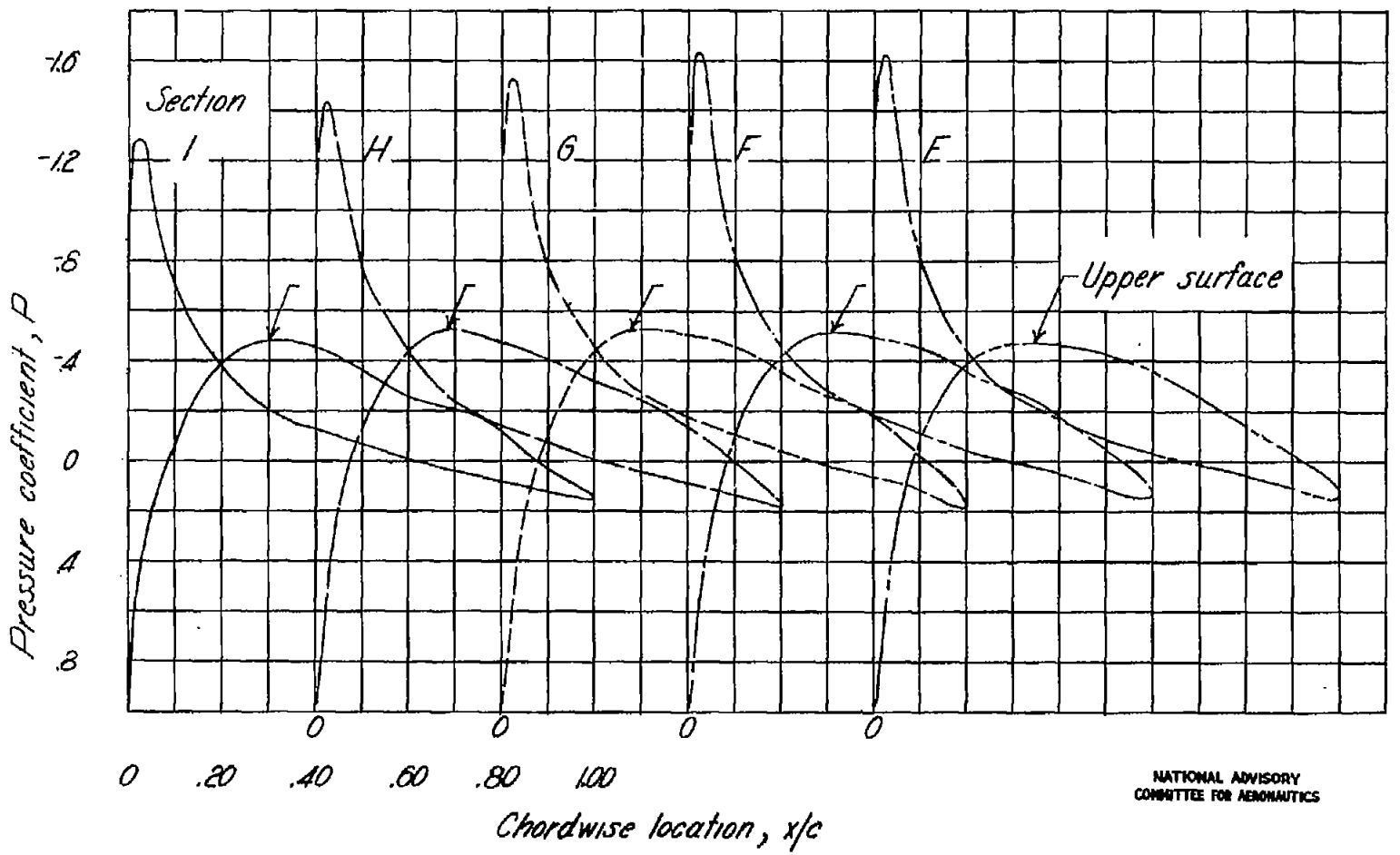

(a) α, -4.1°; q, 98.3 pounds per square foot.

Figure 3.- Measured chordwise pressure distributions over a swept-forward-wing model.

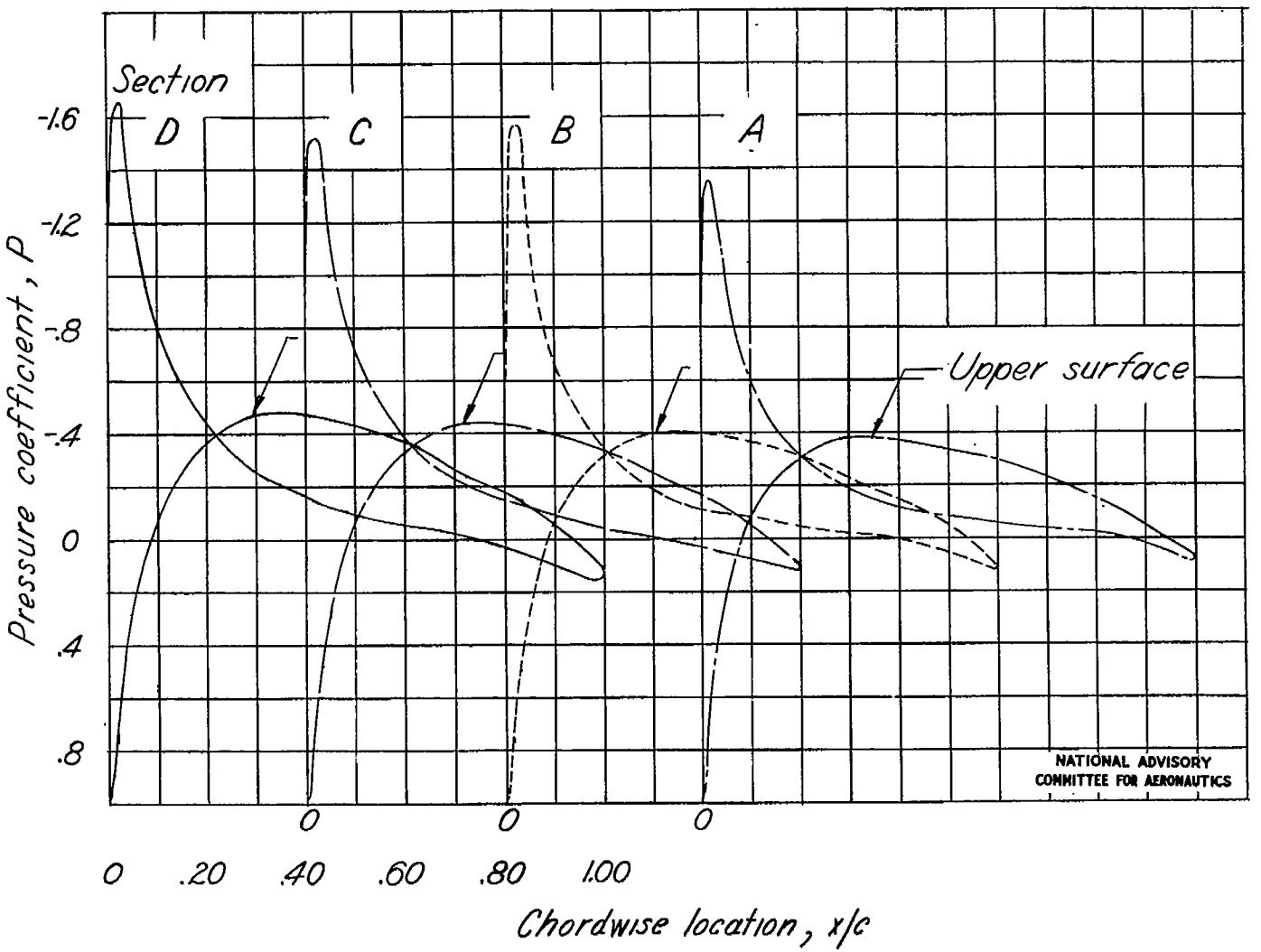

(a) Concluded.

Figure 3.- Continued.

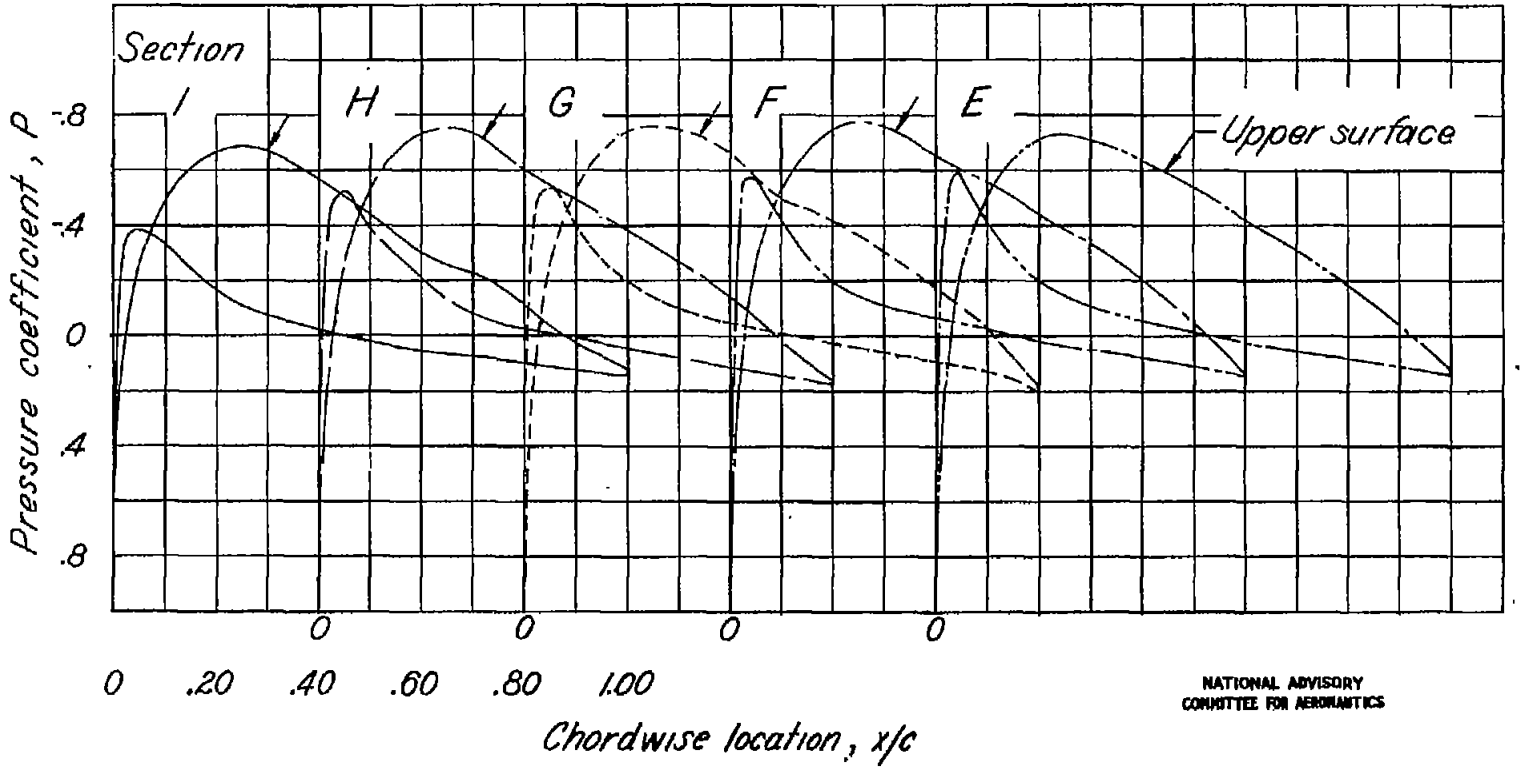

(b) α, 0.5°; q, 98.3 pounds per square foot.

Figure 3.- Continued.

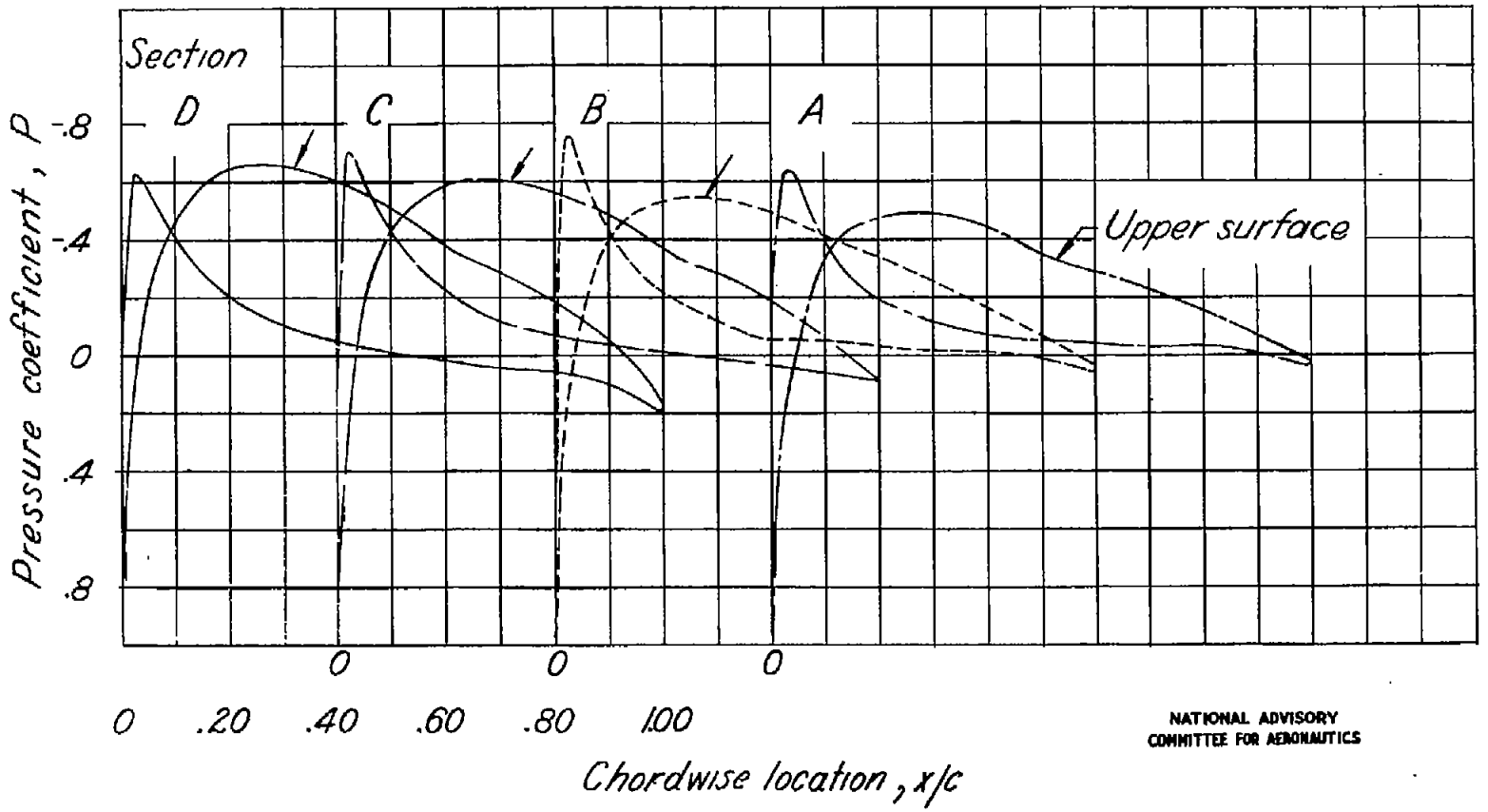

(b) Concluded.

Figure 3.- Continued.

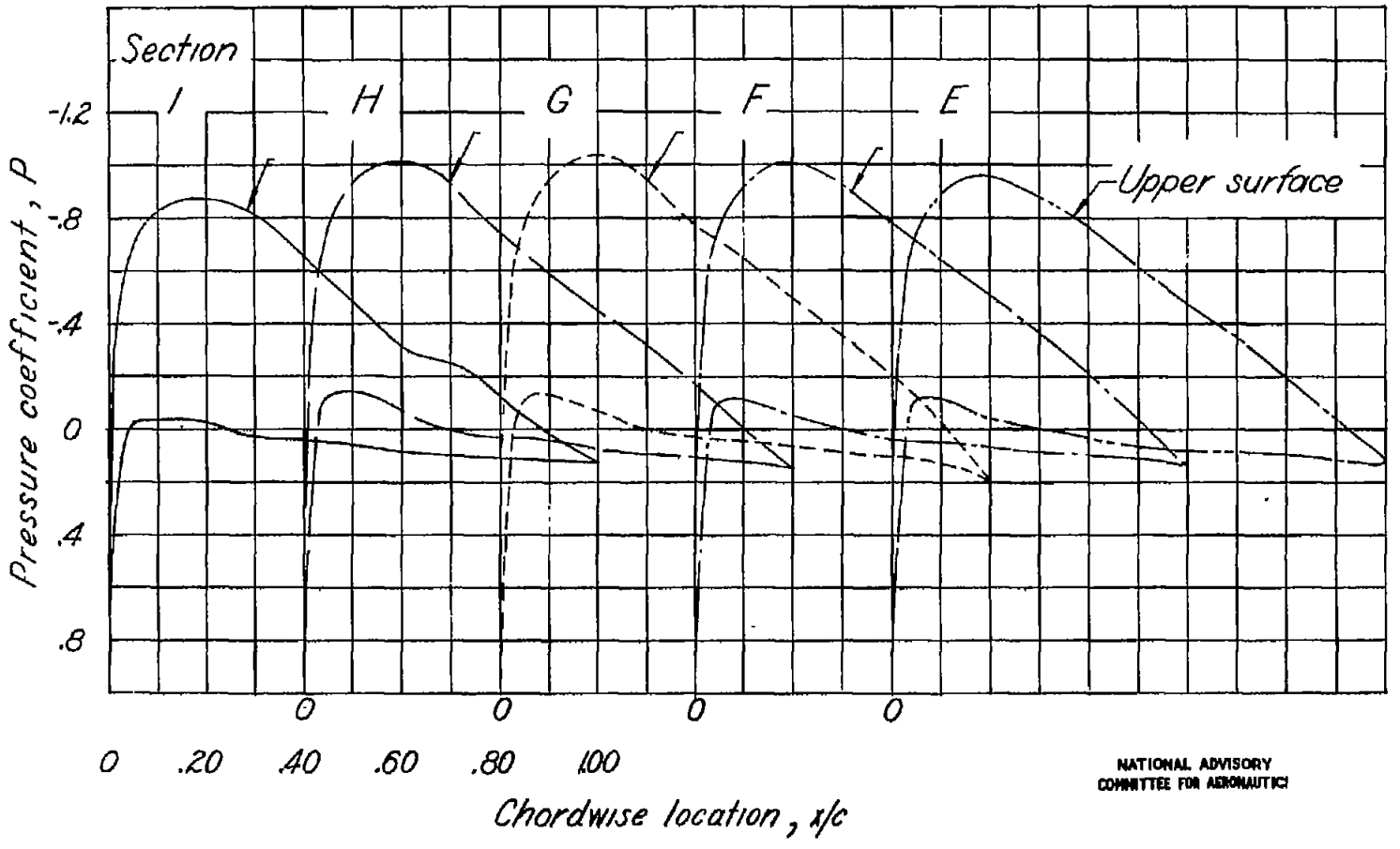

(c) α, 4.0°; q, 98.3 pounds per square foot.

Figure 3.- Continued.

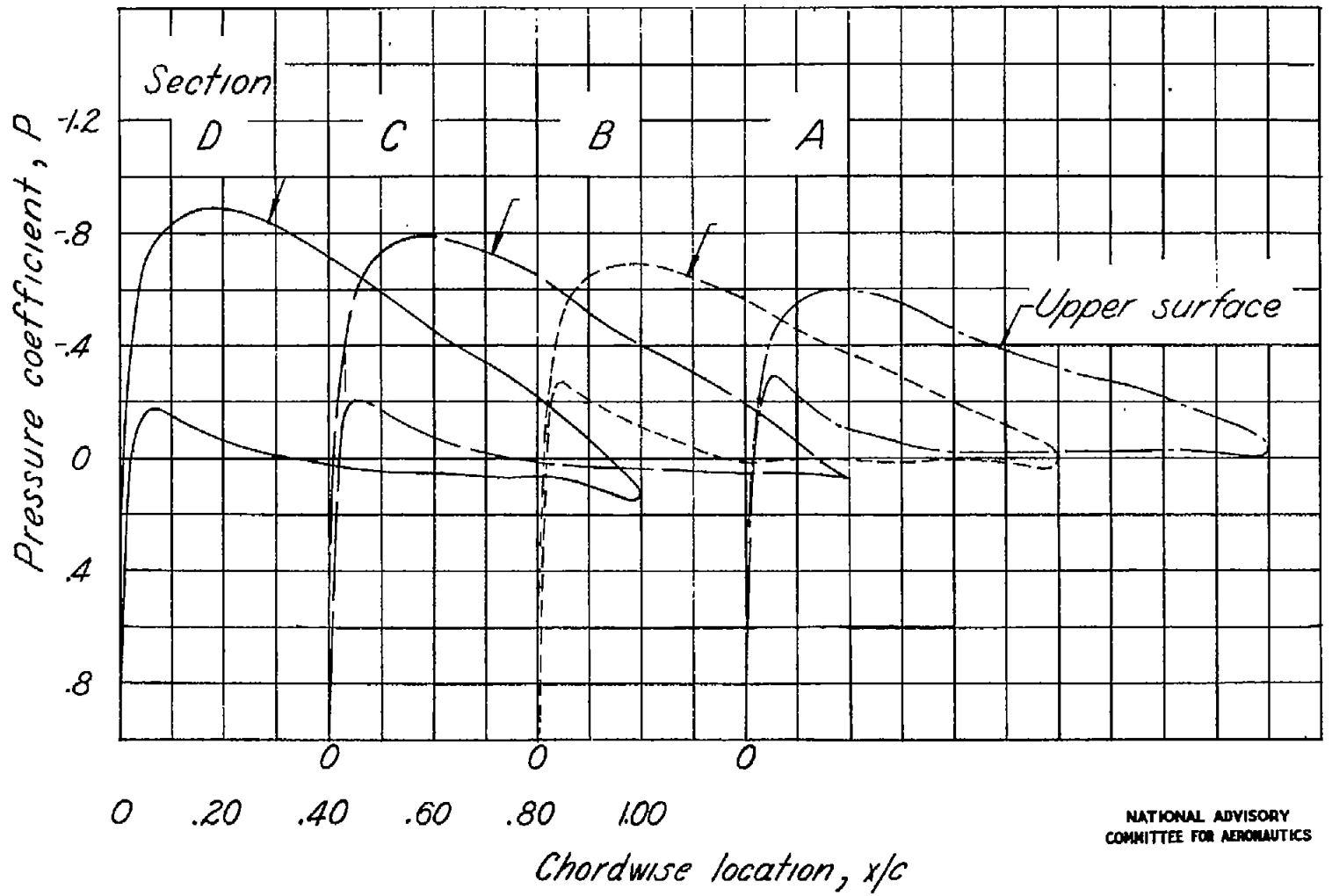

(c) Concluded.

Figure 3.- Continued.

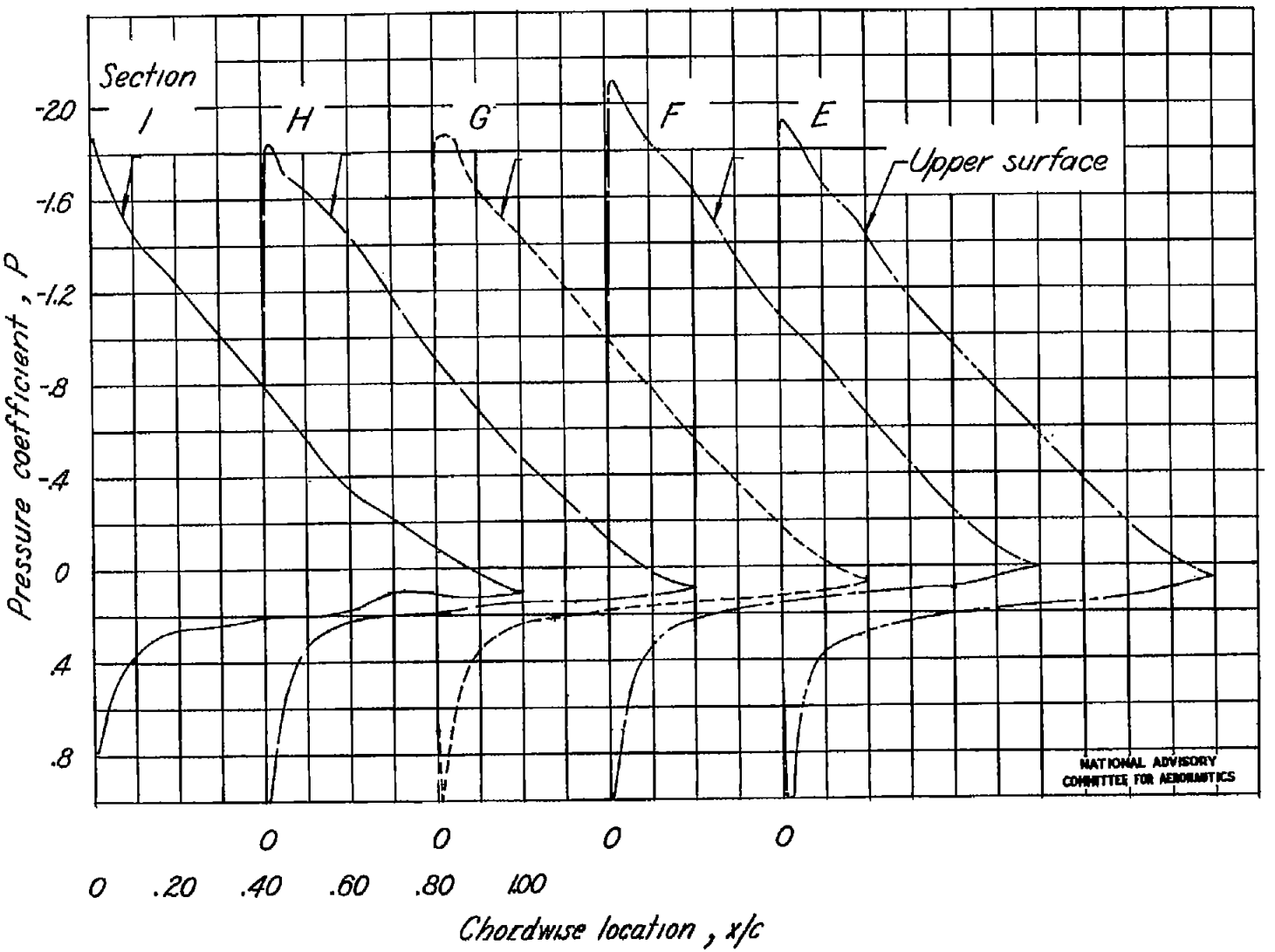

(d) α, 10.9°; q, 39.7 pounds per square foot.

Figure 3.- Continued.

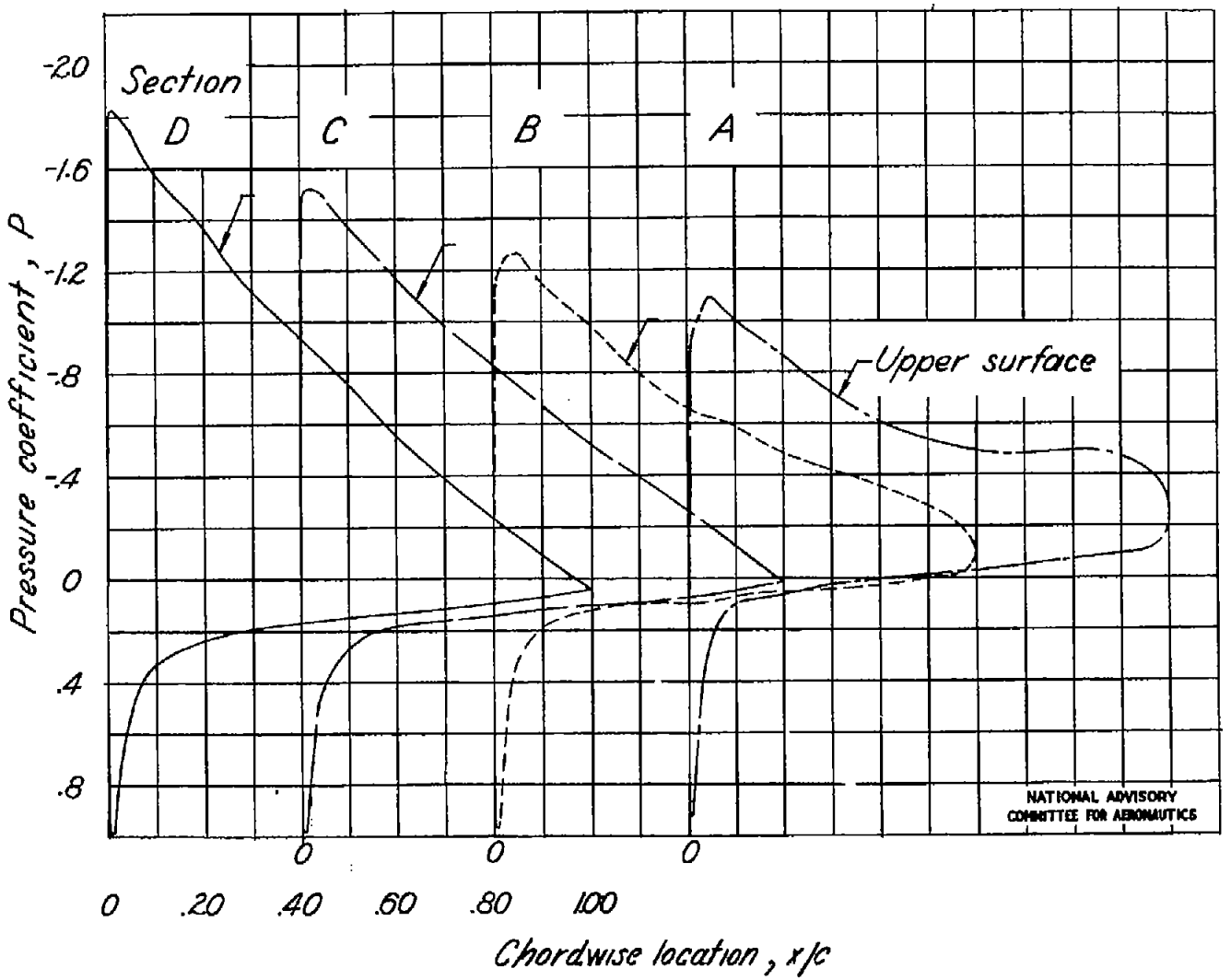

(d) Concluded.

Figure 3.- Continued.

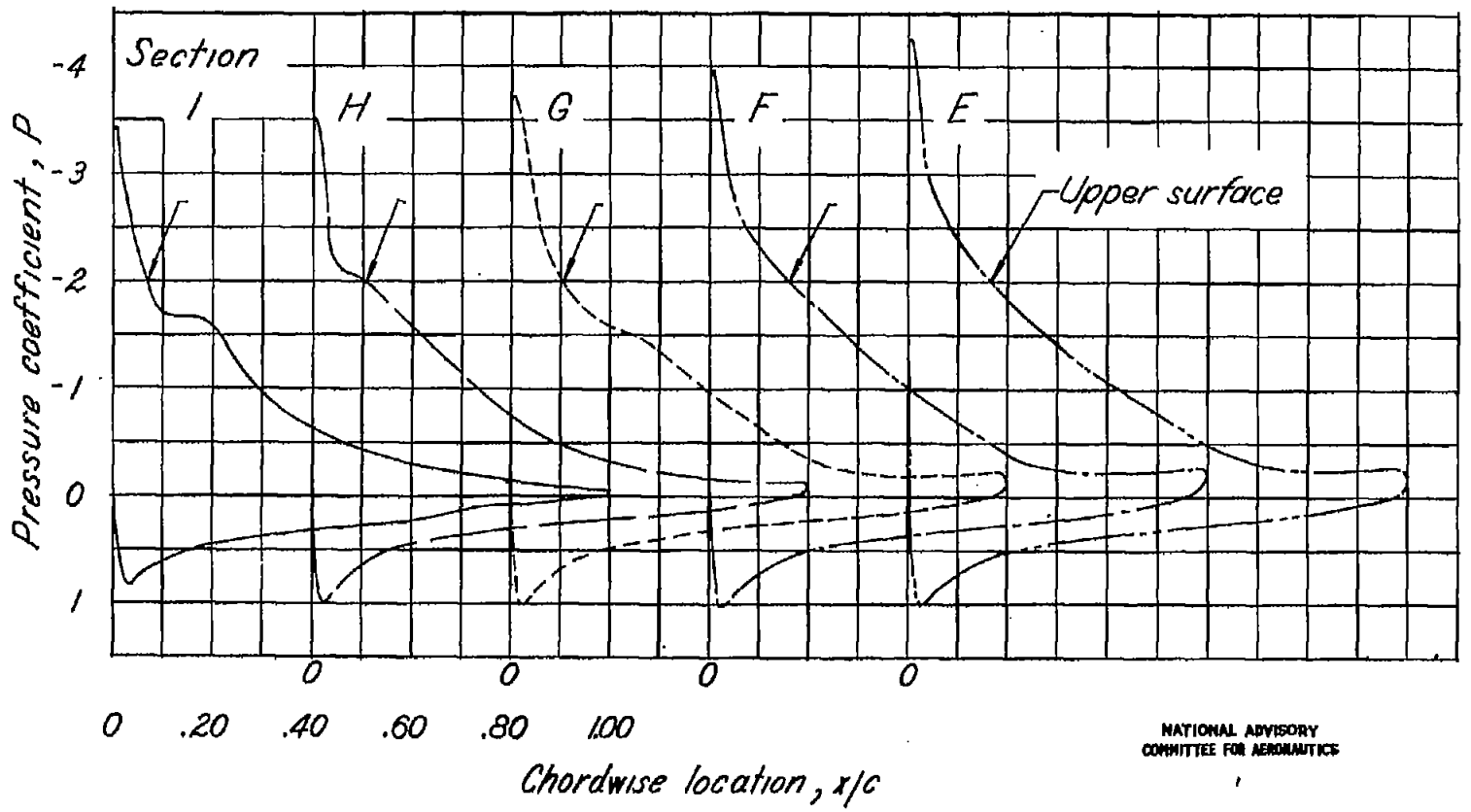

(e) α, 17.2°; q, 39.7 pounds per square foot.

Figure 3.- Continued.

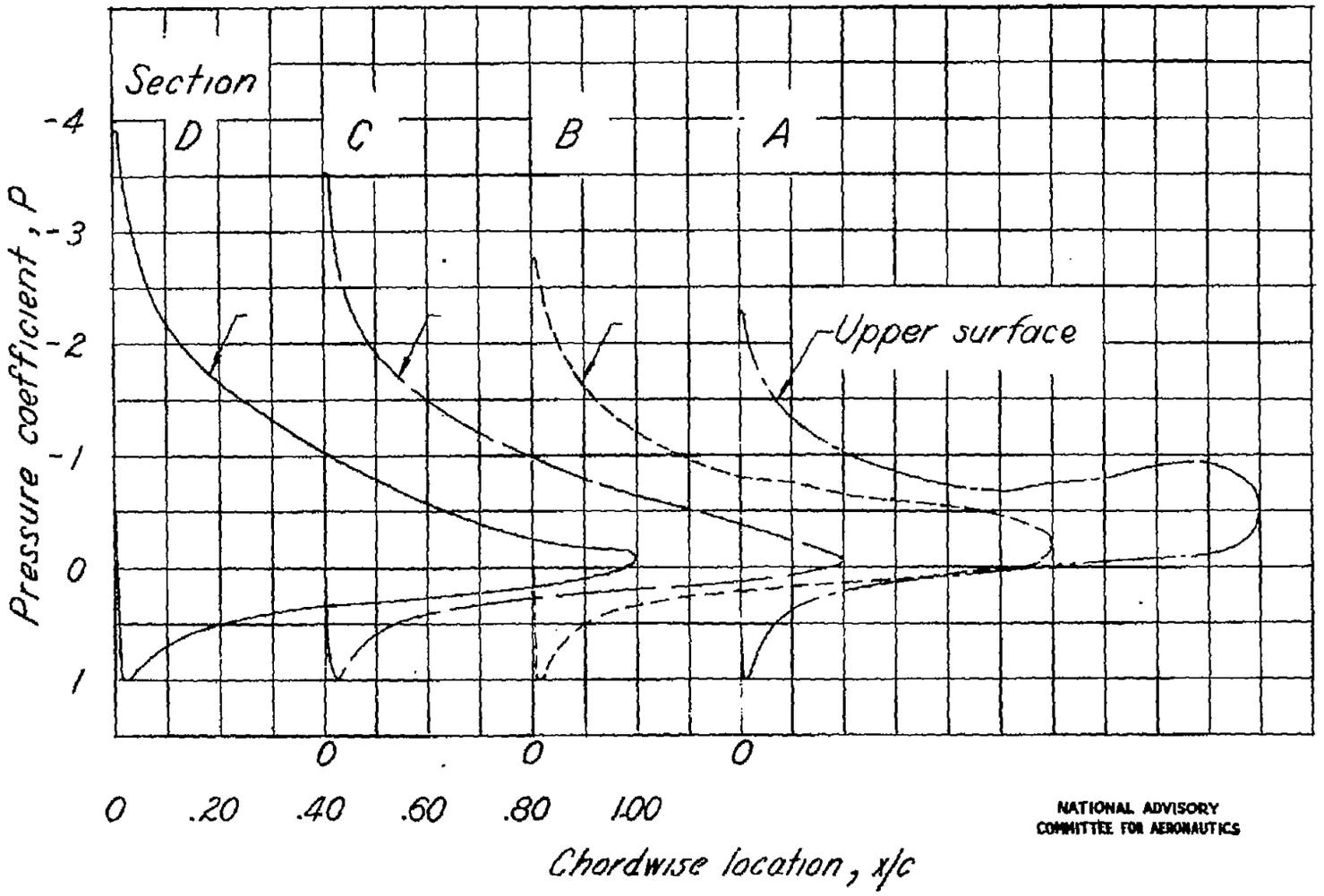

(e) Concluded.

Figure 3.- Concluded.

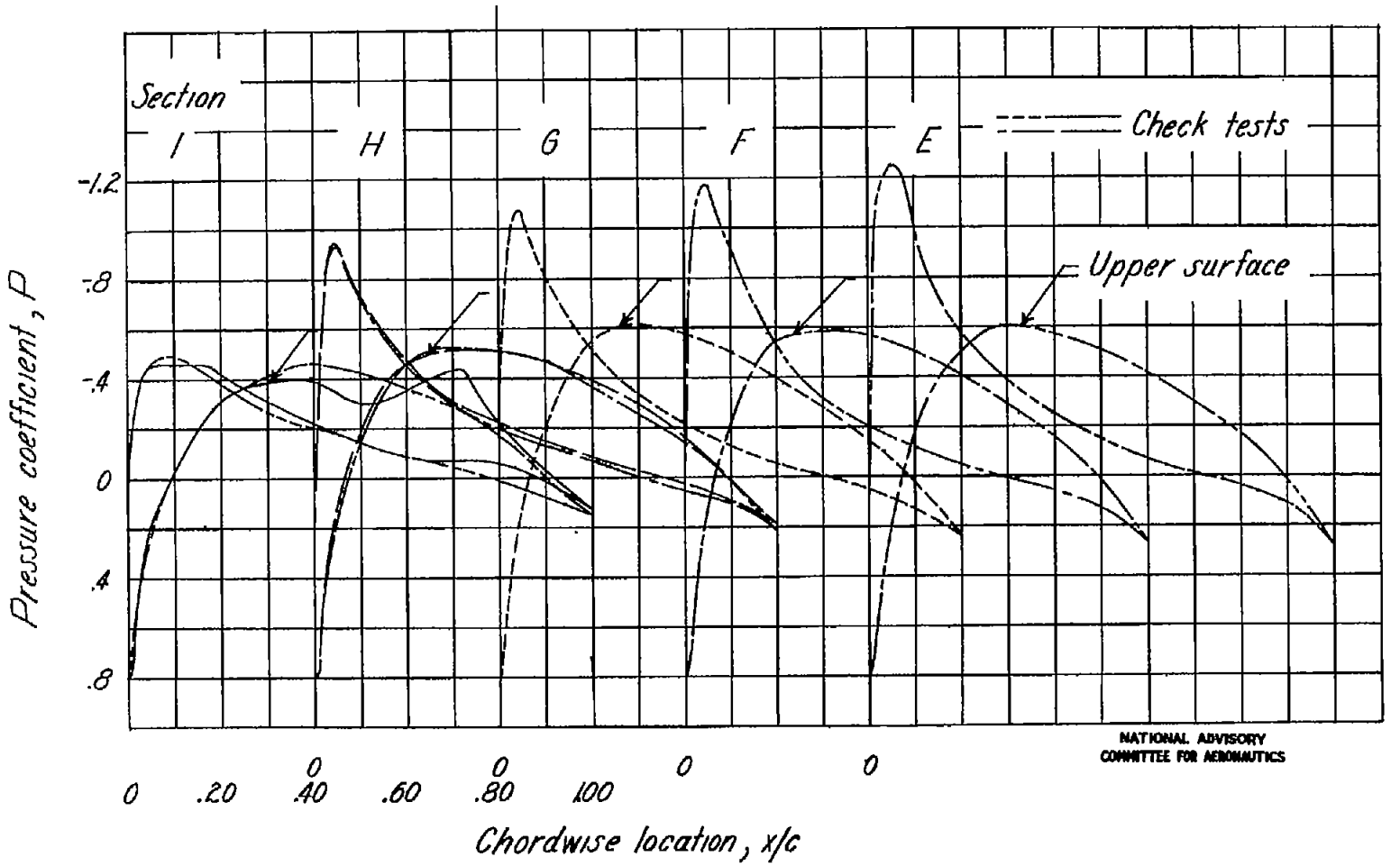

(a) α, -3.0°; q, 98.3 pounds per square foot.

Figure 4.- Measured chordwise pressure distributions over swept-back-wing model.

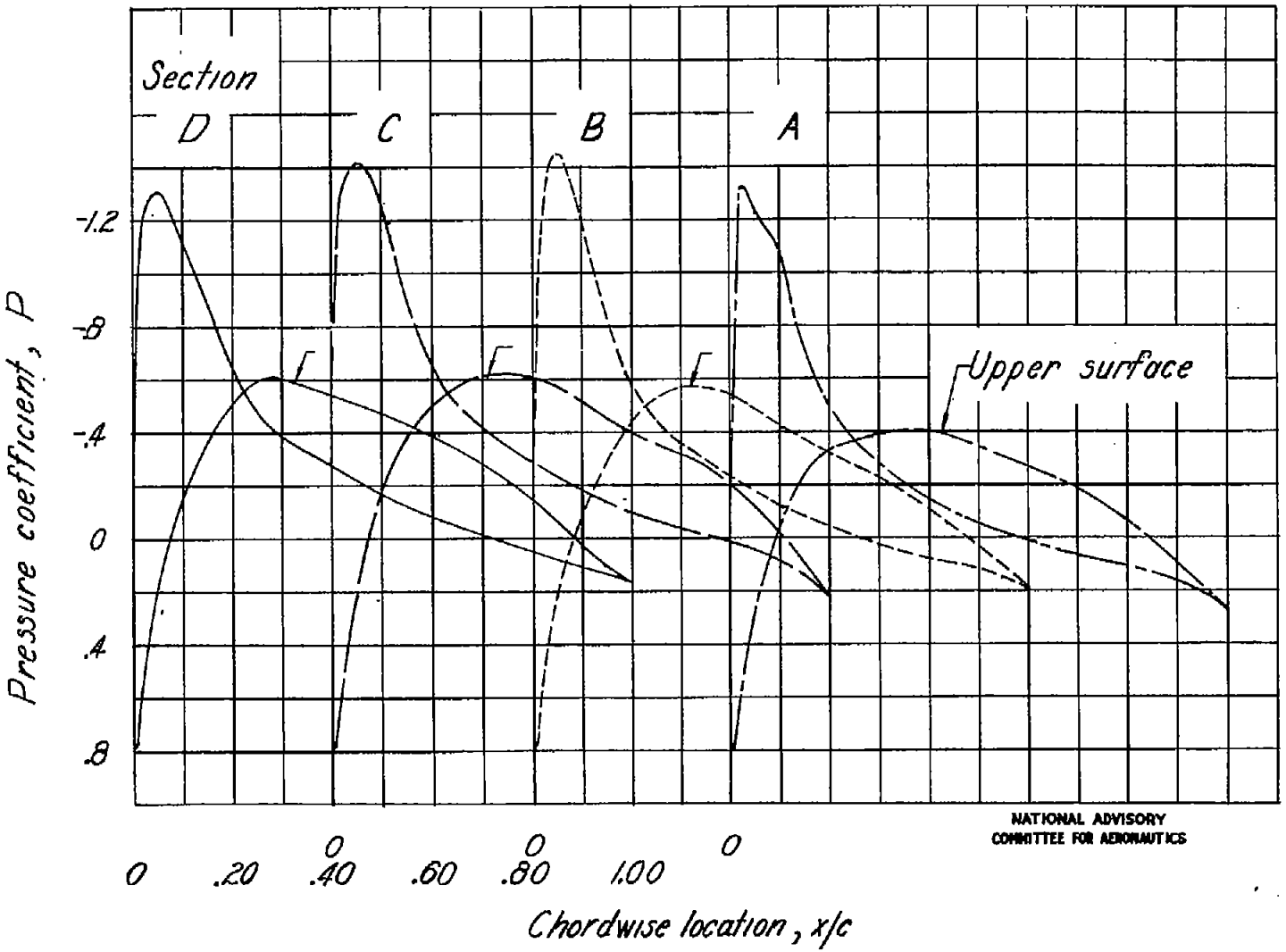

(a) Concluded.

Figure 4.- Continued.

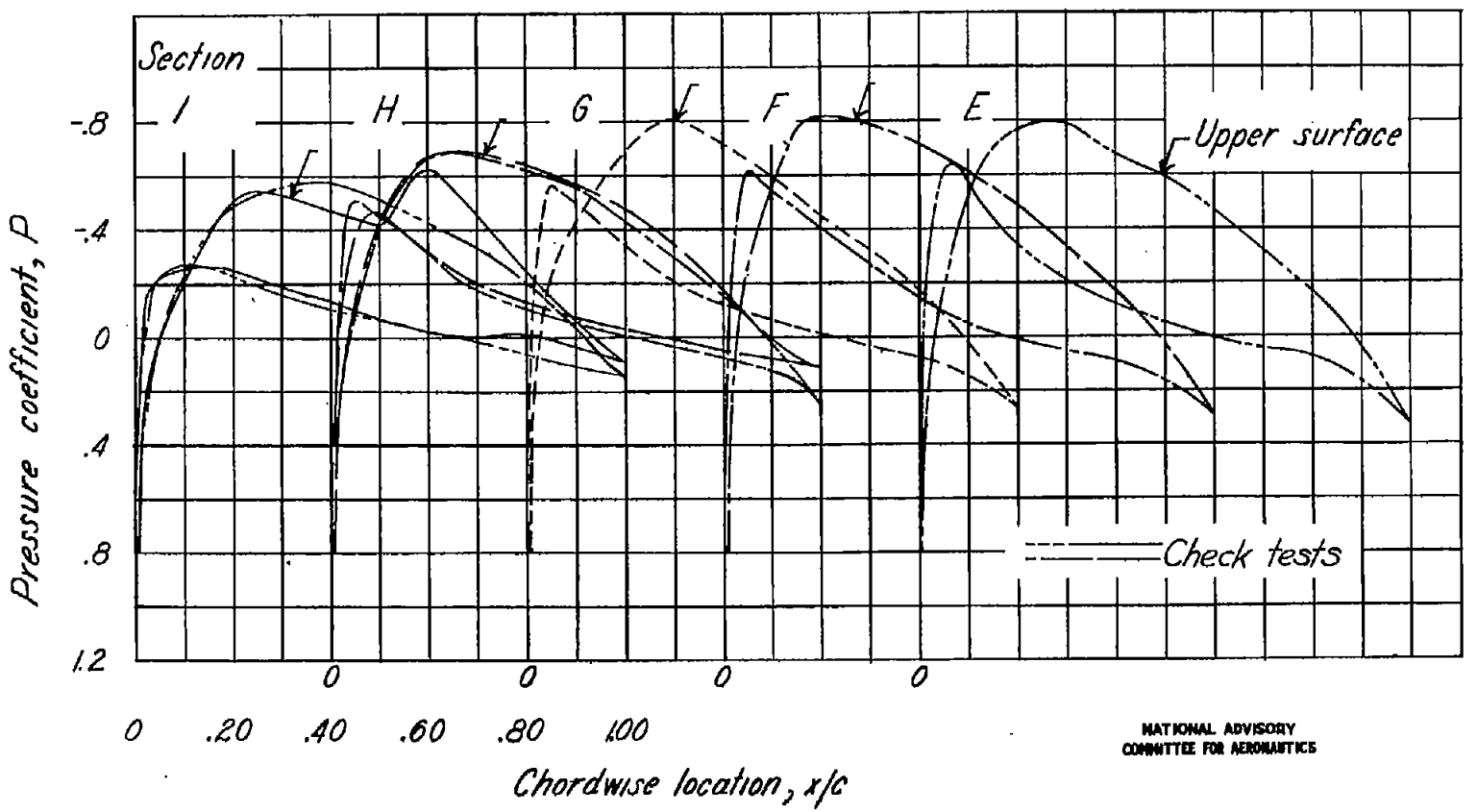

(b) α, 0.2°; q, 98.3 pounds per square foot.

Figure 4.- Continued.

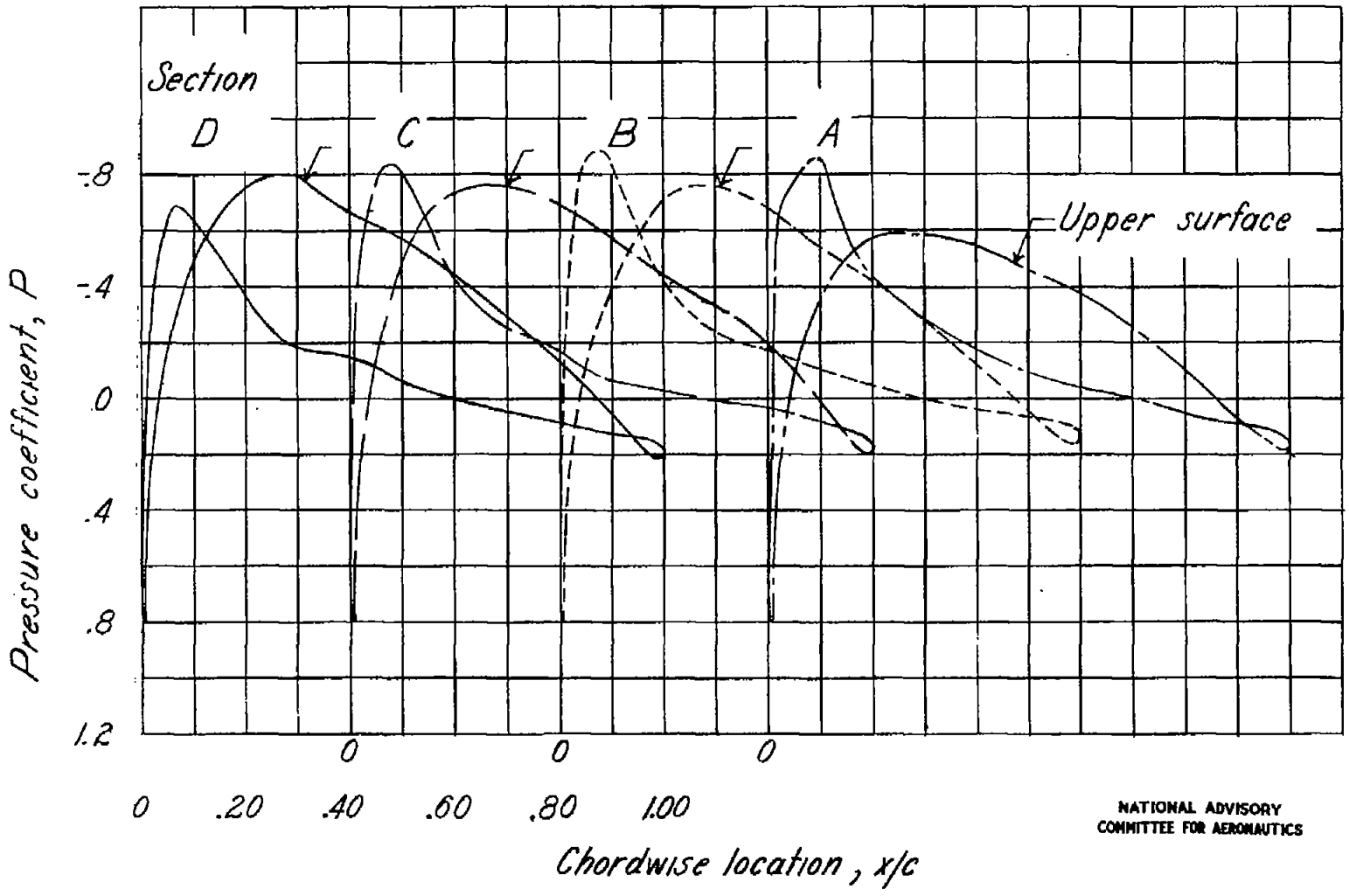

(b) Concluded.

Figure 4.- Continued.

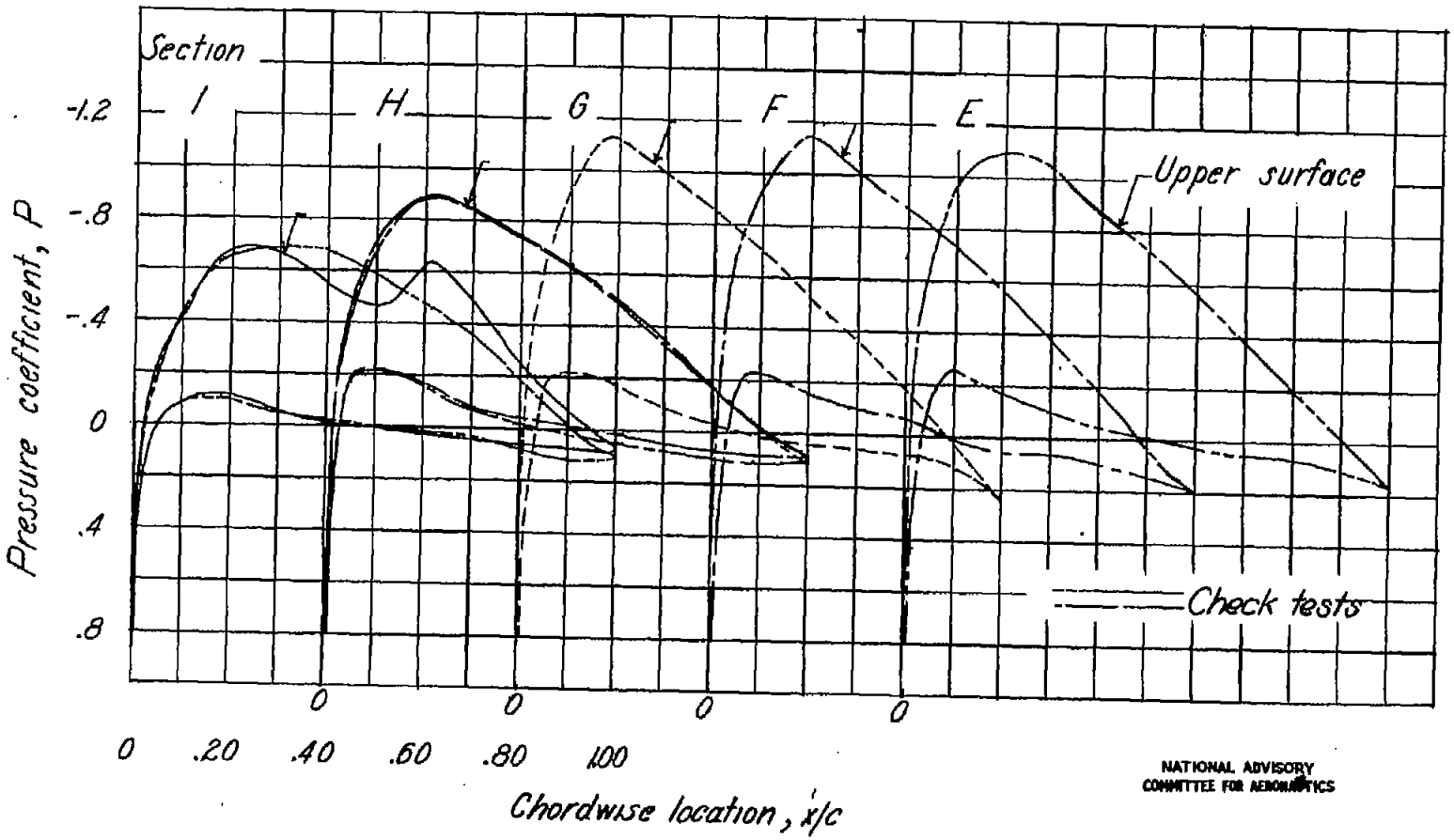

(c) α, 3.4°; q, 98.3 pounds per square foot.

Figure 4.- Continued.

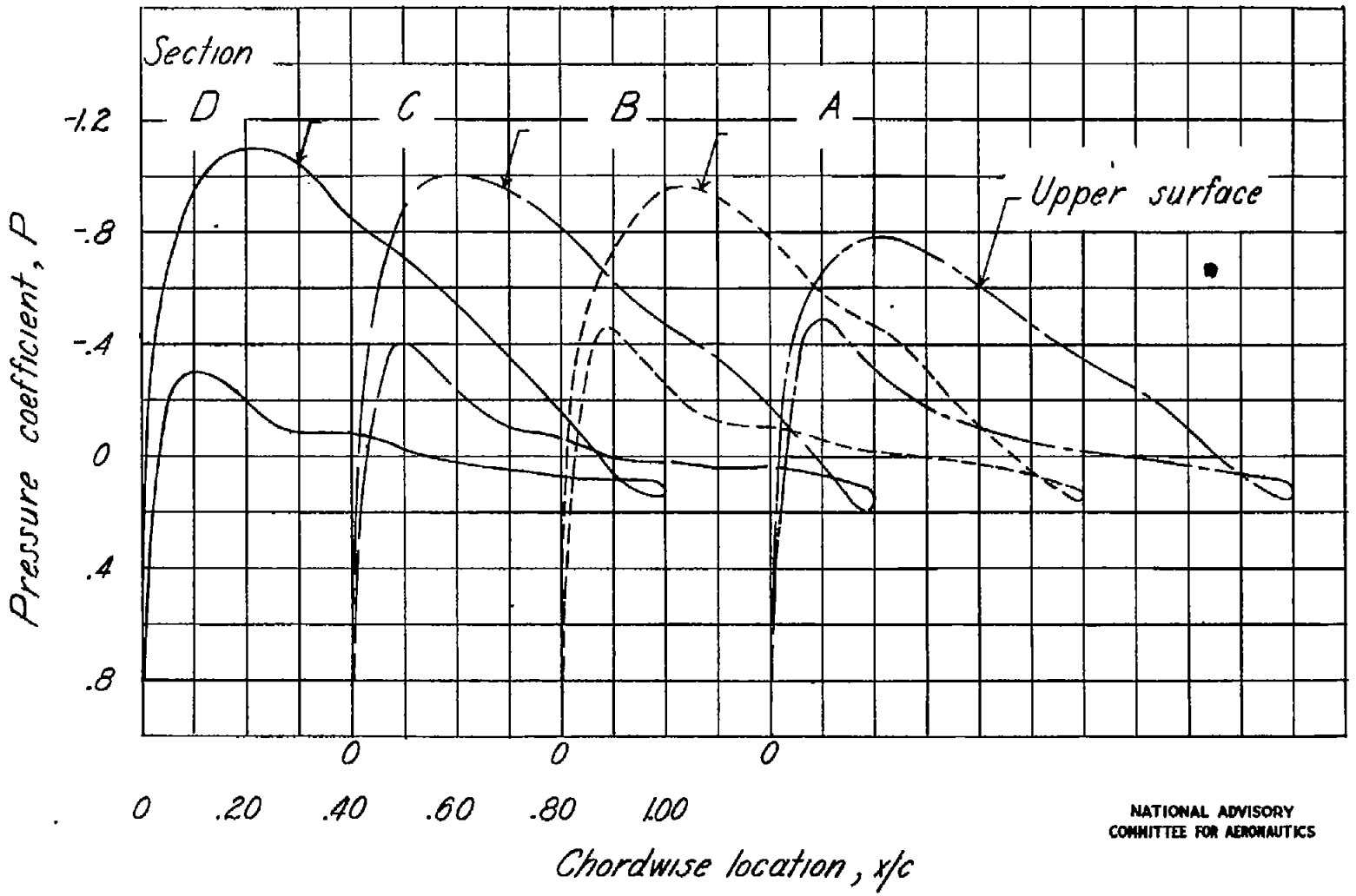

(c) Concluded.

Figure 4.- Continued.

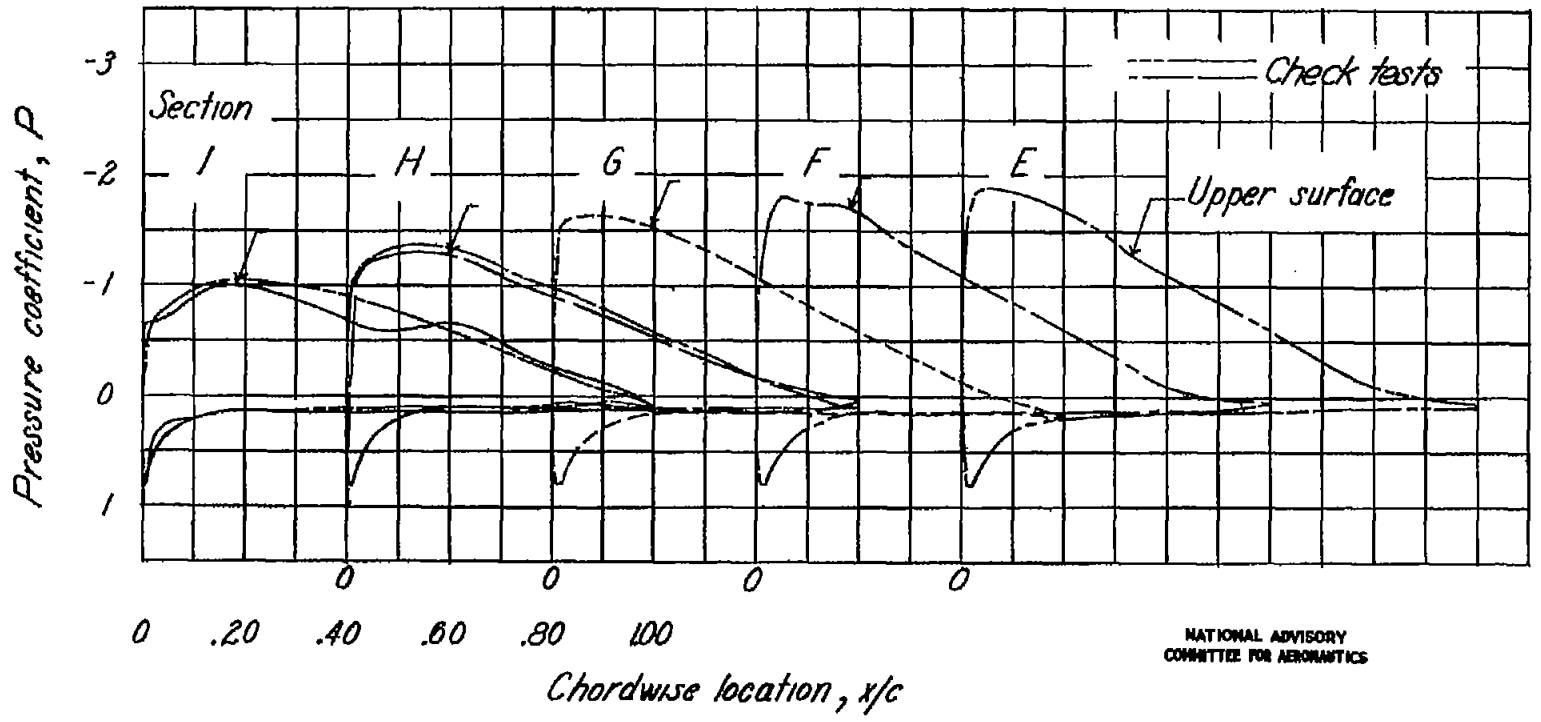

(d) α, 9.8; q, 39.7 pounds per square foot.

Figure 4.- Continued.

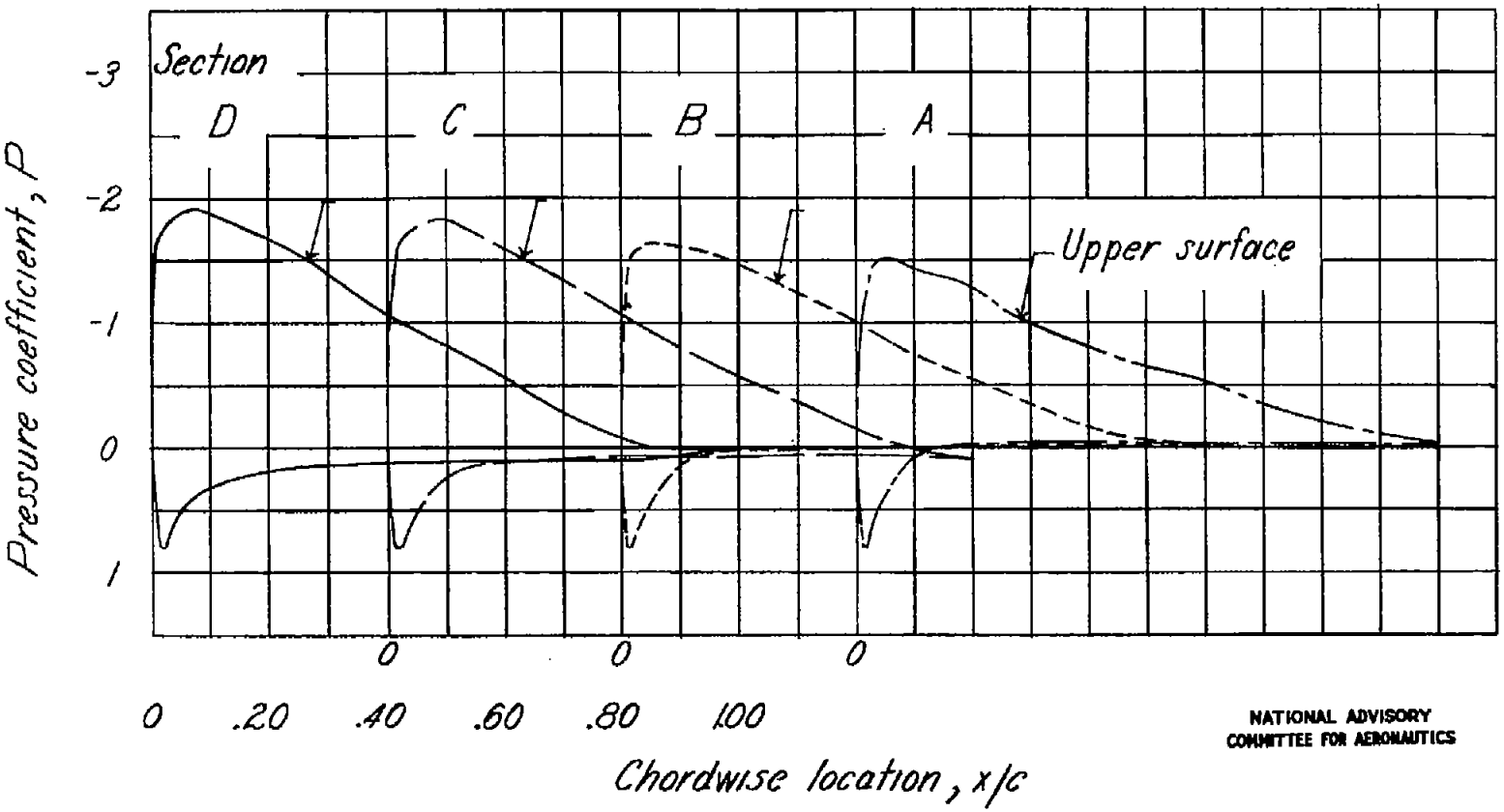

(d) Concluded.

Figure 4.- Continued.

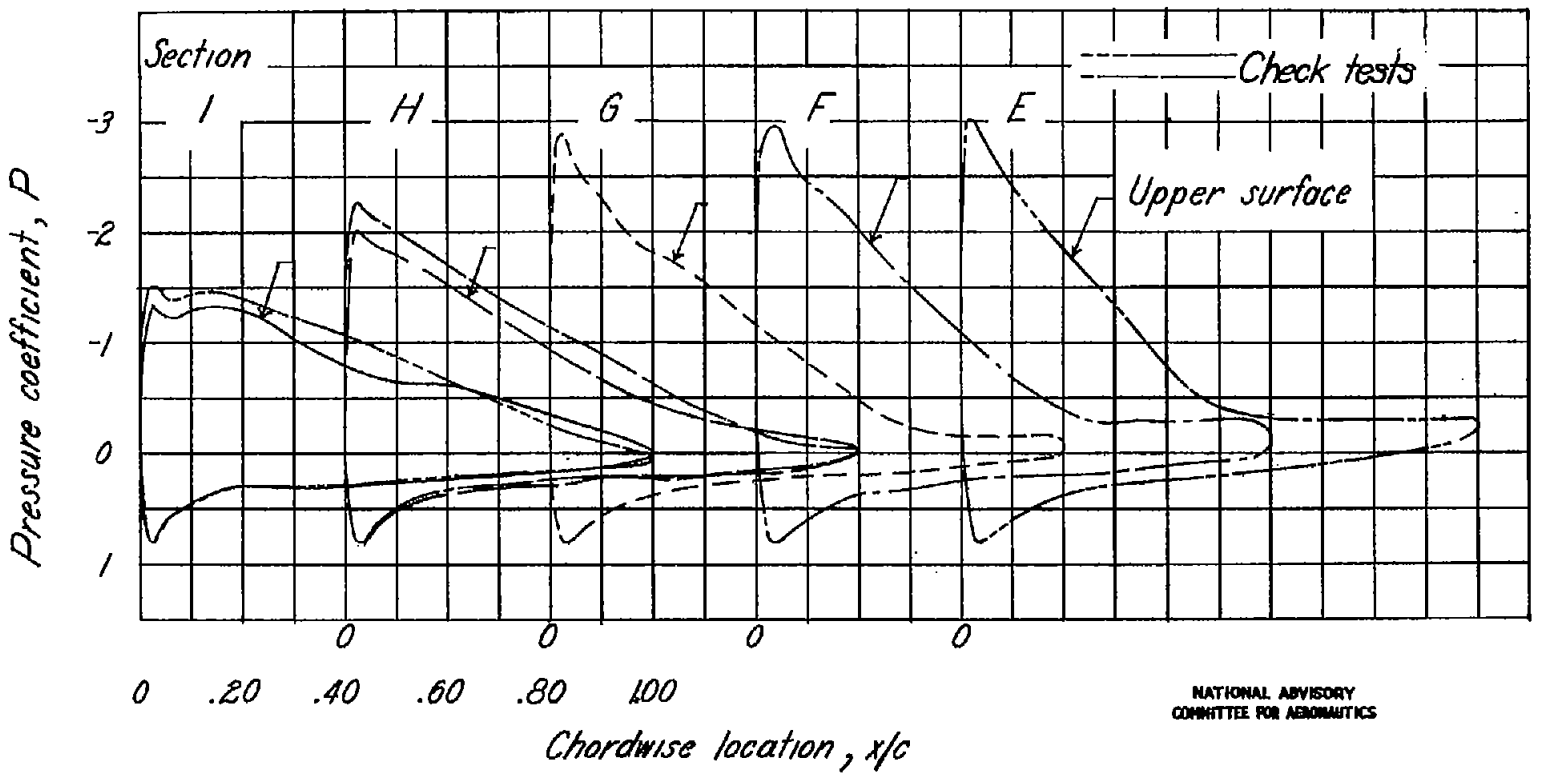

(e) α, 16.3°; q, 39.7 pounds per square foot.

Figure 4.- Continued.

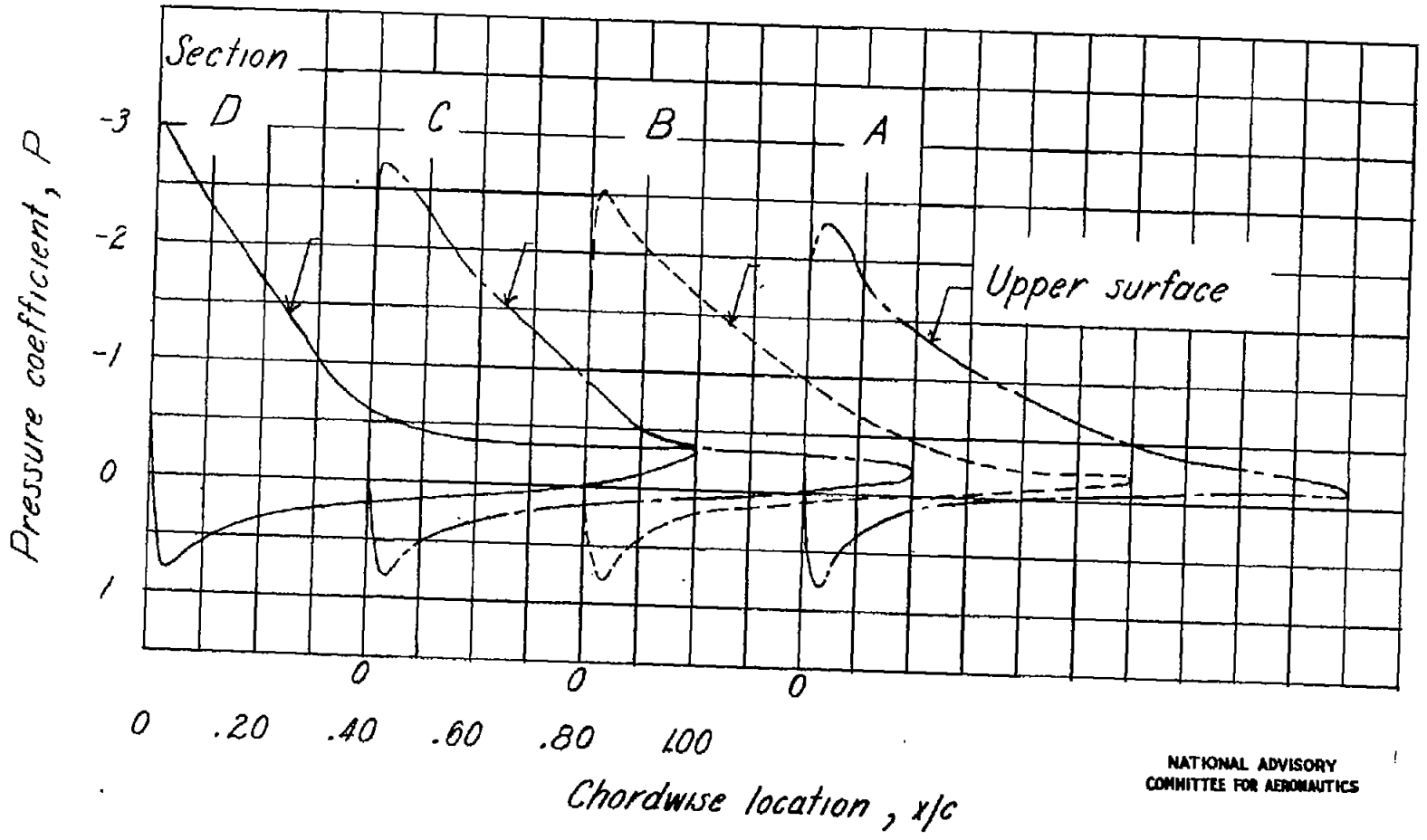

(e) Concluded.

Figure 4.- Continued.

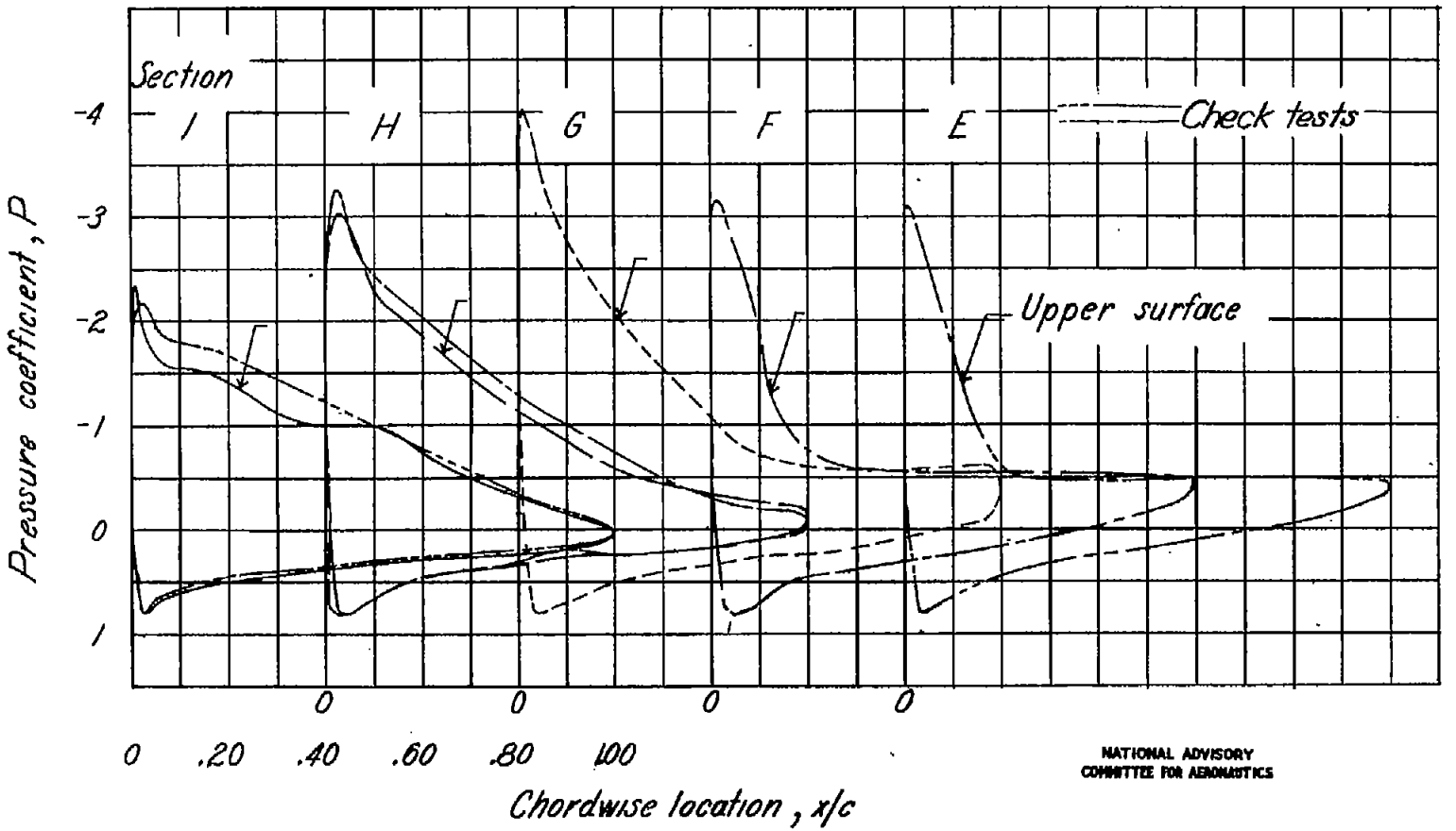

(f) α, 21.4°; q, 39.7 pounds per square foot.

Figure 4.- Continued.

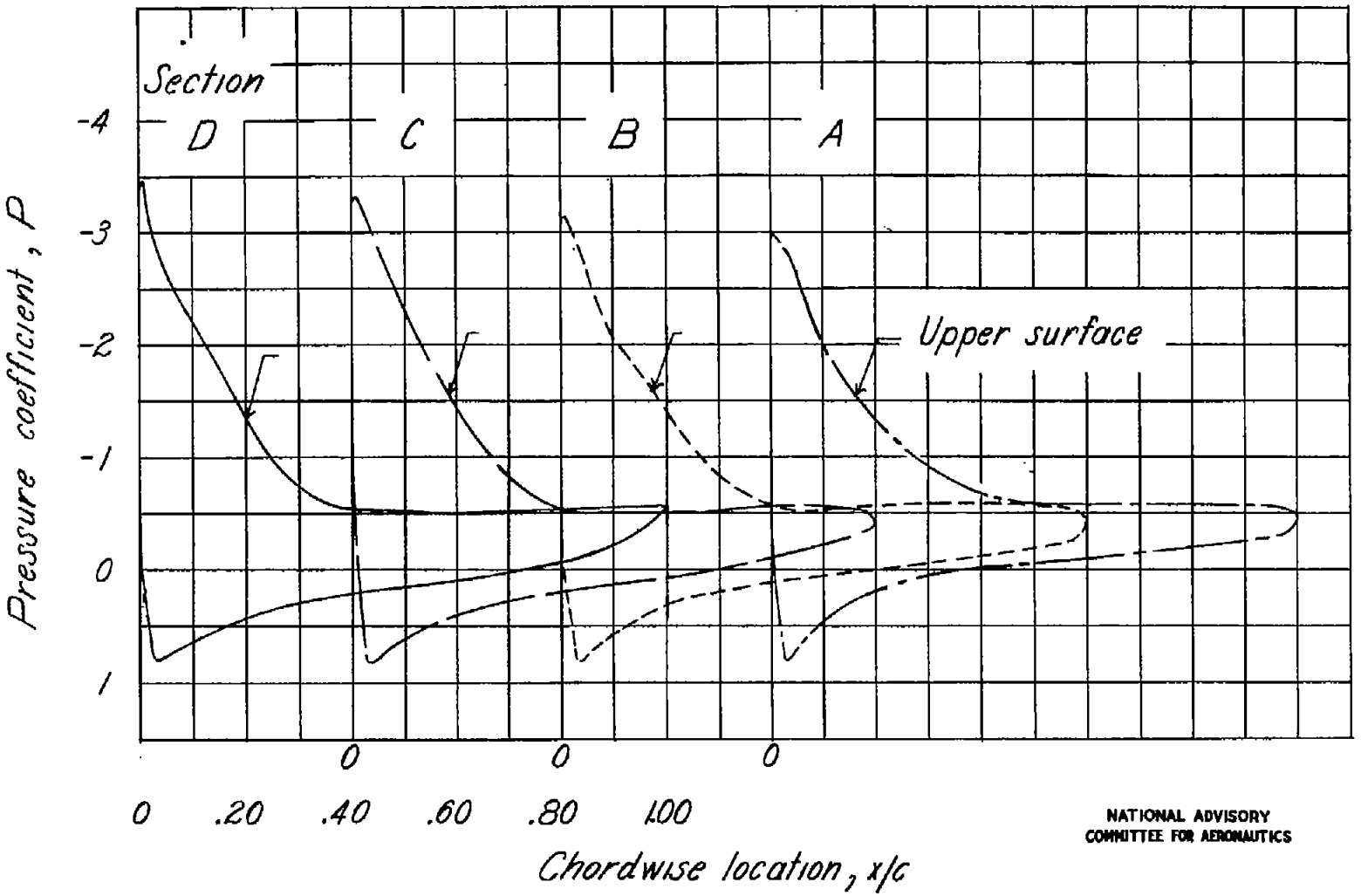

(f) Concluded.

Figure 4.- Concluded.

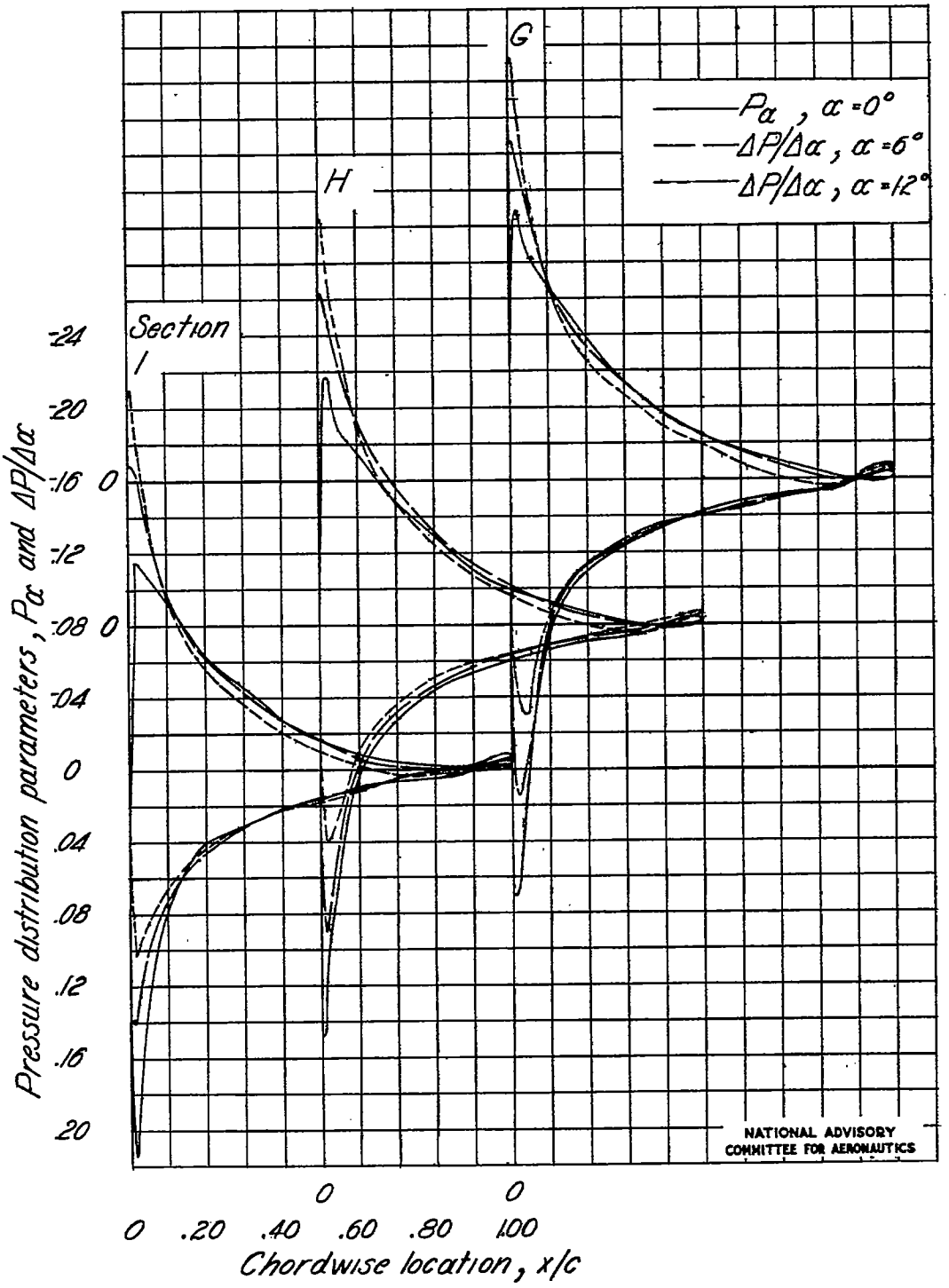

(a) Variation of P_α and $\Delta P/\Delta\alpha$ with chord.

Figure 5.- Curves for determining pressure distribution over the swept-forward wing tested.

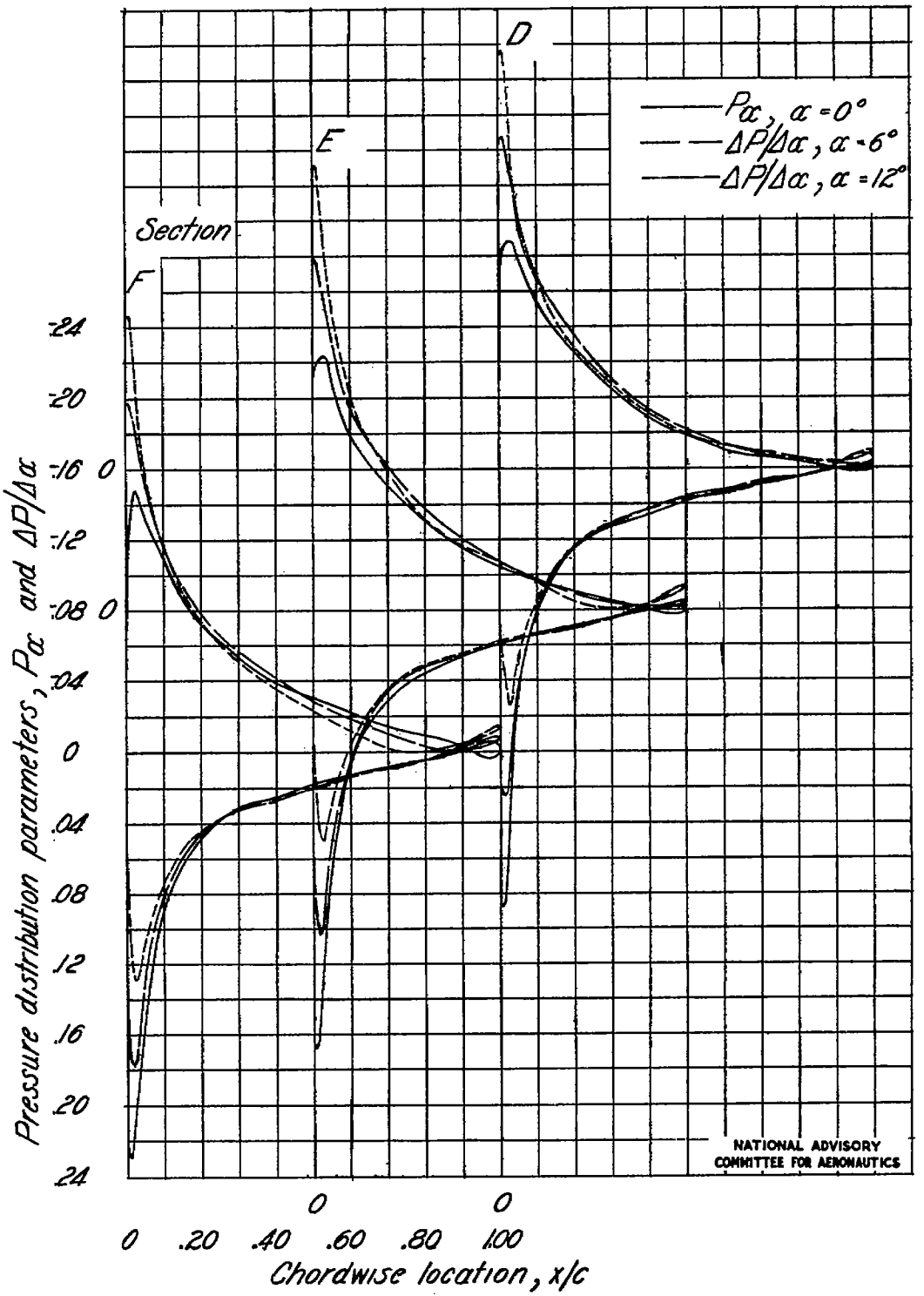

(a) Continued.

Figure 5.- Continued

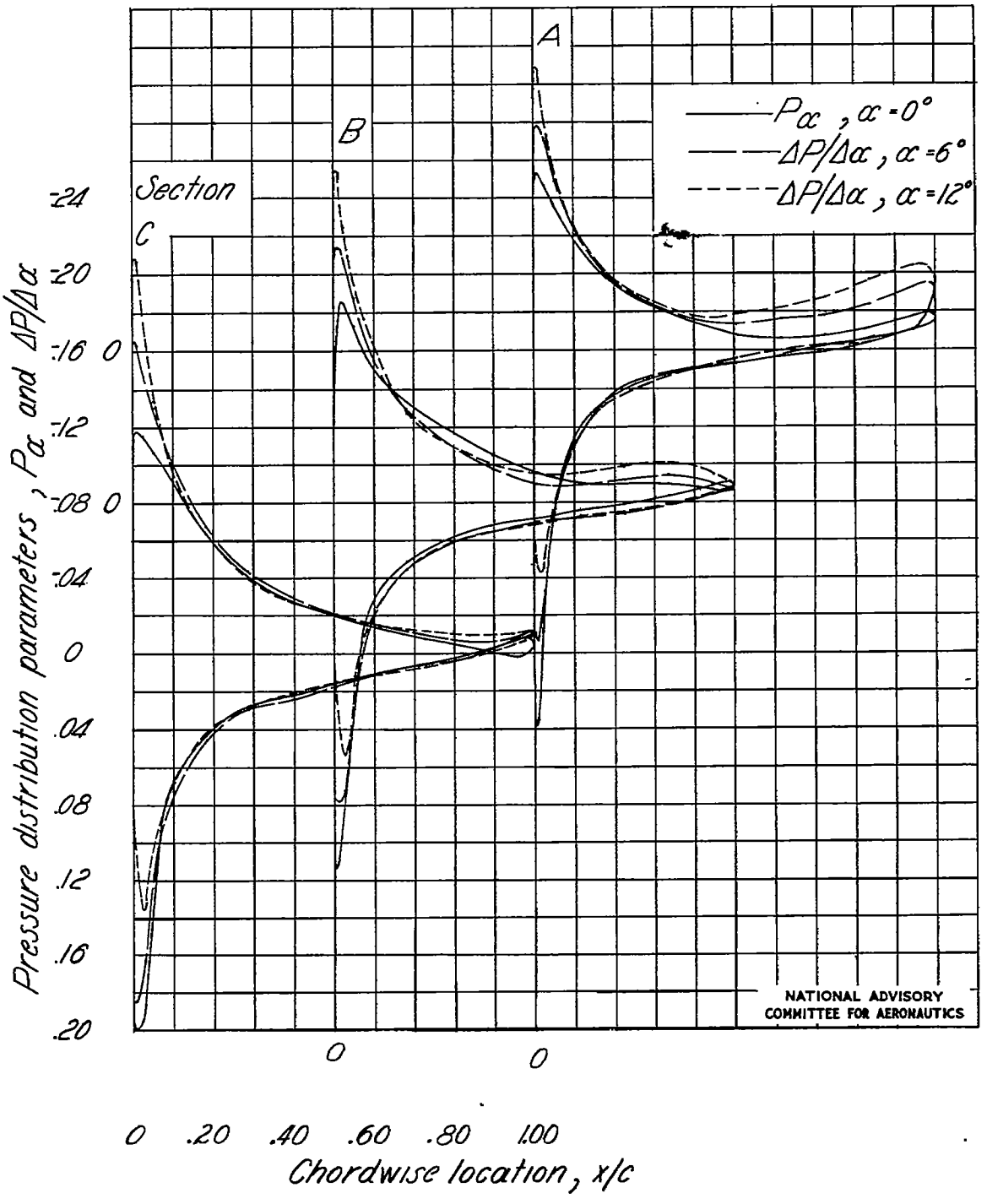

(a) Concluded.

Figure 5.- Continued.

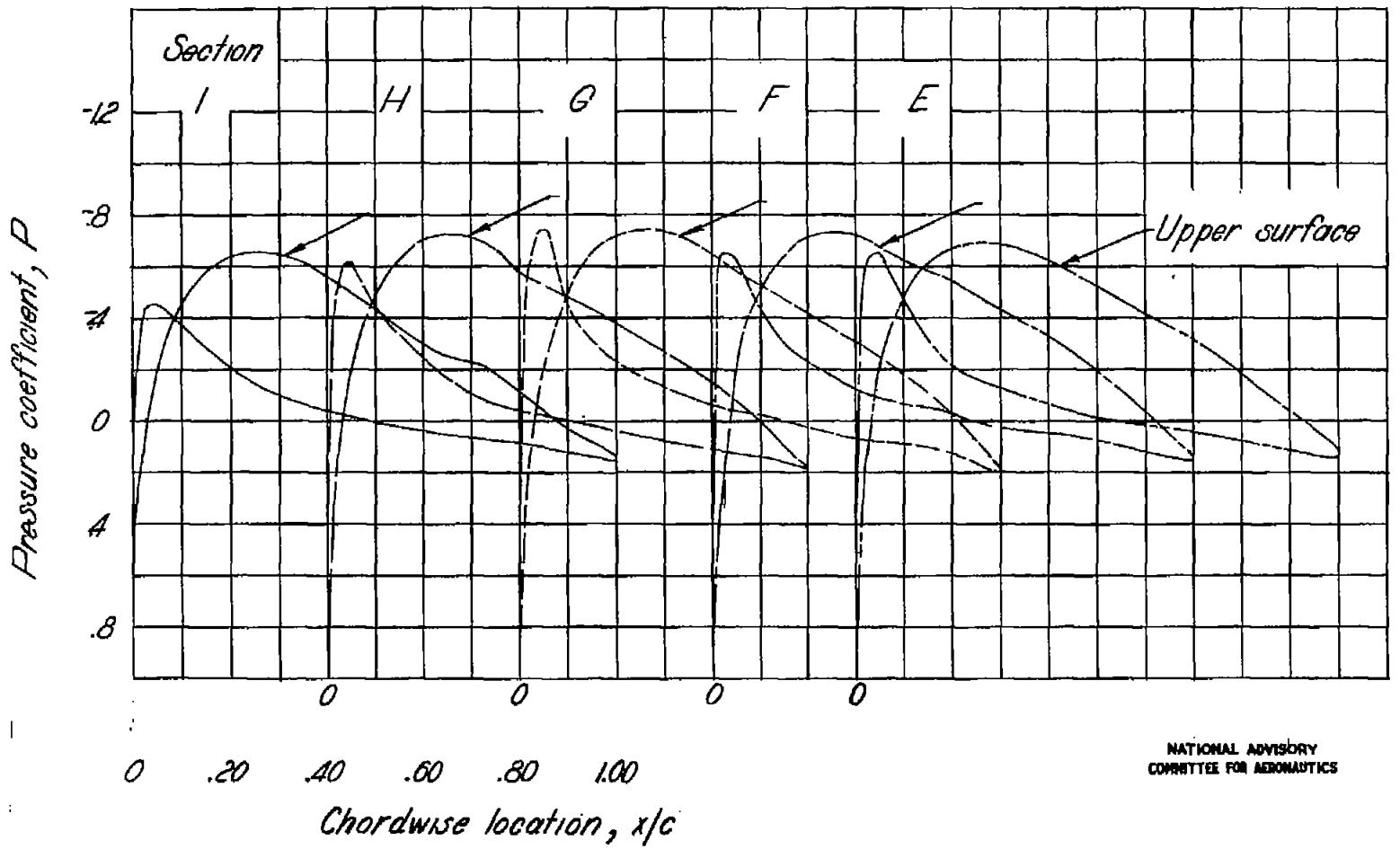

(b) Chordwise pressure distribution for $\alpha = 0^{\circ}$.

Figure 5.- Continued.

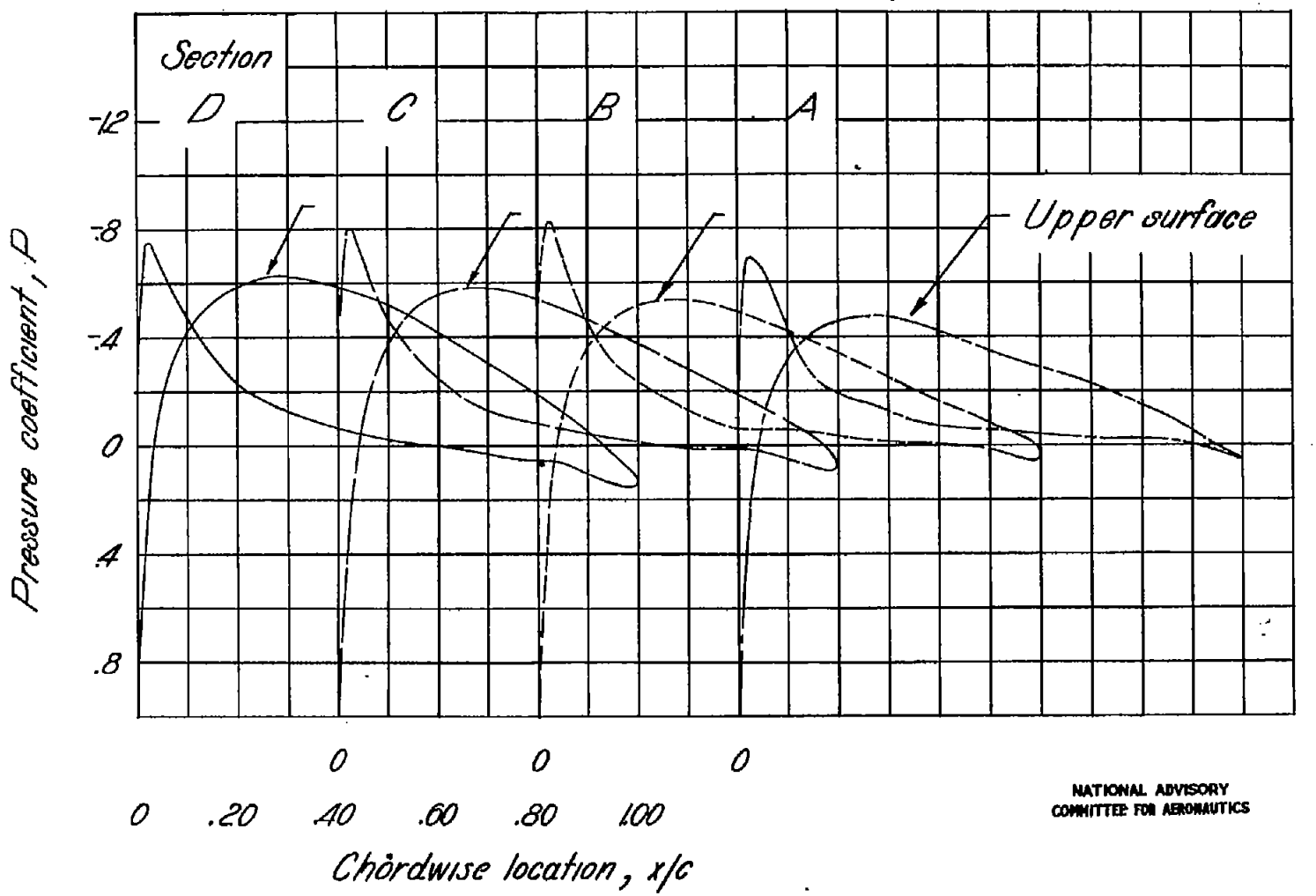

(b) Concluded.

Figure 5.- Concluded.

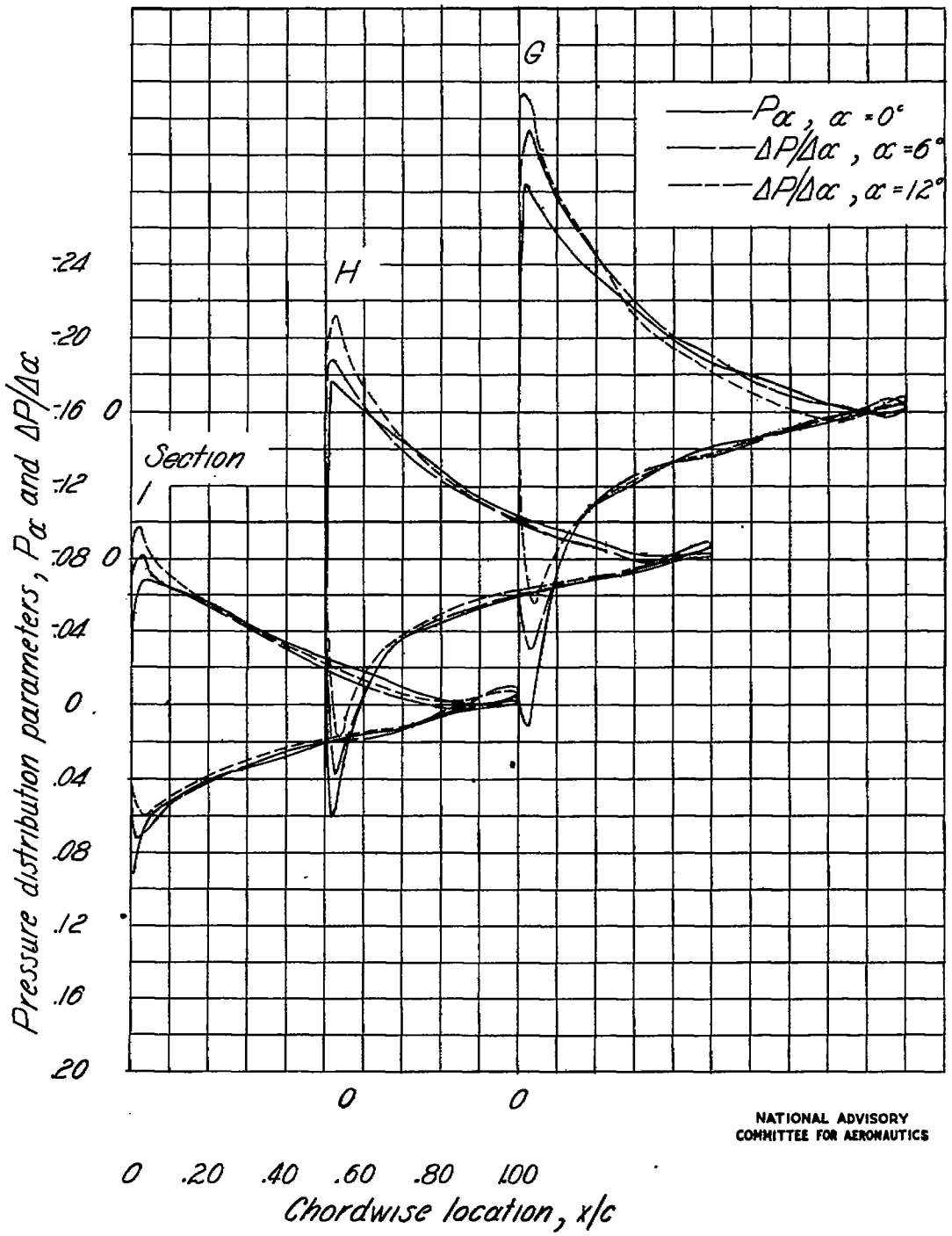

(a) Variation of P_α and $\Delta P/\Delta\alpha$ with chord.

Figure 6.- Curves for determining pressure distribution over the swept-back wing tested.

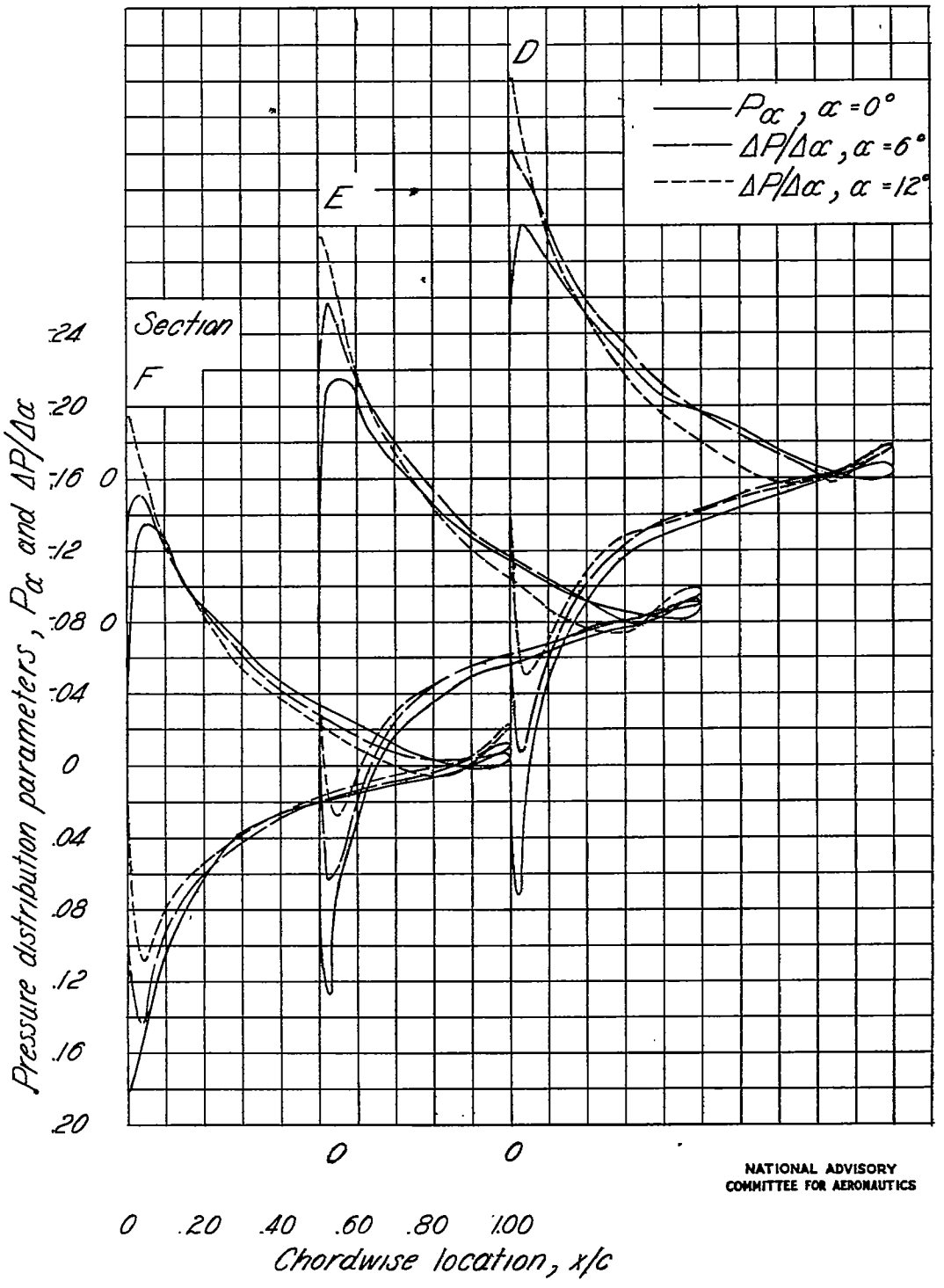

(a) Continued.

Figure 6.- Continued.

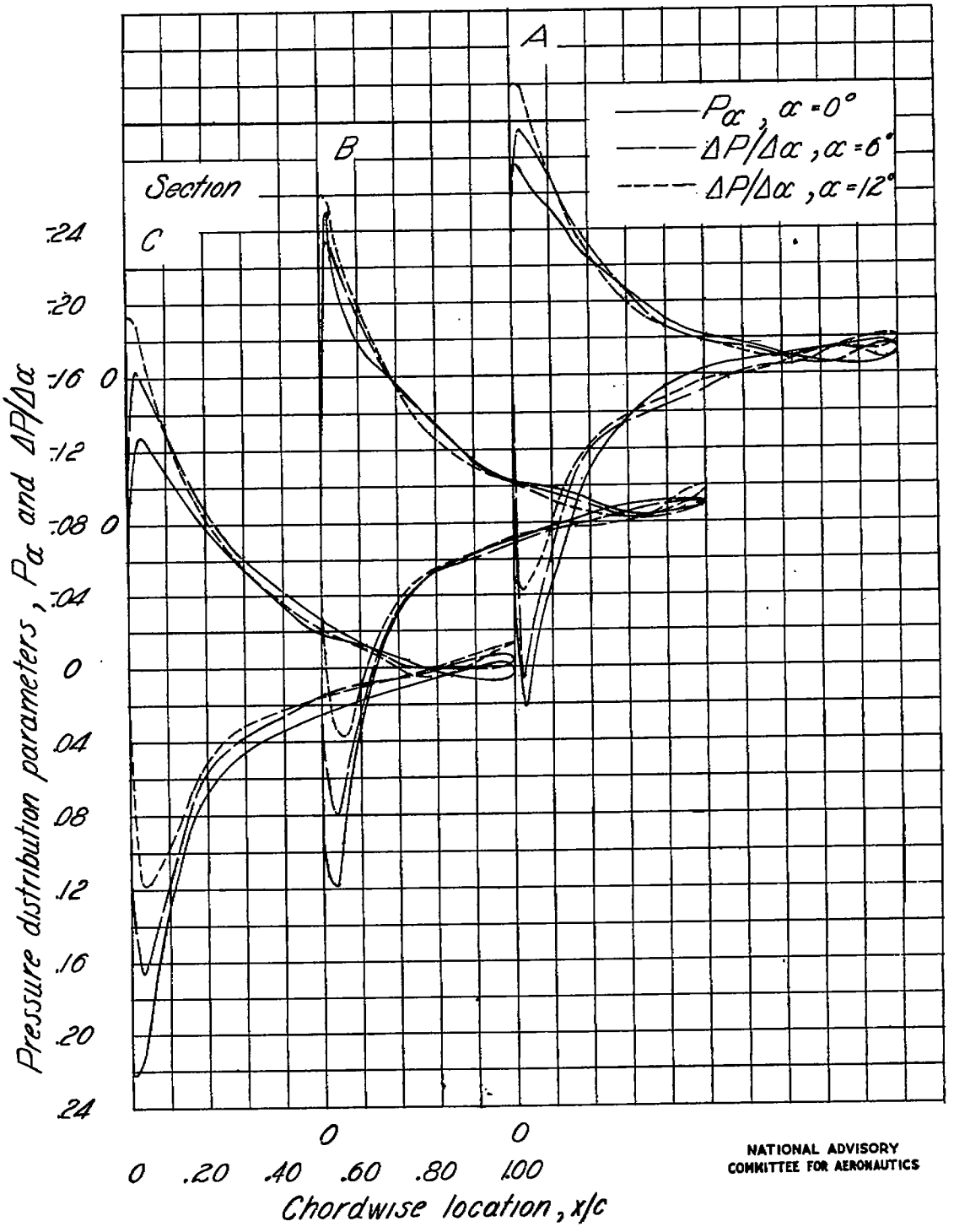

(a) Concluded.

Figure 6.- Continued.

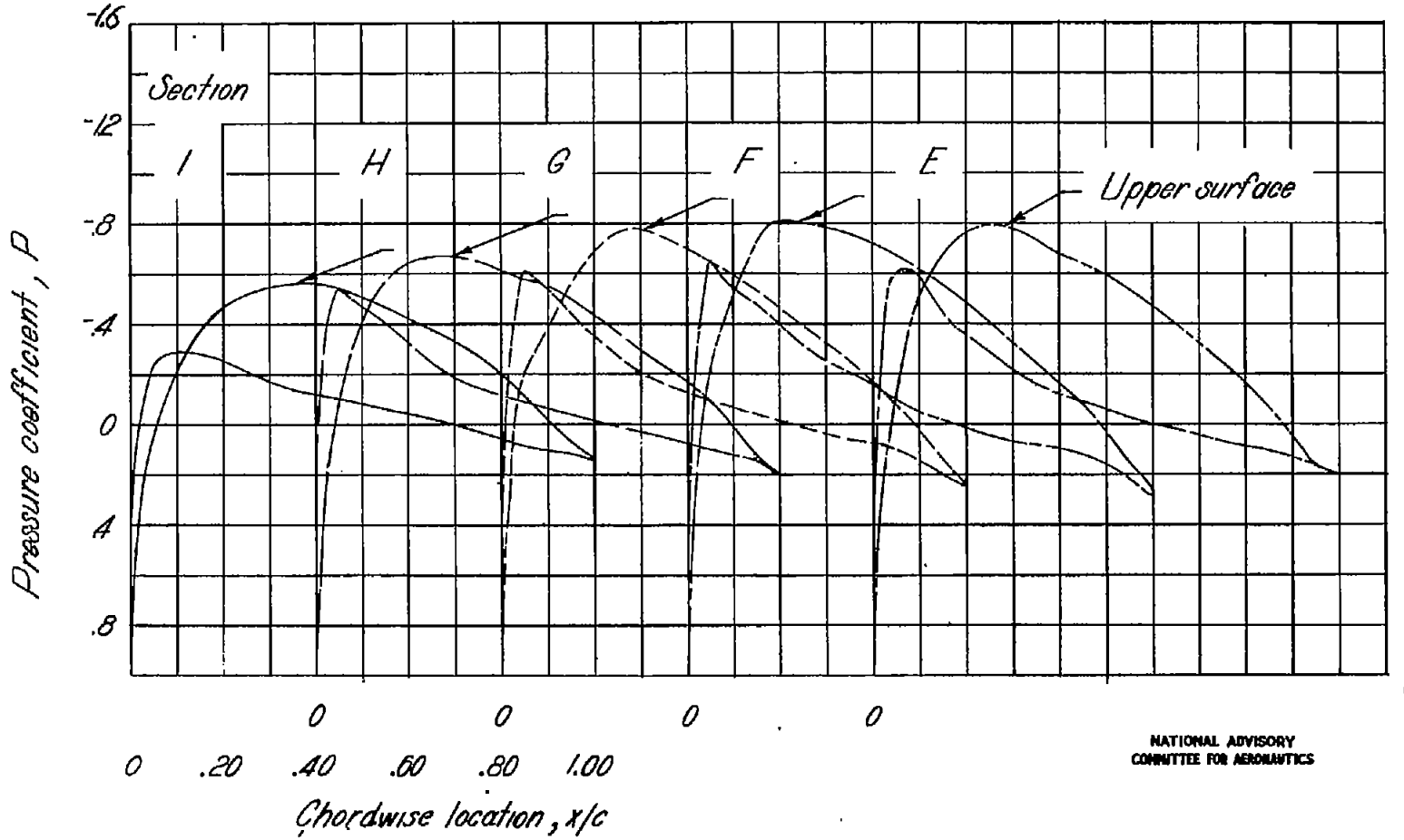

(b) Chordwise pressure distribution for $\alpha = 0^{\circ}$.

Figure 6.- Continued.

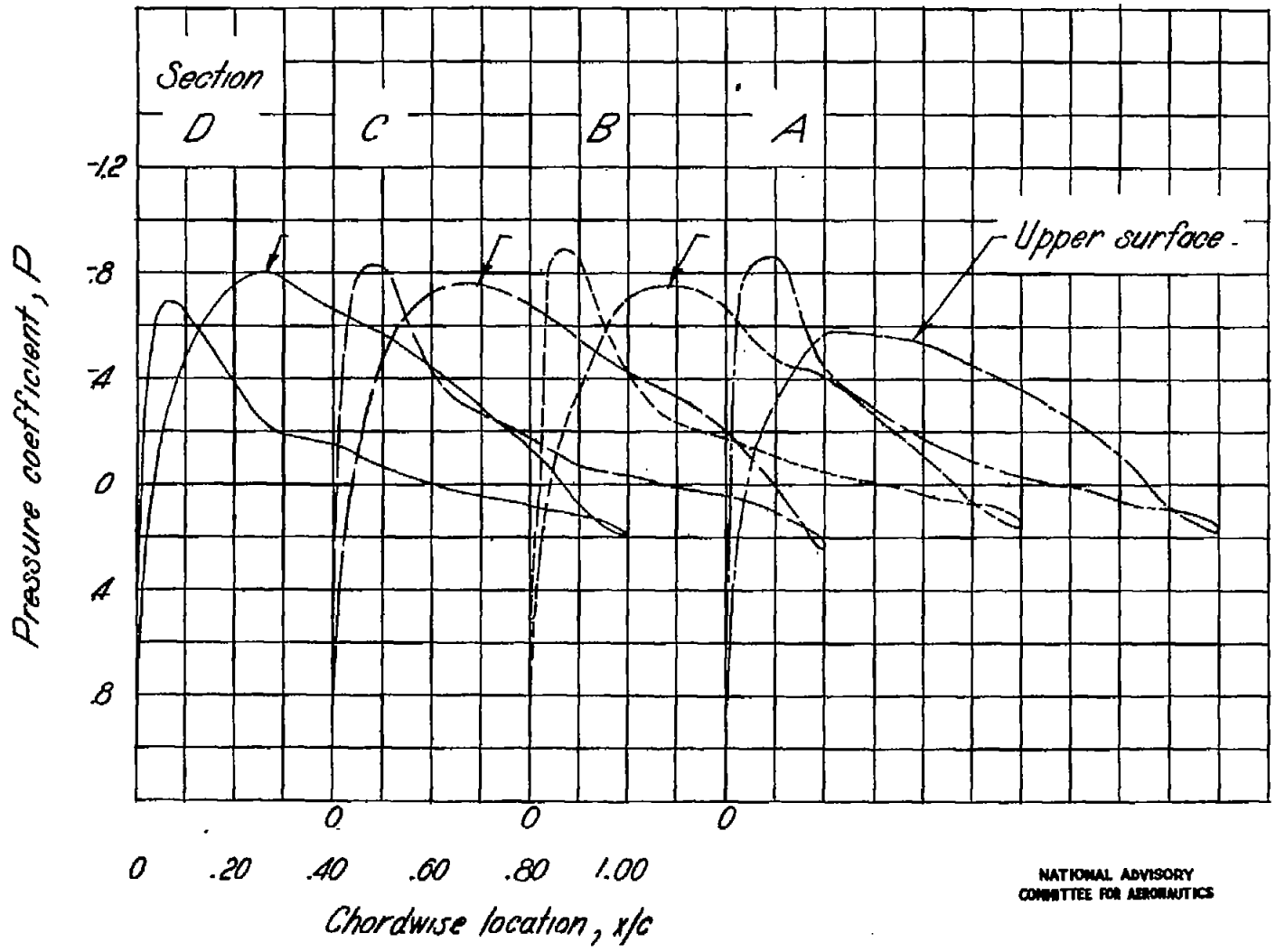

(b) Concluded.

Figure 6.- Concluded.

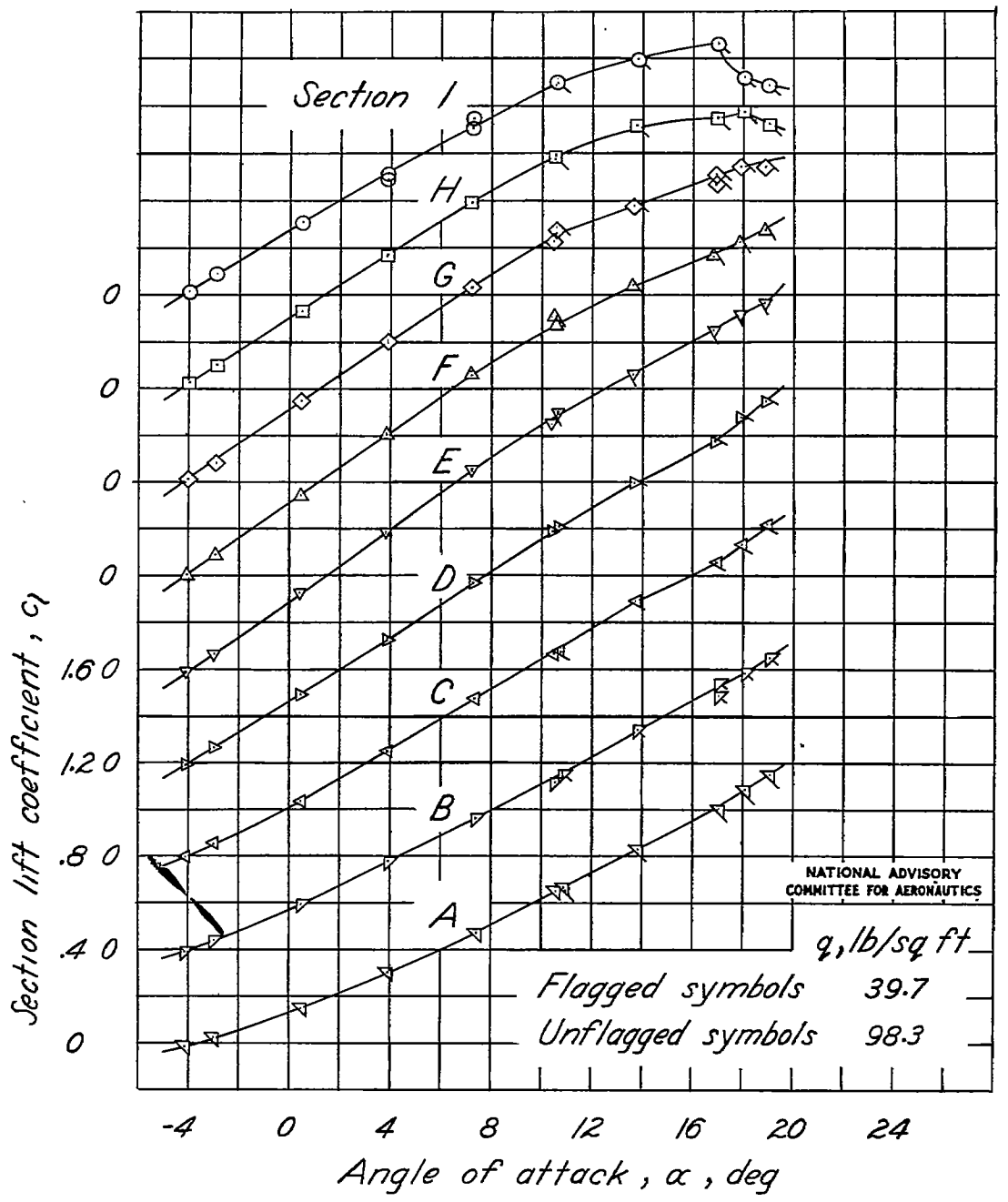

(a) Lift-coefficient curves for various sections.

Figure 7.- Results obtained from integration of section pressure distributions of swept-forward wing.

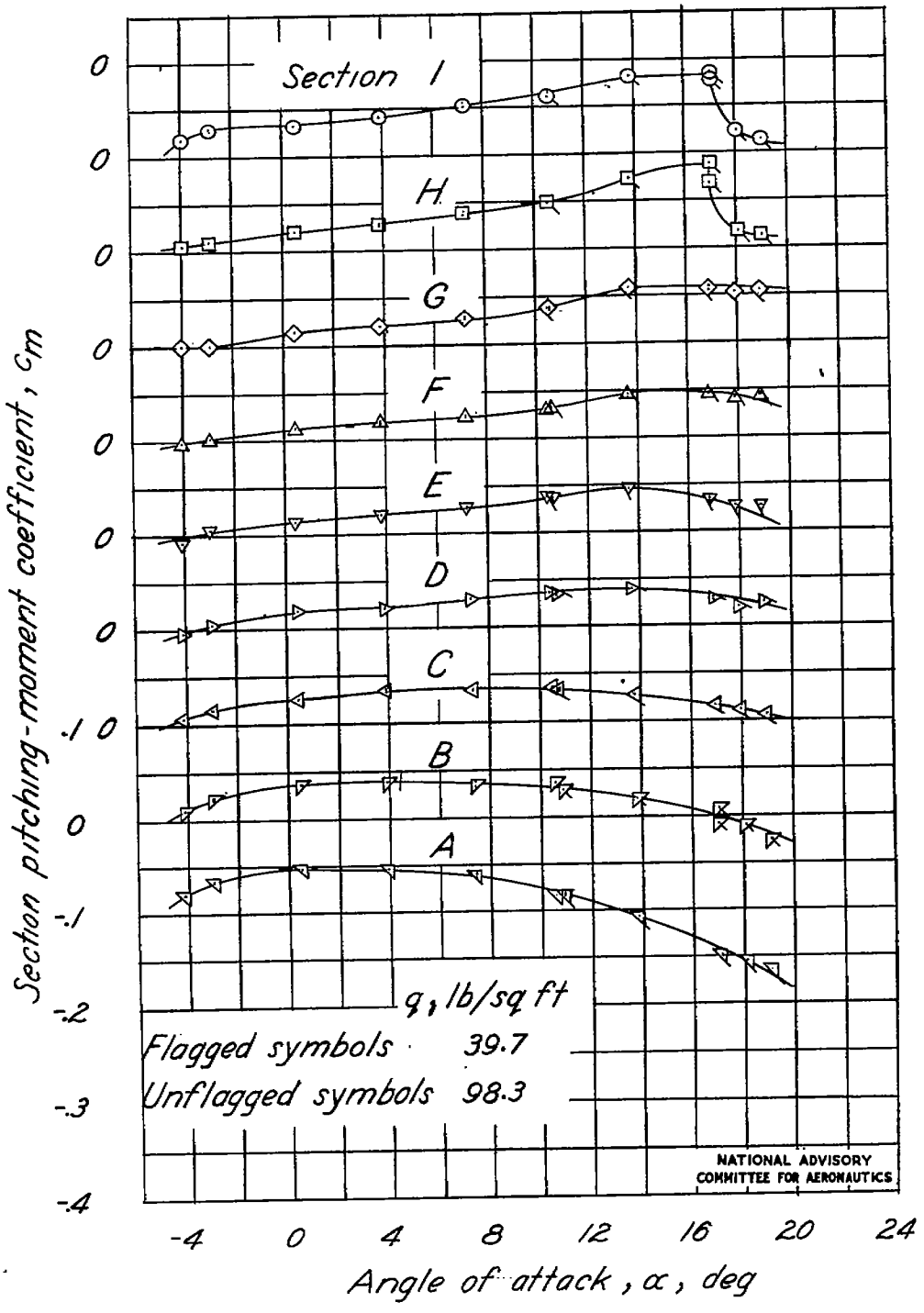

(b) Pitching-moment-coefficient curves for various sections.

Figure 7.- Concluded.

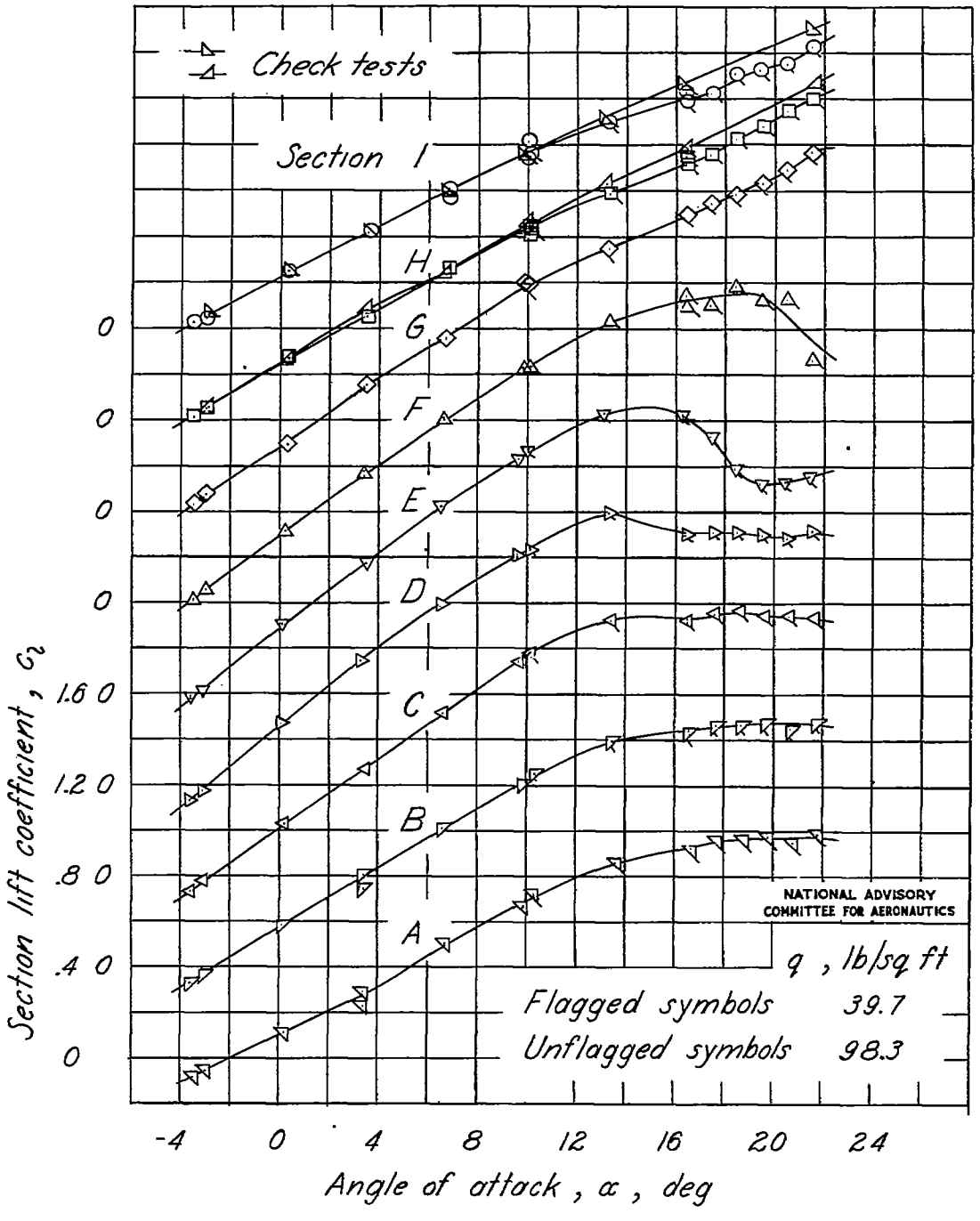

(a) Lift-coefficient curves for various sections.

Figure 8.- Results obtained from integration of section pressure distributions of swept-back wing.

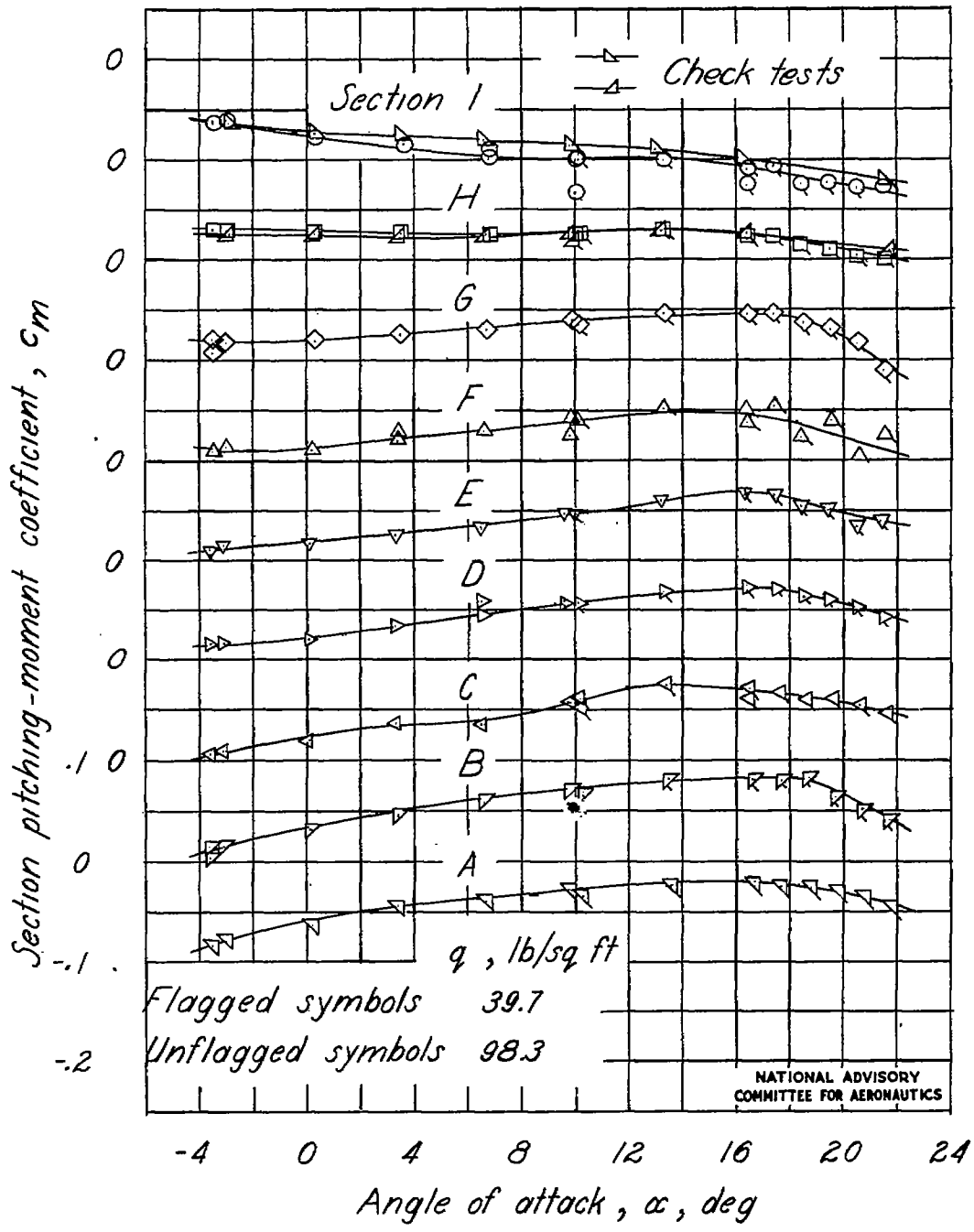

(b) Pitching-moment-coefficient curves for various sections.

Figure 8.- Concluded.

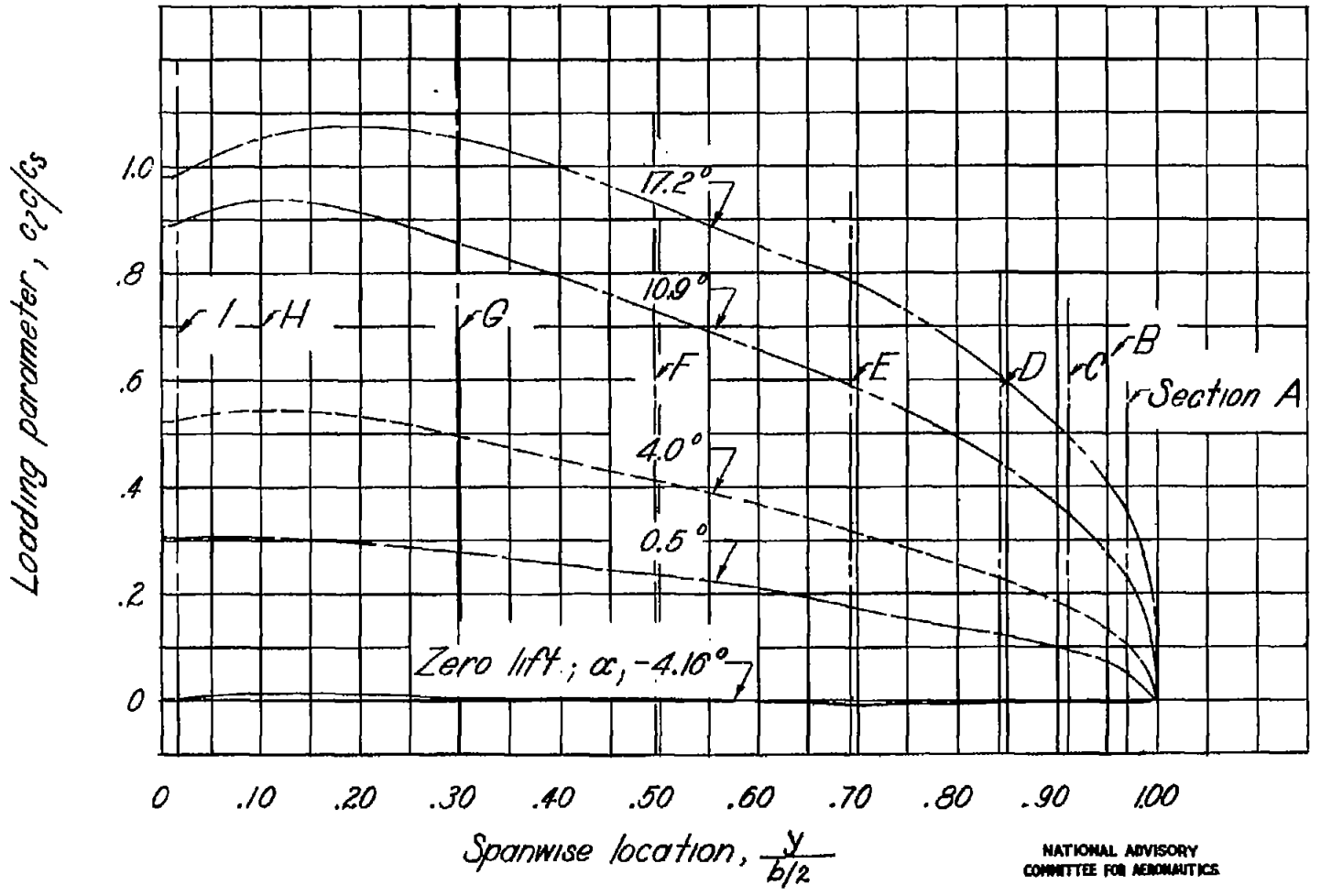

(a) Swept-forward wing.

Figure 9.- Span loading diagrams for the swept-wing models.

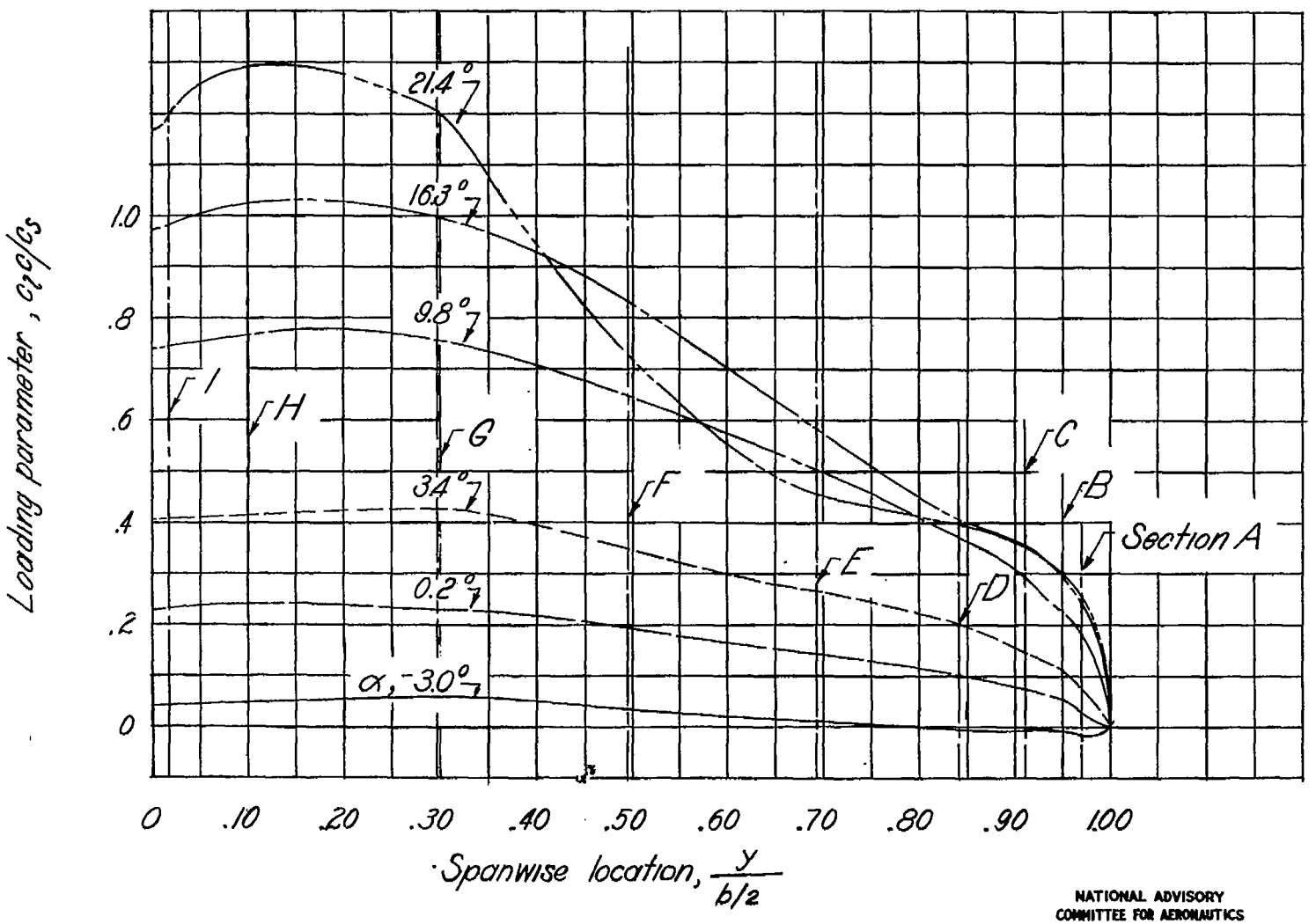

(b) Swept-back wing.

Figure 9.- Concluded.

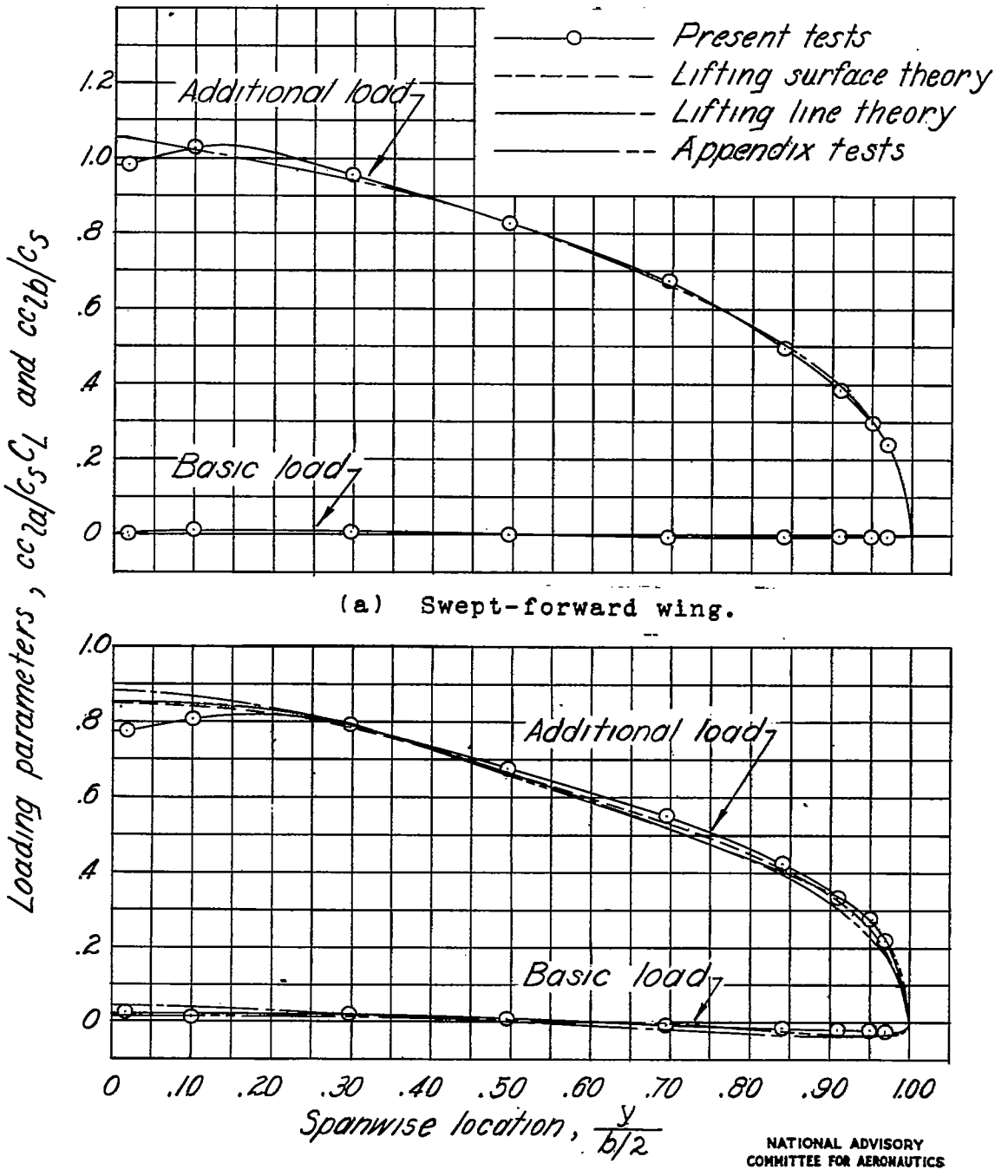

(b) Swept-back wing.

Figure 10.- Comparison of computed and test curves of basic and additional span loading.

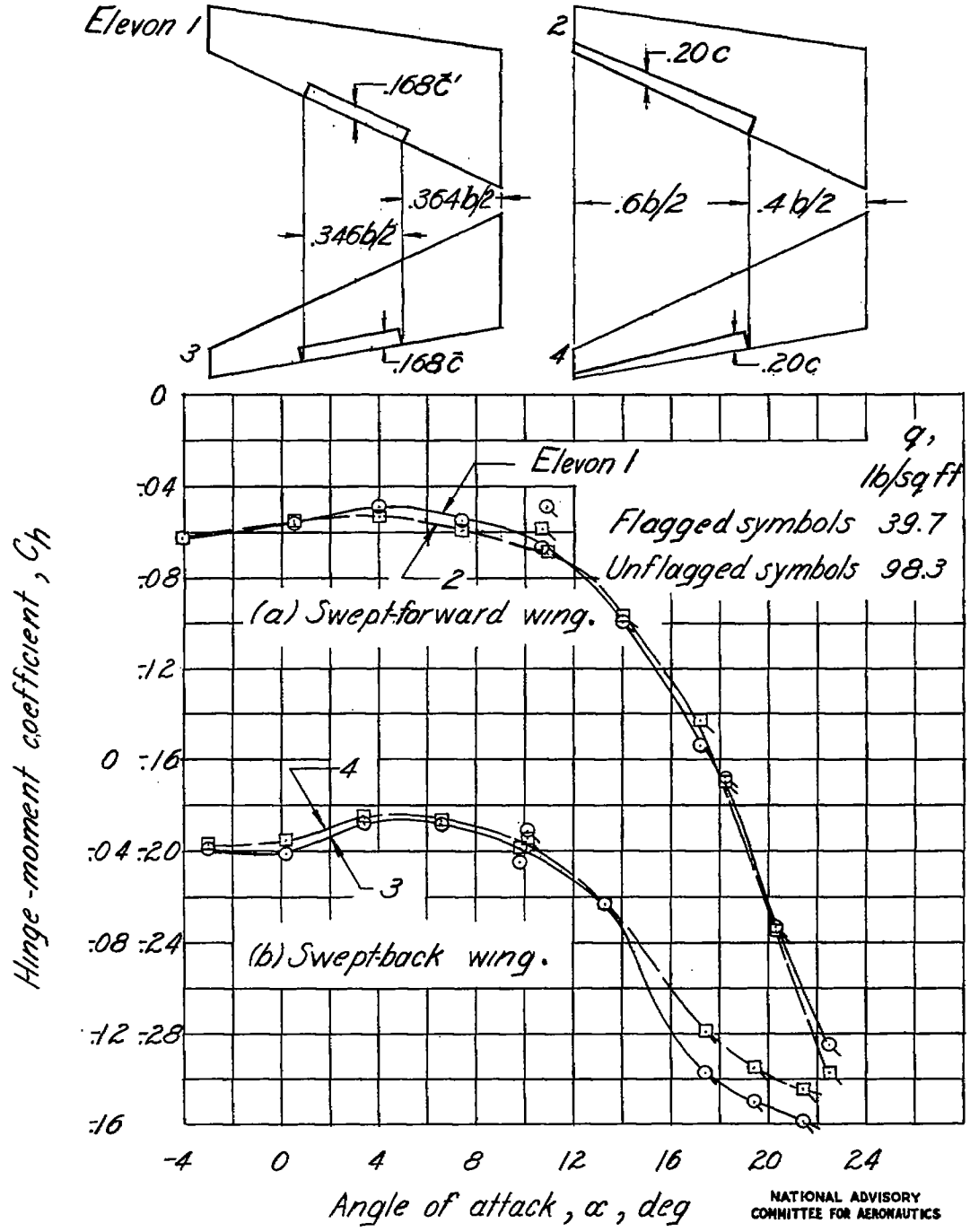

Figure 11.- Variation of elevon hinge-moment coefficient with angle of attack.

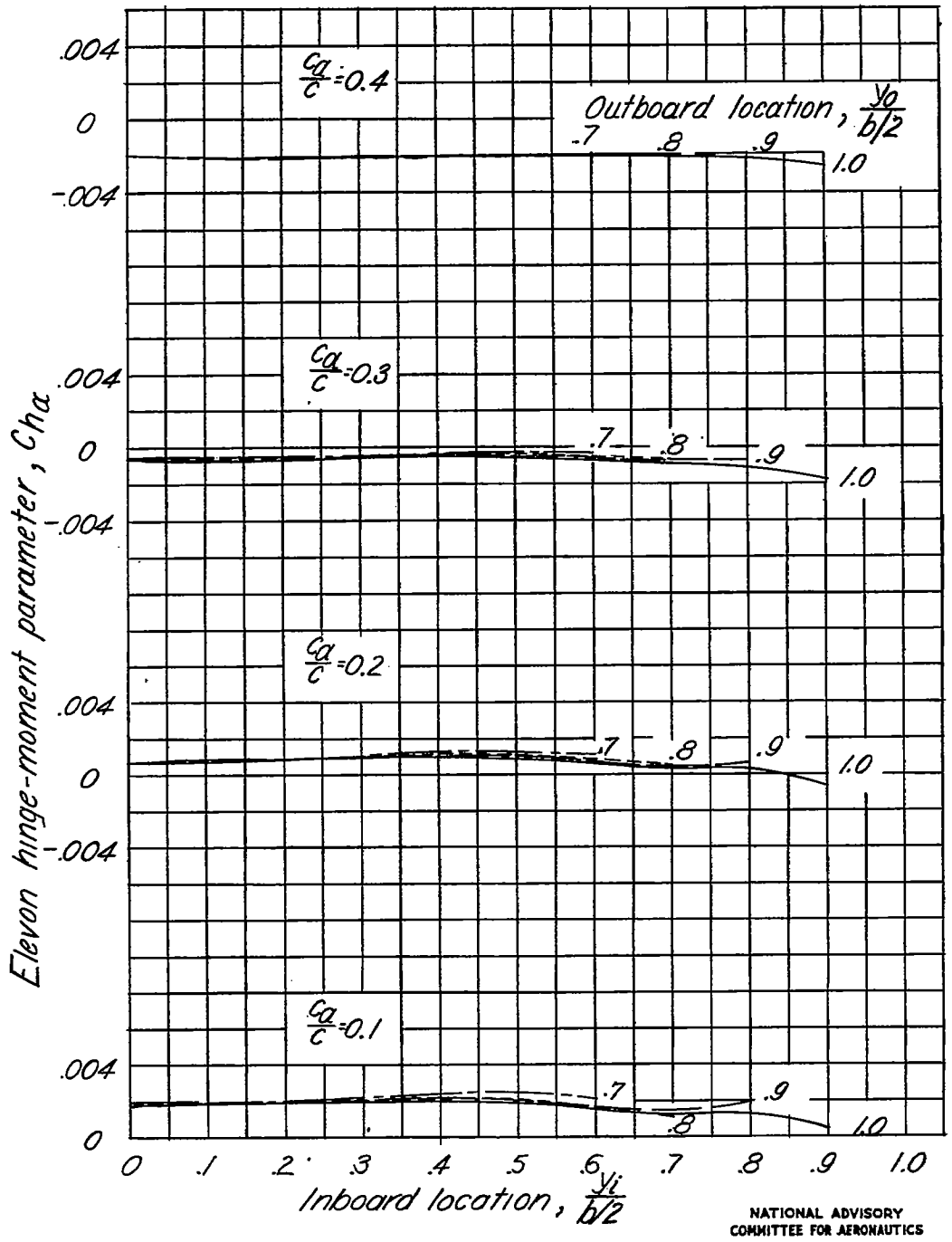

(a) Swept-forward wing.

Figure 12.- Variation of elevon hinge-moment parameter, C_{h_a}, with elevon location.

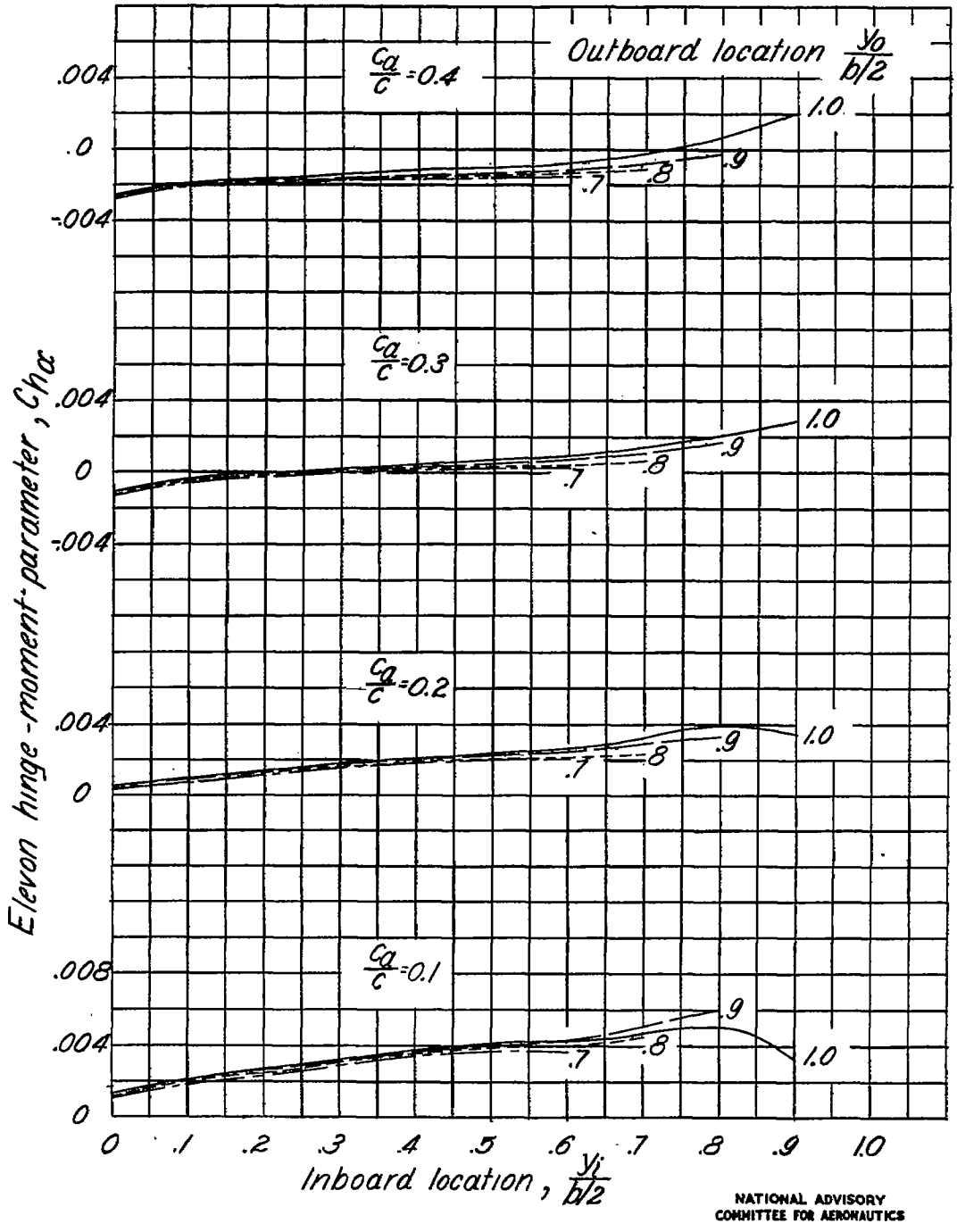

(b) Swept-back wing.

Figure 12.- Concluded.

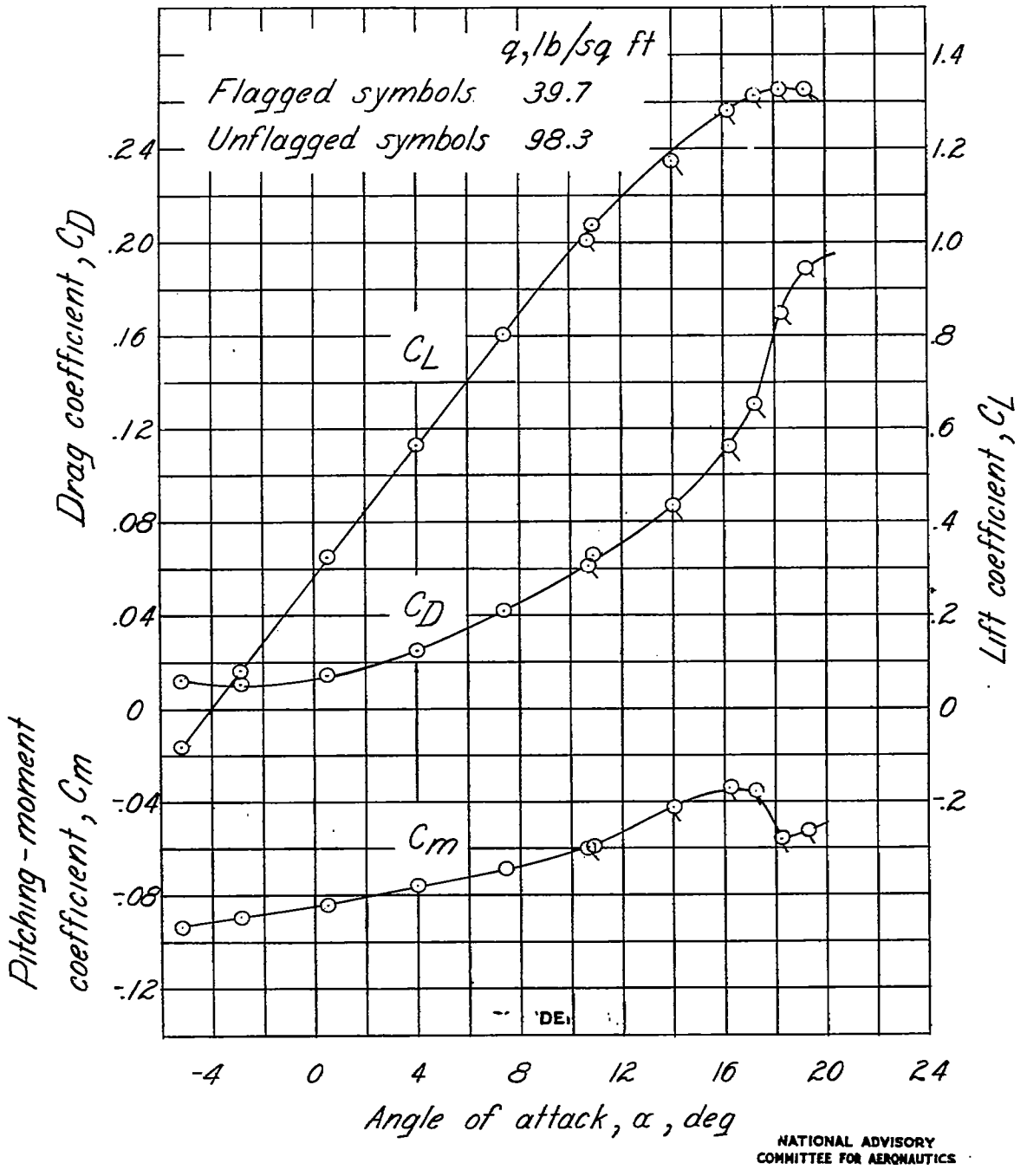

(a) Swept-forward wing.

Figure 13.- Force and moment coefficient data for the sweptwing models.

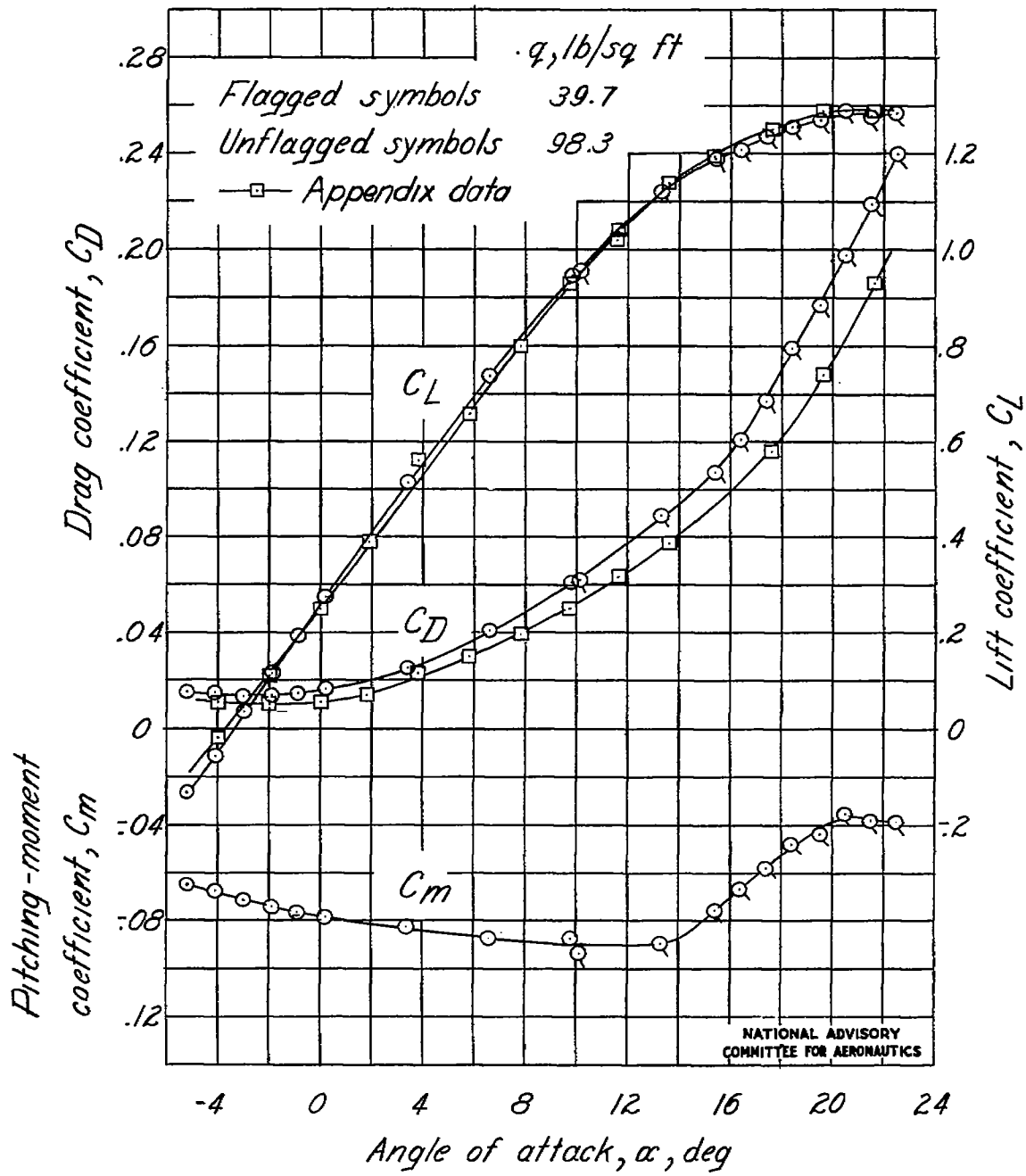

(b) Swept-back wing.

Figure 13.- Concluded.

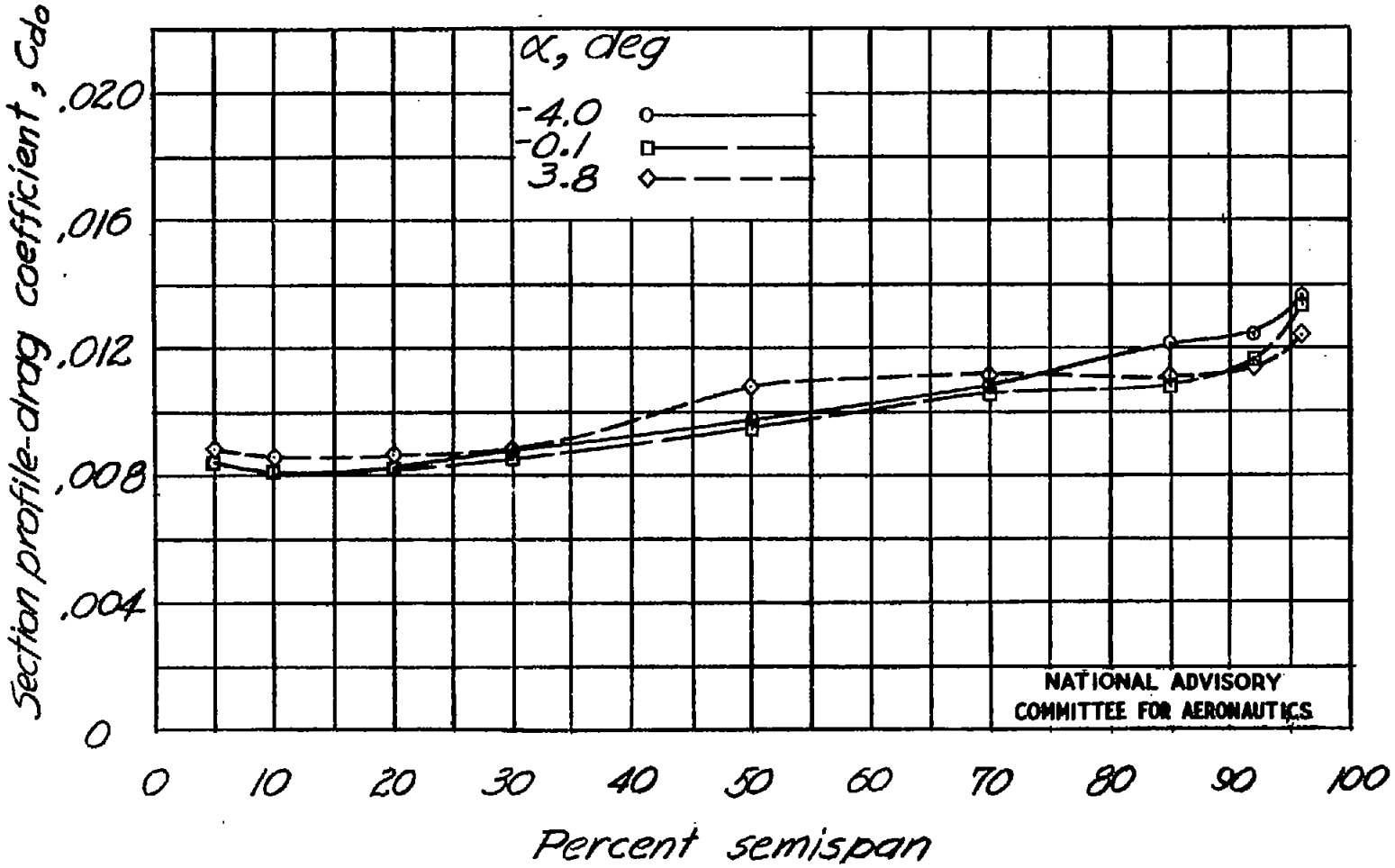

Figure 14.- Spanwise variation of section profile-drag coefficient for the swept-back wing.

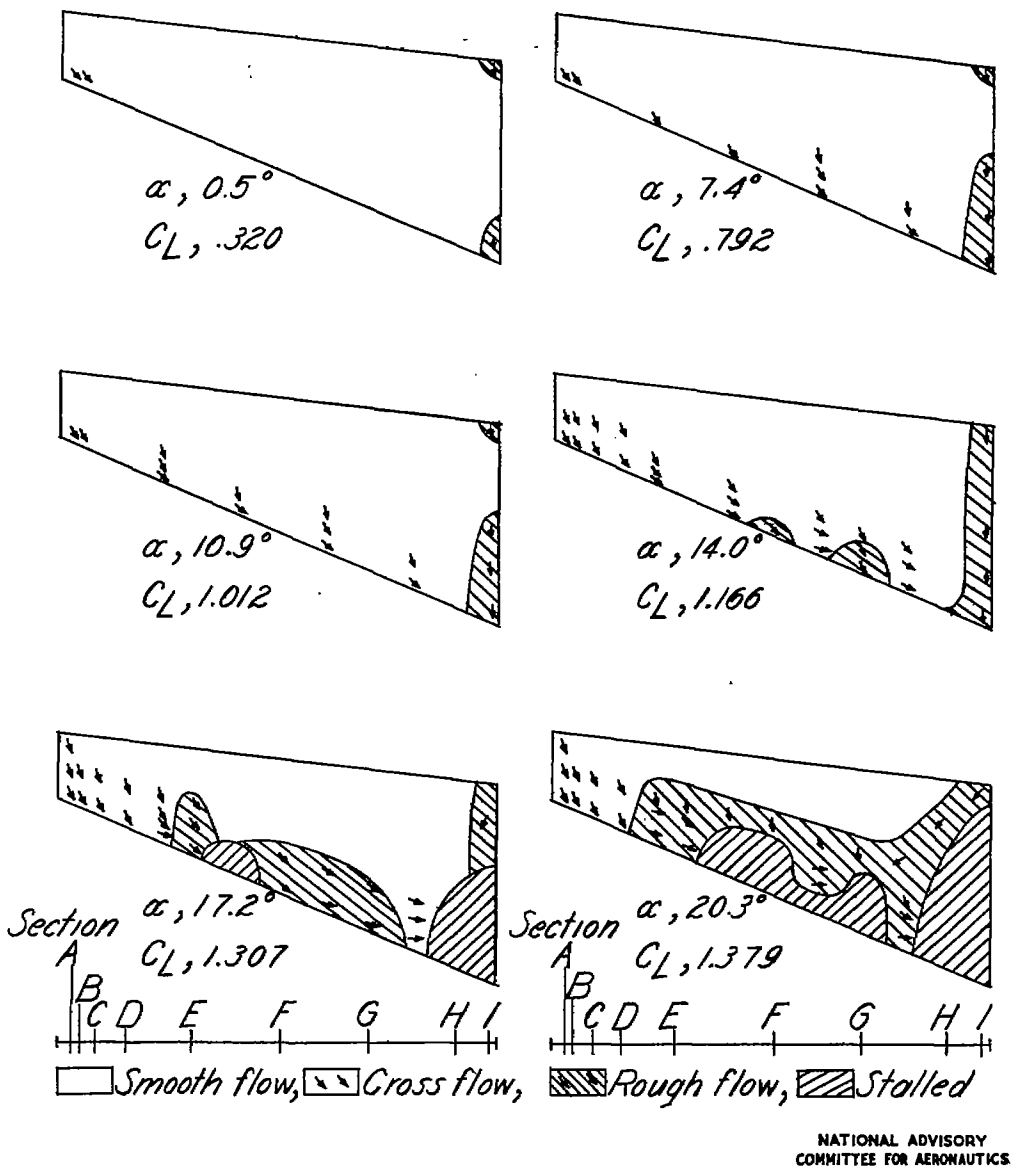

(a) Swept-forward wing.

Figure 15.- Stall patterns of the sweptwing models.

Fig. 15b

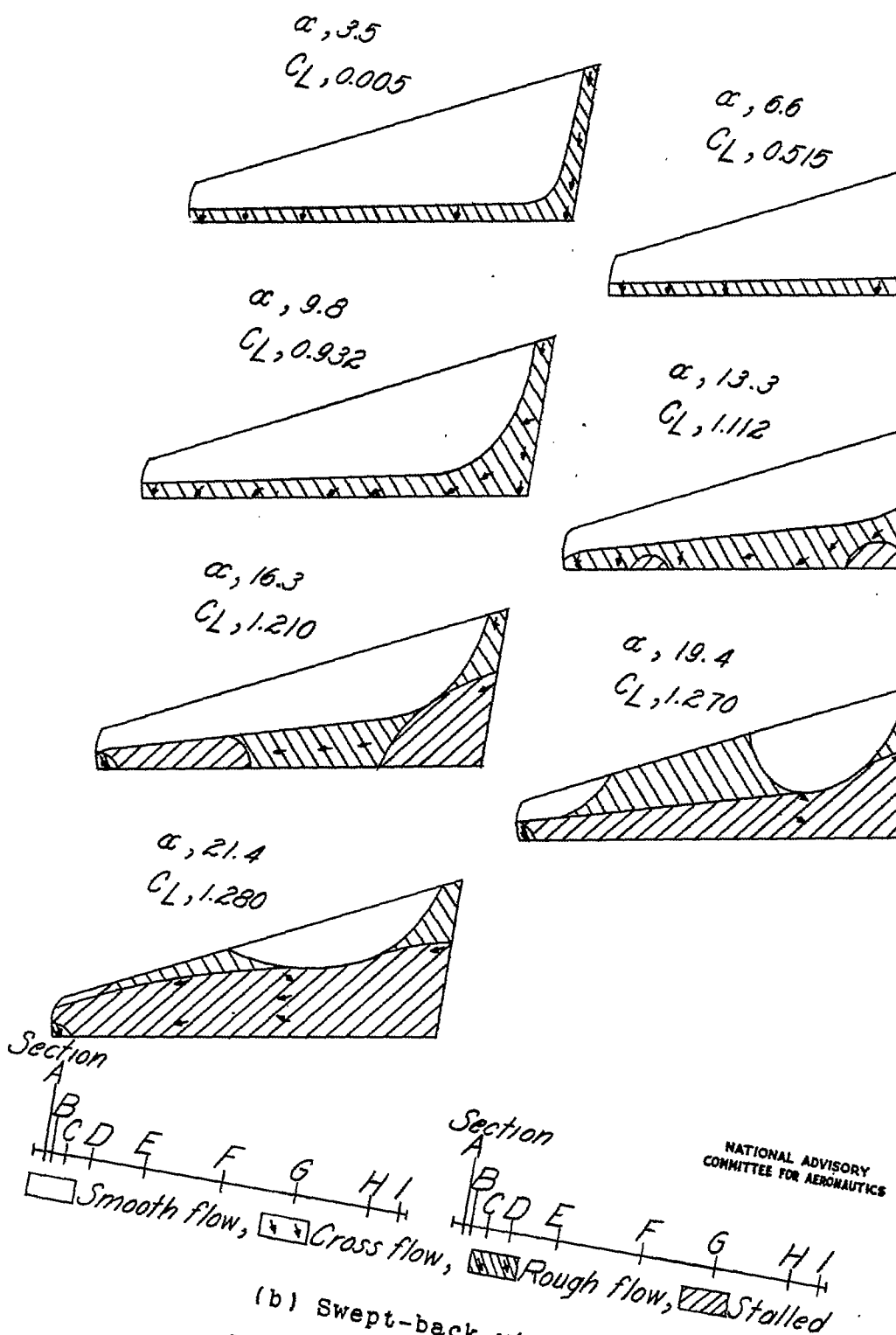

(b) Swept-back wing.

Figure 15.- Concluded.

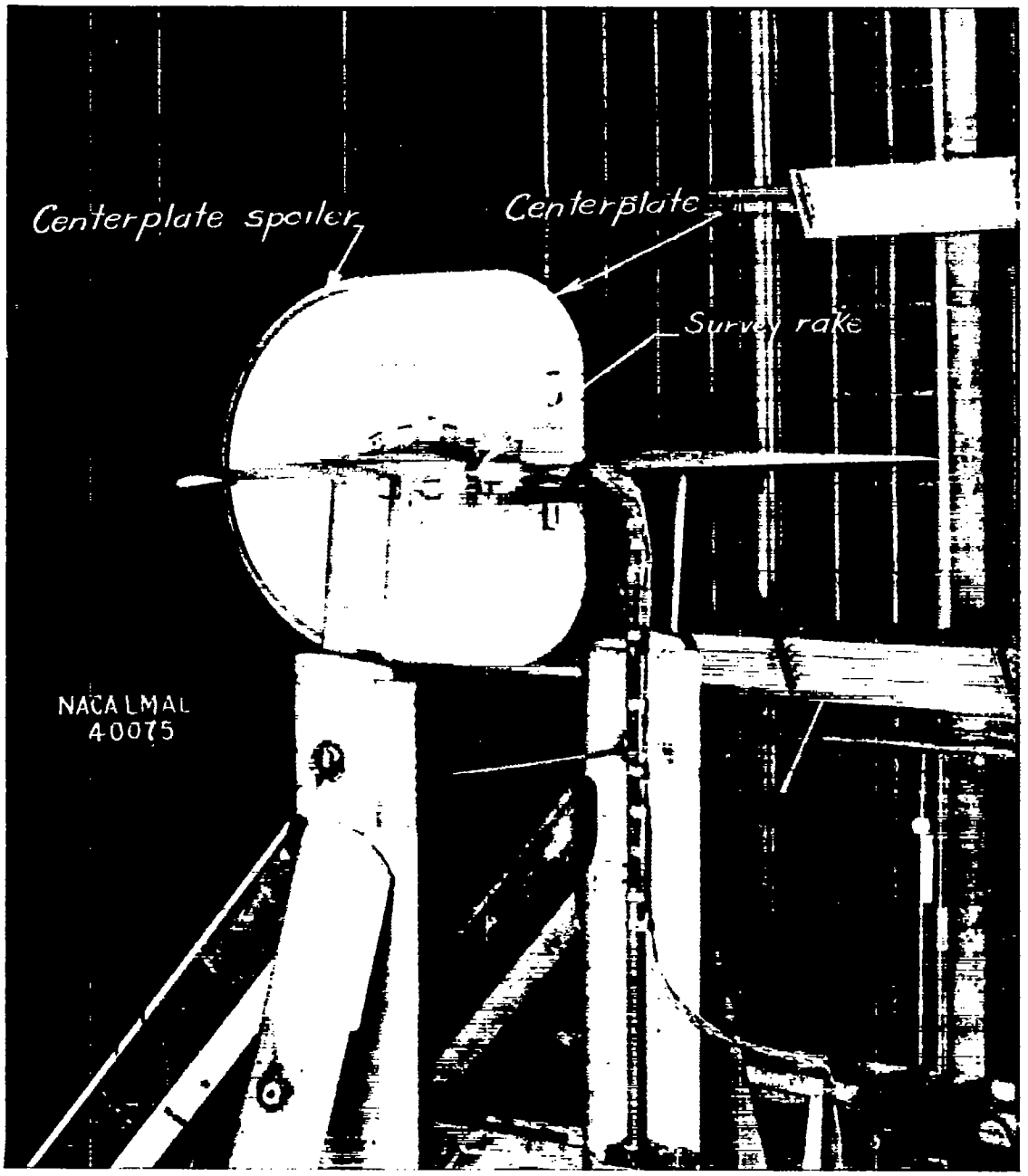

Figure 16.- View of full-span swept-back-wing model installed in the Langley propeller-research tunnel.